TUM

Technische Universität München

All-in-Fiber Frequency Comb Oscillator Development towards Space-Applications

Dissertation

Sebastian Muck Schweyer
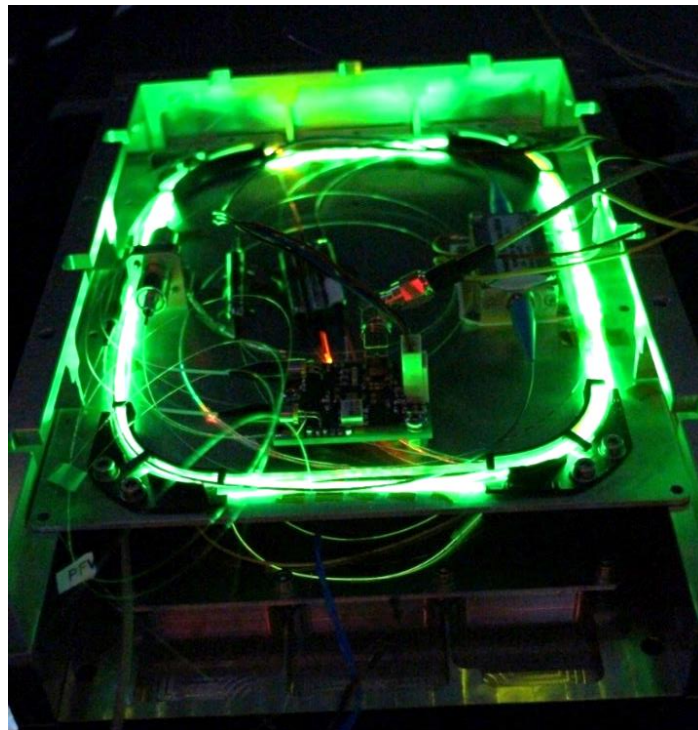
Technische Universität München

Physik-Department

Lehrstuhl für Laser- und Röntgenphysik E11

All-in-Fiber Frequency Comb Oscillator Development towards
Space-Applications

Sebastian Muck Schweyer

Vollständiger Abdruck der von der Fakultät für Physik der Technischen Universität
München zur Erlangung des akademischen Grades eines

Doktors der Naturwissenschaften

genehmigten Dissertation.

Vorsitzende(r):   Prof. Dr. Frank Pollmann

Prüfer der Dissertation: 1. Prof. Dr. Reinhard Kienberger

                          2. apl. Prof. Dr. Karl Ulrich Schreiber

Abstract

Optical frequency combs will play an important role for space-borne applications due to their capabilities of high resolution measurements in the field of spectroscopy, microwave generation, ranging as well as time and frequency transfer. Most of these application include a high stable optical frequency reference such as an optical atomic clock.

To open the accessibility of this technology for the space sector, the mass, size and environmental sensitivity of the frequency comb needs to be significantly reduced, whereas the frequency comb laser shall overtake the stability of the optical reference without any loss in performance.

To achieve this, a robust and compact in-fiber polarization maintaining Erbium frequency comb module was developed, characterized and stabilized in this work. The performance is comparable to (bulky) lab based comb systems, while having a ruggedized in-fiber design and no need of mechanical actuators for stabilization. Thereby a fractional Allan deviation (in-loop) below 10^{-16} was determined, which underlines potential applications in the field of space optical clocks.

The engine of the in-fiber frequency comb module is a femtosecond fiber laser with an integrated electro-optic waveguide modulator based on a semiconductor saturable absorber (SESAM) for pulse generation. Besides this laser, two in-fiber femtosecond lasers based on tapered fiber carbon nanotube absorbers were studied. One oscillator was equipped with an electro-optic modulator and a polarization maintaining design. The other laser was developed to demonstrate the principle of an opto-optical modulator applied to the carbon nanotube absorber. Both lasers were characterized and phase stabilized to a Helium-Neon laser to proof their functionality. Hereby an in-loop stability in the mHz range was measured. Furthermore, a linewidth of the carrier envelope offset frequency below 70 kHz was measured. This was significant lower in comparison to the SESAM based laser (linewidth > 590 kHz).

As an application the big ring laser gyroscope at the Geodetic Observatory Wettzell was stabilized with the SESAM based laser to a H-maser. Due to the stabilization the ring laser frequency drift was reduced by more than 4 magnitudes. In this context the ring laser reached a fractional Allan deviation of 5 10^{-16} at an integration time of 16384 s.

Contents

1 Introduction

In recent years the frequency comb evolved from a sensitive and complex laboratory bread-board setup to a robust and compact system [1, 2]. Frequency combs are used for demanding applications such as optical atomic clocks [3], ultra-low noise microwave signal generation [4], laser spectroscopy [5], absolute distance measurement [6] and frequency/time transfer [7]. This is due their capability of phase-coherent locking to highly stable and low noise microwave and optical references. Thanks to its versatility, the frequency comb [8, 9] will play an important role for space-borne systems in the field of navigation [7, 10, 11, 12], geo-mapping [13, 14, 15], interferometric imaging [16], earth observation [17] and scientific missions [18, 19].

Most of these applications include a highly stable optical reference such as an optical cavity and/or an optical atomic clock (OAC) to determine physical parameters such as space (distance), time and frequency with highest resolution. Hereby the stability of the optical reference needs to be transferred to an optical frequency comb to measure these parameters.

The aim of this thesis was to develop a frequency comb engineering module capable to overtake the sub-Hz stability of modern optical standards without any loss in performance. Additionally, the frequency comb module shall be compact and robust to fit a space-borne instrument. This requires the control and manipulation of ultra-short laser pulses in optical components such as Erbium- and highly non-linear fibers, saturable absorbers and non-linear crystals. Another challenge is to stabilize the frequency comb with a feedback bandwidth beyond the gain response time of the laser oscillator itself.

Frequency combs are generated with solid-state lasers (e.g. Titan Sapphire, Ytterbium doped materials), whispery gallery mode resonators, semiconductor lasers or fiber lasers. Among these laser technologies mode locked Erbium fiber lasers are currently the best candidate for a space-borne system. They can be realized in a compact and robust in-fiber design, while providing the performance of bulky solid-state lasers. Non mechanical actuators for comb stabilization prevent a critical damage to the optical fiber. The commercial and scientific use of Erbium fiber lasers proofs a proper technical readiness level.

The main engine of the frequency comb system is a femtosecond fiber oscillator. Here a polarization maintaining (PM) all-in-fiber SESAM (semiconductor saturable absorber mirror) based femtosecond oscillator with an integrated waveguide electro-optic modulator (EOM) was implemented in the engineering frequency comb module. The EOM is used to achieve a coherent high bandwidth comb stabilization.

Furthermore two femtosecond oscillators with a tapered fiber carbon nanotube (tf-CNT) absorber were studied. The oscillators were also realized in an all-in-fiber design since they promise a better noise performance than a SESAM EOM laser. This is due to the faster sub-ps relaxation time of the CNT absorber. One tf-CNT femtosecond laser was equipped with an intra-cavity EOM, such as the SESAM EOM laser. The other oscillator was specifically built to demonstrate the opto-optic modulation (OOM) principle with a CNT absorber for fast feedback comb stabilization.

The noble prize in physics was awarded in the year 2005 to John Hall and Theodor Hänsch for the demonstration of optical frequency comb technology and contributions in the field of high precision laser spectroscopy [20]. Frequency comb oscillators show two degrees of freedom, which is the repetition rate and the carrier envelope offset frequency. Both need to be stabilized/known to obtain a fully referenced frequency comb. The three oscillators were compared to each other by stabilizations and measurements of the CEO beat and of a comb mode at 633 nm, respectively.

As a verification measurement the big "G" Helium-Neon laser gyroscope located at the Geodetic Observatory Wettzell [21] was stabilized to an H-maser via the SESAM EOM comb oscillator. The goal here was to reduce the gyroscope's long-term drift to improve the measurements of physical effects related to variations in the Earth rotation.

This thesis is structured as follows: In the next section the theory is explained to understand how a frequency comb works, how oscillators are characterized and how pulses are generated in femtosecond Erbium fiber lasers. The femtosecond oscillators and optical interfaces to generate a CEO beat and an optical beat with a HeNe laser are introduced in section 3. In section 4 the oscillators are characterized. In section 5 actuators for comb stabilization are characterized. Consequently the femtosecond oscillators are stabilized and compared against each other.
The stabilization of the "G" laser is demonstrated in section 6. Finally the setup, characterization and stabilization of the all-in-fiber frequency comb module is presented in 7. A summary and outlook of the work is given in section 8.

2 Theory

2.1 Frequency Comb Principle

In general every mode-locked laser oscillator emitting ultrashort (femtosecond) pulses is an optical frequency comb. Such a laser emits a train of pulses (see Figure 2-1 a,), where the temporal spacing of consecutive pulses is indirect proportional to the laser repetition rate $f_{rep}=v_g/L$. Whereas v_g is the pulse's group velocity and L is the resonator length.
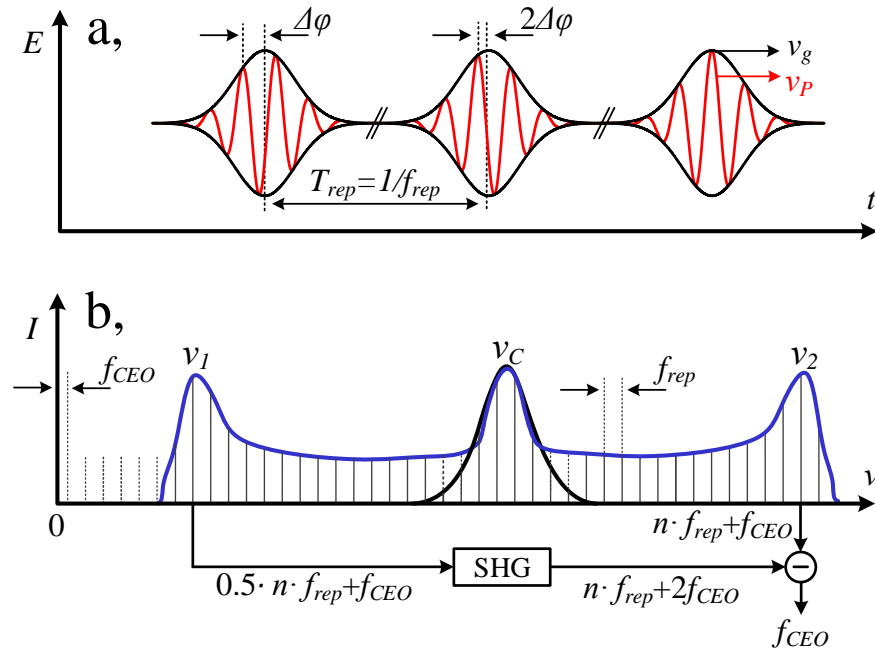
Figure 2-1: A frequency comb based on femtosecond pulse train in the temporal a, and spectral domain b,.

According to the Fourier theorem, a periodic repeating signal in the time domain leads to a periodic pattern in the spectral domain. Out of this reason the optical spectrum of the pulse train shows discrete lines (see Figure 2-1 b,) separated by f_{rep}. The frequencies of these discrete lines correspond to the mode-locked longitudinal modes of the femtosecond laser. The envelope (black bold line) of the comb modes has a Gaussian like shape, which is here given by the time-bandwidth limited Gaussian pulses in the temporal domain. The harmonic mode pattern is shifted by the carrier envelope offset frequency f_{CEO} resulting from a time dependent phase delay between the pulse's envelope and electric field. Concerning $\Delta\varphi_{CEO}$ as the change of the relative phase from pulse to pulse the f_{CEO} frequency is expressed as:

$$f_{CEO} = \frac{\Delta\varphi_{CEO}}{2\pi} f_{rep} \qquad (2.1)$$

Consecutive pulses show a phase delay, since the phase velocity v_p of the electric field (red line) is different compared to the envelopes (black line) mean group velocity v_g. The difference in the group and phase velocity is given due to dispersive effects and is described in detail in [22]. The frequency of the *n*-th comb mode is then described as:

$$v_n = n \cdot f_{rep} + f_{CEO} \tag{2.2}$$

If f_{CEO} and f_{rep} is well known, any other frequency within the comb's spectral range can be estimated. However, in order to realize a fixed frequency ruler, both degrees of freedom, f_{rep} and f_{CEO}, need to be stabilized. Out of this reason, a frequency comb is often defined as a frequency comb when both frequencies are fully fixed.

Therefore f_{rep} and f_{CEO} need to be measured and referenced to an optical or radio frequency (RF) standard. The repetition rate is determined by measuring the output light of the laser oscillator with a photo diode. A measured RF spectrum of an oscillator with a repetition rate of 80 MHz is illustrated in Figure 2-2.
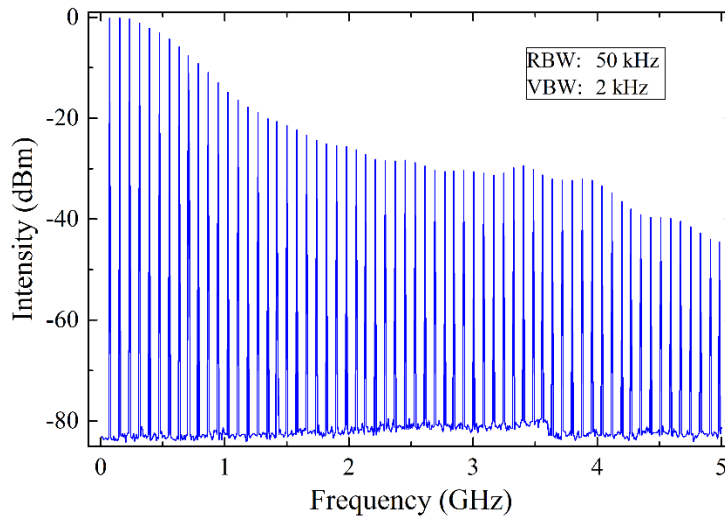
Figure 2-2: Frequency spectrum of a femtosecond fiber laser's repetition rate.

In theory, the f_{CEO} is defined as $f_{CEO}=v_c(1-v_g/v_{ph})$, where v_c is the laser's carrier frequency resulting to $f_{CEO}\approx$1-3 THz for fiber lasers [23, 24]. Thereby it is more sophisticated to obtain f_{CEO}, since there is no detector available fast enough to observe the instant change in the phase of the pulse's carrier frequency in respect to the envelope. Out of this reason *1f-2f* interferometry [25] is used in this thesis to mix f_{CEO} down ($f_{CEO}\pm kf_{rep}$) to a measurable value with a f_{CEO} frequency in a typical range of some tens to hundreds of MHz.

Therefore the comb oscillator output spectrum needs to be expanded to a bandwidth with equal or more than one octave. To do so, the laser pulses are fed into a highly nonlinear medium such as a photonic crystal fiber (PCF), a highly nonlinear fiber (HNF) or a silicon

nitride (SiN) waveguide. Due to nonlinear processes a supercontinuum (SC) is generated, which is depicted as a blue solid line in Figure 2-1 b,. The lower frequency part v_1 is frequency doubled via a second harmonic generation process and is superimposed with the light from the SC's higher frequency part v_2. The f_{CEO} frequency is obtained by measuring the interference signal between $2v_1$ and v_2 with a photodiode resulting to:

$$2v_1 - v_2 = 2\left(0.5 \cdot n \cdot f_{rep} + f_{CEO}\right) - \left(n \cdot f_{rep} + f_{CEO}\right) = f_{CEO} \qquad (2.3)$$

The f_{CEO} is then often stabilized via the self-referencing method[1], where f_{CEO} is phase stabilized directly to f_{rep}. For stabilization, f_{rep} is in generally controlled via tuning the optical length in the cavity with actuators such as fiber stretchers, electrical optical phase modulators (EOM) or piezo mounted free space mirrors. On the other side, the f_{CEO} is controlled by loss/gain modulation of the cavity by means of actuators such as pump power modulation, graphene modulators, electro-optic intensity modulators or opto-optical modulation. An overview on these actuators is given in chapter 0. Other approaches are 2f-3f interferometry [26] or the generation of an CEO free comb via difference frequency generation [27].

2.2 Requirement on Frequency Stability and Optical Referencing

The performance requirement on the frequency comb laser oscillators was that the stability of a modern optical clock shall be transferred to the comb modes without any loss in performance. In general the clock performance is quantified by the fractional stability and accuracy of the clock frequency. In Figure 2-3 the fractional stability of two radio frequency standards as well as a strontium optical atomic clock (OAC) is shown. The black line shows the fractional stability as a function of integration time for a passive H-maser in a Galileo satellite [28]. The ACES (Atomic Clock Ensemble in Space) mission carries an active H-maser and a Cesium fountain. Its combined stability is depicted by the red-curve. Modern OACs such as the Strontium neutral clock from JILA [3] show a stability, which is about two orders of magnitude better than the best space-clock ACES (launch planned in 2019).

---

[1] Example: The f_{rep} @ 100 MHz of a comb is converted to 25 MHz by an electric frequency divider (n_d=4). The f_{CEO} ($\Delta\varphi_{CEO} = 2/4\ \pi$) is then phase locked to the 25 MHz signal.
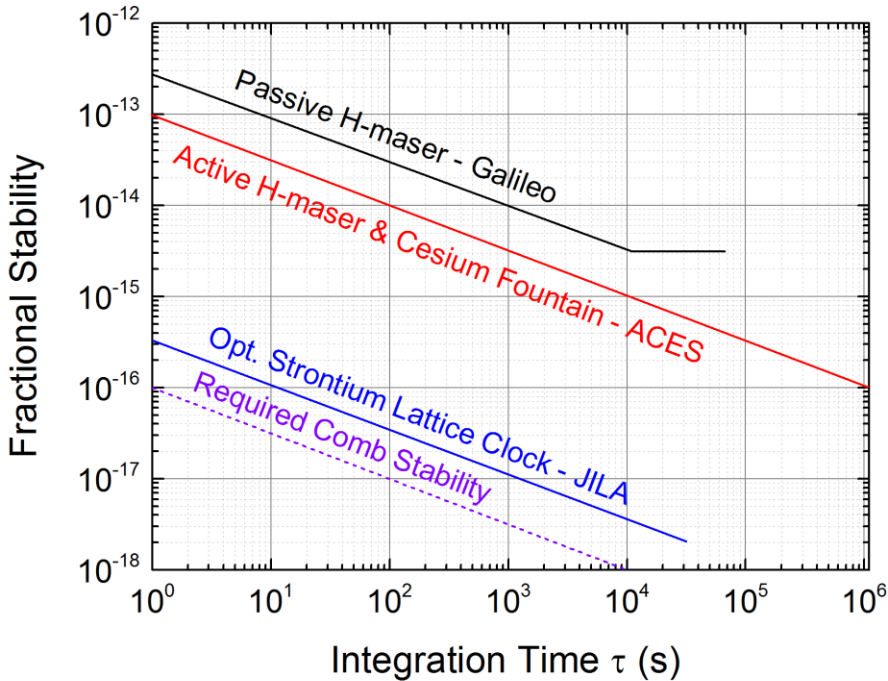
Figure 2-3: Fractional stability of space radio frequency standards and a modern optical atomic clock.

Hereby, the frequency comb stability needs to be below this stability. Therefore a fractional comb stability of $\leq 1\cdot 10^{-16}$ at an integration time of 1 s and fractional stability of $\leq 1\cdot 10^{-18}$ at an integration time of 10000 s was aimed for the comb performance.
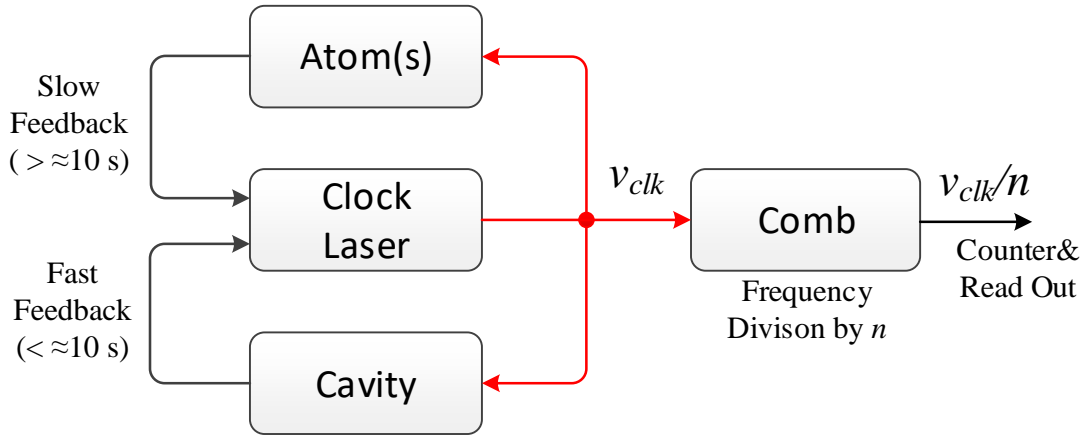
Figure 2-4: Frequency comb as an optical frequency divider for an optic atomic clock.

In order to understand this requirement, the referencing of a comb to an optical frequency is briefly explained in the following. Figure 2-4 shows a simplified sketch of an optical clock principle. Hereby a narrow linewidth laser is locked to a high finesse cavity to guarantee a

short-term stability better than 10^{-15} in an observation period of some seconds. For long-term stability the laser is probed and referenced to an atomic transition.

Since the frequency of the clock laser ($\approx 10^{15}$ Hz) could not directly be measured with e.g. photodetectors (response of $< 10^{10}$ Hz), a frequency comb is used as a frequency divider to transfer the stability from the optical to the RF domain. Therefore, an optical beat between the clock laser and a comb tooth is generated as illustrated in Figure 2-5. The clock laser frequency is then given by:

$$v_{CLK} = n_{clk} \cdot f_{rep} + f_{CEO} + f_{opt} \tag{2.4}$$

The comb tooth ($n_{clk} \cdot f_{rep}$) is referenced to the clock laser by a phase stabilization of the optical beat f_{opt}. Hereby the f_{opt} beat is locked whether to a RF-synthesizer signal or to the repetition rate itself, such as often applied for self-referencing of f_{CEO} [29].
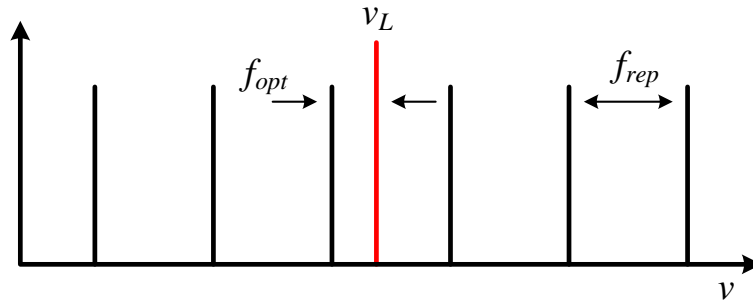
Figure 2-5: Optical beat generation between a comb mode and a single mode laser.

Since the comb is now phase stabilized to the clock laser, all other comb modes overtake the properties of the clock laser such as phase noise and long-term stability. This means that the absolute frequency stability is divided down to the RF-domain by the number of comb modes resulting to:

$$f_{rep} = \frac{v_{CLK} - f_{CEO} - f_{opt}}{n_{clk}} \tag{2.5}$$

The clock laser of the neutral Strontium clock has a fractional stability of $3 \cdot 10^{-16}$ at a frequency of 435.11 THz, which means that the frequency stability of the phase stabilized CEO beat and optical beat is below $3 \cdot 10^{-16}$ or 435.11 THz$\cdot 3 \cdot 10^{-16} = 130$ mHz. The frequency of the Sr-clock laser is close to the HeNe laser frequency (473.6 THz) in this thesis, which was used for stability measurements. For this reason, the Sr clock was here exemplary selected as illustration.

2.3   Fixed Point Frequency and Comb Noise

This chapter gives a summary on the dynamics of fiber frequency combs as well as on their noise properties. These properties build an important basis for the characterization and stabilization of femtosecond oscillators which is depicted in section 4 and section 5, respectively. Non stabilized frequency combs have a minimum linewidth at a specific spectral position, where phase noise of f_{rep} and f_{CEO} almost cancels each other out. This position is called fixed point frequency v_{fix}. The comb modes show around this point a breathing like motion, which is also often described with an expanding/contracting elastic band model (see Figure 2-6). The fixed point model is discussed in detail in [23,30,31].
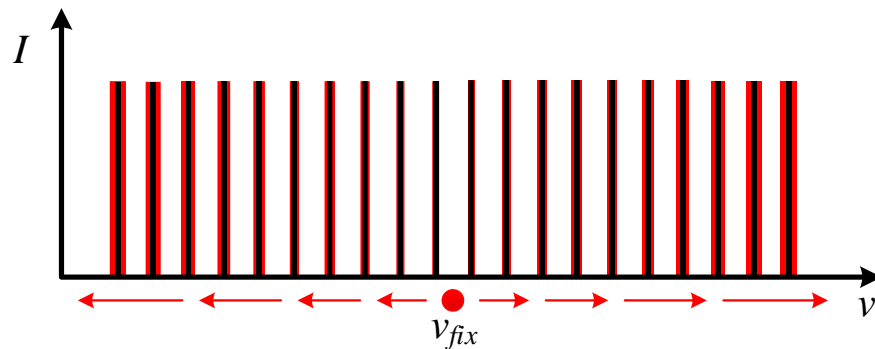
Figure 2-6: Breathing motion of frequency comb teeth around a fixed point frequency vfix.

Since the laser is driven by pump power, the breathing motion is dominated by intensity noise of the pump laser. In this context the fixed point is experimentally estimated by changing the pump currents set-point and observing the simultaneous change in f_{rep} and f_{CEO}:

$$v_{fix} = f_{rep} \cdot \frac{df_{CEO}/dP}{df_{rep}/dP} = f_{rep} \cdot \frac{df_{CEO,P}}{df_{rep,P}} = f_{rep} \cdot n_{fix,P} \approx v_c \qquad (2.6)$$

Hereby the fixed point frequency often lies within the range of the laser's carrier frequency ($\approx$192 THz for Erbium fiber comb lasers). Around this point, pump power variations lead to a fluctuation between group and phase delay in the laser cavity, while the phase delay is constant.

In a more detailed level, pump power variations effect the energy, the spectral width, carrier frequency and the peak power of the intra-cavity pulse. The resulting change in the pump power dependent repetition rate and CEO frequency is extensively described in [24, 32] leading to equation (2.7) and (2.8):

$$\left(\frac{df_{rep}}{dP}\right) = -f_{rep}^2 \left[\beta_2 \frac{d\omega_C}{dP} + \omega_{rms}\beta_3 \frac{d\omega_{rms}}{dP} + \Omega_g^{-1}\frac{dg}{dP} + \frac{\delta}{\omega_c}\frac{dA^2}{dP}\right] \qquad (2.7)$$

Hereby the first term from equation (2.7) illustrates the pump induced carrier shift ($\omega_c=2\pi\nu_c$) coupled to net cavity dispersion β_2. The second term presents the interaction of the net third order dispersion β_3 associated with changes in the spectral width ω_{rms}. In the third term the resonant contribution of pump induced gain g fluctuations are considered, where Ω_g is the bandwidth of the Lorentzian like gain function. The last term introduces the self-steepening contribution from the lumped fiber nonlinearity δ and the amplitude A of the electric field envelope.

$$\frac{df_{CEO}}{dP} = \frac{\beta_0}{2\pi}\left(\frac{df_r}{dP}\right) + \frac{f_{rep}}{2\pi}\left(\frac{d\varphi_{spm}}{dP}\right) \qquad (2.8)$$

The equation for pump dependent changes in the CEO frequency is subdivided into two sections. Section one describes shifts in the carrier envelope term, where pump induced changes in the repetition rate are multiplied by the lumped average fiber propagation constant β_0. The other term accounts for the shifts in the carrier phase from pump power induced self-phase modulation φ_{spm}.

However, different perturbations in the laser's cavity have different fixed point values. E.g. changes in the cavity path length mainly influence the repetition rate and so show a fixed point at low frequencies with 1-3 THz. A fixed point near 0 Hz would mean that the group and phase velocity fluctuates by the same amplitude, while their ratio keeps the same [31]. Various noise sources impact the frequency comb performance [33], which are assigned whether to intra or extra cavity noise:

$$S_{vn} = \underbrace{\left(S_{vn}^{length} + S_{vn}^{loss} + S_{vn}^{pump} + S_{vn}^{ASE}\right)}_{\text{intracavity noise}} + \underbrace{\left(S_{vn}^{SC} + S_{vn}^{shot noise} + S_{vn}^{length,ext}\right)}_{\text{extracavity noise}} \qquad (2.9)$$

Hereby $S_{vn}(f)$ represents the frequency noise power spectral density (PSD), which describes the frequency jitter of a comb mode n at an relative offset frequency f ($f = 0$-$f_{rep}/2$). The PSD for phase and frequency noise is discussed in section 2.4. The intra-cavity noise is given by the sum of length fluctuations S_{vn}^{length} [34], loss variation S_{vn}^{loss} [24], pump noise S_{vn}^{pump} [35,36] and quantum noise by amplified spontaneous emission S_{vn}^{ASE} [34,37,38]. Intra-cavity noise contributes to the linewidth of the comb teeth, while extra-cavity shot noise and noise from supercontinuum generation adds amplitude noise to the comb modes. The amplitude noise limits the signal-to-noise ratio (SNR) of the measured comb line frequency. Furthermore, the comb performance can be limited by environmentally induced path length changes. This counts in particular for an optical path, which is not included within the laser feedback chain

for stabilization (out-of-loop). Out of this reason, single branch comb lasers [39] or active stabilization of the path lengths [40] were proposed for applications demanding high stability ($\leq 10^{-18}$) such as in the field of optical atomic clocks or frequency and time transfer. Another approach is to use a multi-branch system [41], showing the same optical path length in each branch, which is damped from mechanical vibrations and temperature controlled.
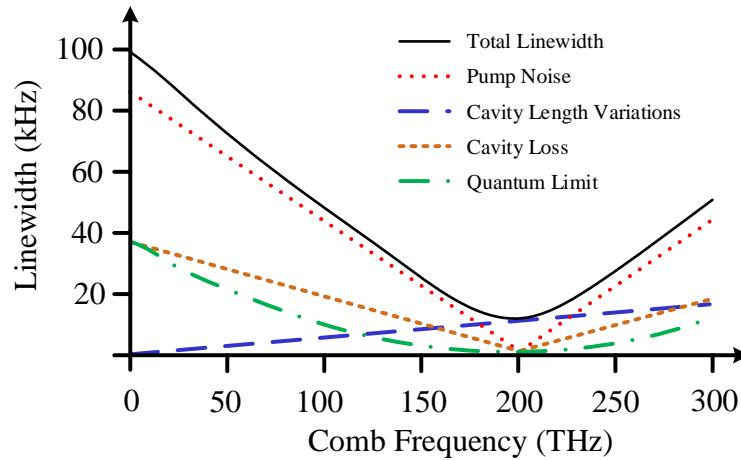
Figure 2-7: Contribution of different perturbations to the linewidth of comb modes for a free running frequency comb laser [24].

Figure 2-7 shows the contribution of the noise sources to the overall comb linewidth with respect to the laser frequency. In this illustration, the f_{CEO} has a linewidth of 100 kHz. The f_{CEO} linewidth of fiber comb lasers depends on its design and lies within a range of 10-1000 kHz. Solid state lasers such as mode locked Ti-Sapphire oscillators reach a free running f_{CEO} linewidth in the sub-kHz range. The comb modes' noise scales quadratic in respect to the fixed point frequency.

$$S_{vn} = \left(v_n - v_{fix} \right)^2 \cdot S_{fix}\left(f \right) \tag{2.10}$$

The impact of perturbations on the frequency noise of a comb mode near 266 THz is exemplary shown in Figure 2-8. In combination with Figure 2-7 this presents a good picture on the magnitude and frequency characteristics of the various noise sources and how they do impact the comb's performance. In terms of frequency characteristics the environmental noise dominates below 500 Hz from the mode's central frequency. Pump noise has the highest contribution from 500 Hz to about 50 kHz. From 50-500 kHz the noise is dominated by quantum-limited noise.
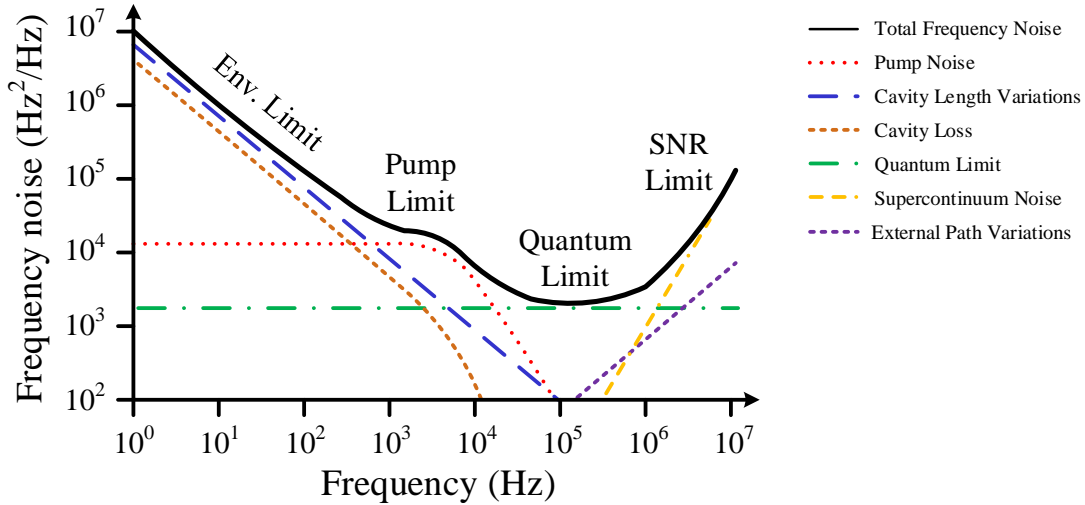
Figure 2-8: Contribution of different perturbations to the frequency noise spectra of a comb mode at 266 THz [24].

The frequency noise introduced by pump power intensity noise shows a low pass frequency response function. In this context, the pump's relative intensity noise $S_{RINpump}(f)$ is converted within the oscillator to frequency noise given by:

$$S_r^{Pump}(f) = B \frac{1}{1+\left(f/f_{3dB}\right)^2} S_{RINpump}(f) \qquad (2.11)$$

Where the constant $B=(Pdf_{rep}/f_{rep}dP)^2$ represents the coupling efficiency from intensity to frequency noise. The -3 dB bandwidth f_{-3dB}, which is in the range of 1-30 kHz for fiber lasers, depends on the laser oscillator's gain dynamics as well as on the net cavity dispersion. The equation for cavity loss variations is similar to that from pump noise, which leads to:

$$S_r^{loss}(f) = B \frac{1}{1+\left(f+f_{3dB}\right)^2} S_{loss}(f) \qquad (2.12)$$

The fixed point frequency is near the carrier frequency, when concerning pump-induced loss. However, this could dramatically change considering other loss mechanisms introduced via environmental perturbations. Hereby the PSD for $S_{loss}(f)$ decreases by $1/f$.

Length changes in the cavity are caused due to mechanical and acoustic vibrations and temperature fluctuations. Hereby the frequency noise for length changes decreases with 1/f and is given by:

$$S_r^{length}(f) = \left(\frac{f_{rep}}{v_{group}^L}\right)^2 S_{length}(f) \qquad (2.13)$$

Such as for every pulsed laser the quantum limit is determined by amplified spontaneous emission (ASE) noise. The ASE leads to noise in the pulse energy, carrier phase, frequency and timing [38,42,37,34]. Hereby the ASE noise contributes to the phase jitter and timing jitter of the laser pulses. The timing jitter's contributes to the linewidth, which has its vicinity at the laser's fixed point. The phase noise contribution adds to all modes and results from the Schawlow-Townes Limit [43, 34].

2.4 Frequency and Time Characterization of Oscillators

The performance of a frequency comb is characterized by the phase noise $S_\phi(f)$ and frequency stability of f_{CEO} and f_{rep}. Frequency stability measurements depict the long-term stability of a frequency comb in the temporal domain. On the other side, phase noise measurements of f_{rep} and f_{CEO} show the comb limitation in the frequency domain. Nevertheless, the phase noise measurement is also used to predict the comb's performance in the short-term time scale [44]. The repetition rate and the CEO frequency is detected with a photodetector. Hereby the sinusoidal oscillations of the photodetector voltage is given as [45]:

$$V(t) = V_0 + \varepsilon(t)\sin\left(2\pi v_C t + \phi(t)\right) \tag{2.14}$$

With V_0 = peak voltage, $\varepsilon(t)$ = temporal amplitude fluctuations, v_c = carrier frequency and $\phi(t)$ = temporal phase fluctuations.

Hereby, the amplitude fluctuations do not contribute to the frequency stability of the oscillator. The instantaneous frequency at a specific time is the sum of the carrier frequency and the derivative of the total phase:

$$v(t) = v_c + \frac{1}{2\pi}\frac{d\phi}{dt} \tag{2.15}$$

The fractional frequency stability $y(t)$ is then:

$$y(t) = \frac{\Delta f}{f} = \frac{v(t) - v_c}{v_c} = \frac{1}{2\pi v_0}\frac{d\phi}{dt} \tag{2.16}$$

The phase noise is defined as the power spectral density (PSD) of the phase fluctuations $\phi_{rms}^2(f)$ within a certain Fourier frequency band. Hereby $\phi_{rms}^2(f)$ results from the Fourier transform of the autocorrelation function of $\phi(t)$ in an equivalent noise bandwidth (EN-BW).

$$S_\phi(f) = \phi_{rms}^2(f)\frac{1}{BW} = 2 \cdot \frac{\left|F\left\{\phi(t)\right\}\right|^2}{BW}; \quad \left[S_\phi(f)\right] = \frac{rad^2}{Hz} \tag{2.17}$$

$S_\phi(f)$ is the PSD of phase fluctuations per 1 Hz bandwidth at a frequency offset f away from the carrier frequency v_c. Phase noise analyzer and spectrum analyzer often measure the double sided PSD of phase fluctuations, which is:

$$\mathrm{L}(f) \equiv \frac{10 \log_{10} S_\phi(f)}{2}; \quad \left[\mathrm{L}(f)\right] = \frac{dBc}{Hz} \tag{2.18}$$

The units dBc/Hz (dBc: **dec**i**b**els relative to the **c**arrier) describes ratio of the power of phase fluctuations in one sideband to the total signal power in the carrier signal for 1 Hz bandwidth. Instead of phase noise, also the term of frequency noise within frequency comb and laser specifications is used. The frequency noise is directly related to the phase noise as:

$$S_v(f) = f^2 \cdot S_\phi(f); \quad \left[S_v(f)\right] = \frac{Hz}{Hz^2} \tag{2.19}$$

Another parameter to specify oscillators is the integrated phase noise. Often it is difficult to compare different comb lasers by the value of the integrated phase noise, since the phase noise is integrated over a different frequency area. A true specification would be here to integrate the phase noise up to the Nyquist frequency, which would be $f_{rep}/2$. The integrated phase noise is given by:

$$\phi_{jitter} = \sqrt{\int_{f_2}^{f_1} S_\phi(f) df}; \quad [rad] = \phi_{jitter} \tag{2.20}$$

Further the timing jitter, which in this thesis describes the pulse-to-pulse timing jitter, is estimated from the integrated phase noise as

$$\tau_{rms} = \frac{\phi_{jitter}}{2\pi v_C}; \quad [\tau_{rms}] = s \tag{2.21}$$

We use the phase noise $S_\phi(f)$ to quantify the combs in the frequency domain within a frequency range of 1 Hz up to $f_{rep}/2$ (~40 MHz) or a time scale from microseconds to one second. For longer timescales the frequency stability is measured via phase sensitive frequency counters. A frequency counter measures the number of zero crossings of the oscillations within a specific gate time τ_{gate} (1 s in this thesis). Optionally, the absolute phase at the end of the gate time is also estimated. By this information, the (averaged) frequency $\overline{y}$ is determined. This measurement is repeated, whereby the counter shall be dead time free, meaning that no time gap during the measurements occurs. An Allan deviation algorithm is applied to the frequency measurements to evaluate the oscillator's stability over time and to quantify specific behavior such as noise types or perturbations. The standard Allan (see equation

(2.22)) deviation takes the difference of measured frequency values in a time interval of τ and generates an averaged value for each τ [45]:

$$\sigma_y(\tau) = \sqrt{\frac{1}{2(M-1)} \sum_{i=1}^{M-1} \left(\bar{y}_{i+1} - \bar{y}_i\right)^2}$$ (2.22)

With $\tau = \tau_{gate} \cdot m$, $M = t_{total}/\tau$ and t_{total}=total measurement time. The overlapping Allan deviation is preferred over the standard Allan deviation since it takes all measurement values into account to generate a result. The overlapping Allan deviation is given as:

$$\sigma_y(\tau) = \sqrt{\frac{1}{2m^2(M-2m+1)} \sum_{j=1}^{M-2m+1} \left\{ \sum_{i=j}^{j+m-1} \left[\bar{y}_{i+m} - \bar{y}_i\right] \right\}^2}$$ (2.23)

An overview on the different Allan deviations is found in the handbook of frequency stability analysis of W.J. Riley [46], whereas counters and their field of application are studied in [47,48,49].

In this thesis the linewidth of the free running lasers is defined as the full width of the half maximum (FWHM) of the Lorentzian shaped peak function. Whereas a phase or frequency noise measurement compromises the full information of the laser line shape, a rough evaluation of the laser's performance is derived by its linewidth. In [50] the laser line shape as a function of frequency noise is studied assuming Lorentzian like peak forms. Hereby the β-separation line is introduced which is:

$$S_v(f) = 8\ln(2)f / \pi^2$$ (2.24)

Hereby frequency noise above the β-separation line contributes to the laser's linewidth where frequency noise below the β-separation line (higher frequencies) rather adds noise to the wings of the laser line. Figure 2-9 shows the β-separation line (red) and the frequency noise spectrum of a laser beat (blue). Please note that the Lorentzian peak is not in scale with the frequency noise spectrum, since it is illustrated for explanation purpose only. The frequency noise shows an intersection with the β-line at about 20 kHz. This means if the noise below this frequency could be suppressed via a feedback loop, a coherent phase stabilization would be achieved with a delta peak (green line). Subsequently the β-line helps to determine the feedback bandwidth (here > 20 kHz) which is necessary to obtain a coherent phase lock with a sub-radian integrated phase noise level. However, also a coherent peak with an integrated noise of some radians can be reached with a slightly smaller locking bandwidth [51].
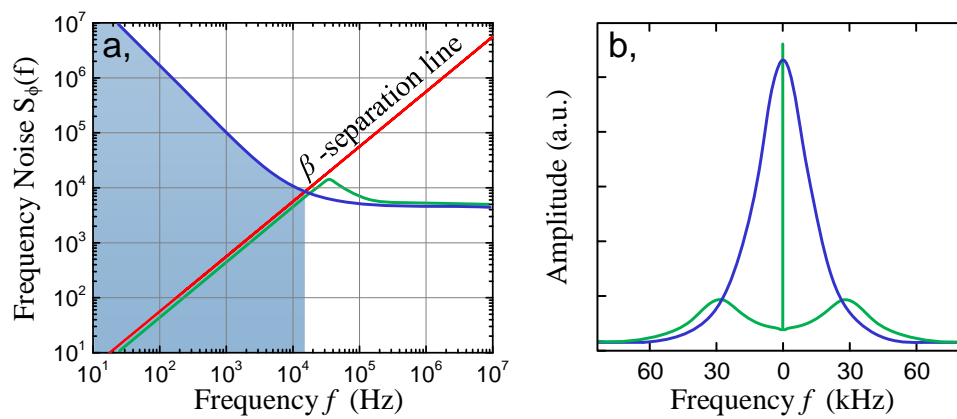
Figure 2-9: Frequency noise spectrum for a Lorentzian line shape (blue line) as well as frequency noise spectrum of a stabilized oscillator, with a noise level below the β-separation line resulting in a coherent peak.

2.5 Erbium Fiber Femtosecond Laser
2.5.1 Pulse Generation in Fiber Lasers

Frequency combs based on compact and reliable mode-locked Erbium fiber lasers reach nowadays highest stability ($< 10^{-17}$ @ $\tau = 1$ s) and low phase noise levels (< 100 mrad), which are comparable to bulky Titan Sapphire solid state lasers. In combination with nonlinear optical interfaces a wavelength range of 400 – 2200 nm is covered, reaching mostly all clock laser wavelength of interest.

In Figure 2-10 the ground level state of Erbium doped fibers is excited at a wavelength of 980 nm or 1480 nm (resonant pumping). Pump diodes at 976 nm are widely employed for Erbium doped lasers, since they also are used for Ytterbium fibers and are available as a space qualified model. The emission wavelength of Erbium covers a wavelength range of about 1.5 µm to 1.58 µm, with a maximum emission peak at 1530 nm.
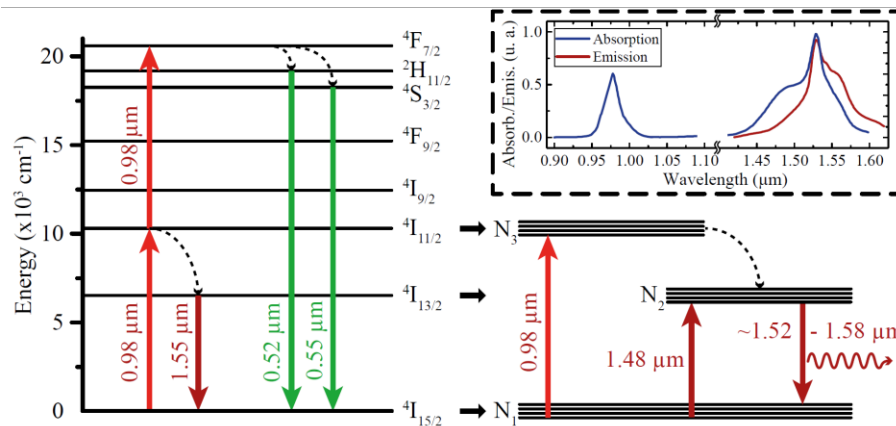
Figure 2-10: Transition states as well as absorption and emission spectrum of an Erbium doped fiber [52].

Femtosecond pulses in fiber lasers are generated via passive mode-locking, which is realized by the nonlinear polarization rotation method (NPR) [53,54], a nonlinear amplifying/optical loop mirror (NALM/NOLM) [55] or via saturable absorption [56]. The NPR technique is not suitable for applications outside of the laboratory since it is highly sensitive to environmental fluctuations. NALM/NOLM lasers on the other side were not considered, because they are very delicate to develop.

In this thesis, lasers based on saturable absorbers were developed and studied. Lasers with a saturable absorber are "relatively" easy to build, scalable in their repetition rate and were already demonstrated in "out-of-laboratory" [1] and space-borne operation [57].

Saturable absorbers are employed in a ring cavity or linear cavity design (see Figure 2-11). The ring cavity consists of the absorber (here: CNT-single walled carbon nanotube), an Erbium doped fiber and a hybrid isolator wavelength division multiplexer (IWDM) with a tap

port to couple out a part of the laser pulse. A WDM combines two different wavelengths to a common port, which is here the pump wavelength (980 nm) and the laser's wavelength (1560 nm). The isolator in the ring cavity allows that the pulse propagates only into clockwise direction.
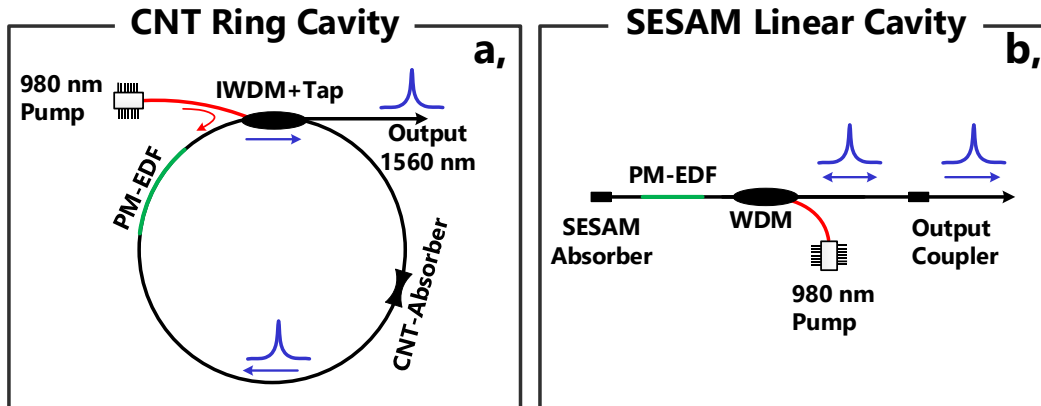
Figure 2-11: Ring and linear cavity of a mode-locked fiber laser with a carbon nanotube and a semiconductor saturable absorber for femtosecond pulse generation, respectively..

In the linear cavity the pulse propagates back and forth between a partial reflective mirror and a reflective absorber (here: SESAM-semiconductor saturable absorber mirror [58]), where a part of the pulse is coupled out at the mirror. The repetition rate of a ring cavity f_{repr} and a linear cavity f_{repl} is given by the cavity length, speed of light and the effective refractive index of the fiber:

$$ f_{repr} = \frac{c}{n \cdot L} \qquad f_{repl} = \frac{c}{n \cdot 2L} \tag{2.25} $$

The transmission (or reflection) of a saturable absorber depends on the intensity of its incident light. This means that the transmission increases towards higher light intensities. A laser shows at the startup a continuous wave (cw) like behavior. However, due to the absorber's properties a spike in the intra-cavity's light intensity is less attenuated compared to the rest of the cw light. Consequently the cavity mode of this spike has a higher gain with respect to the cw light and is amplified by the active fiber. Within some roundtrips other cavity modes next to this cavity modes oscillate with a fixed (mode-locked) temporal phase to each other building up a short pulse such as illustrated in Figure 2-12.
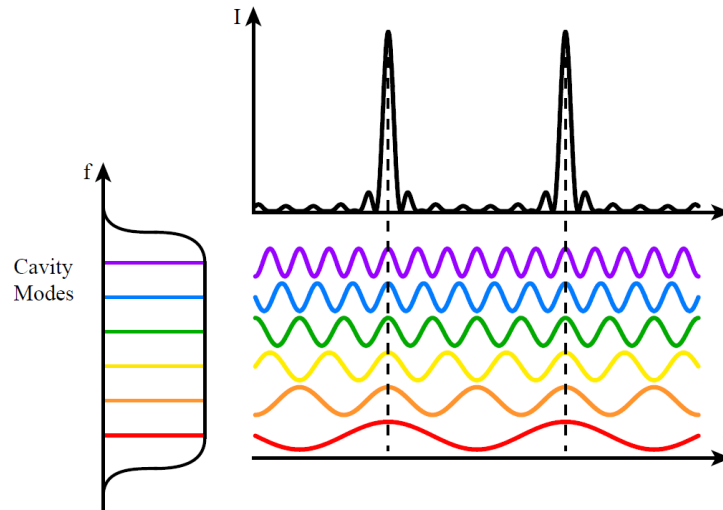
Figure 2-12: Scheme of the superposition of six phase locked cavity modes resulting in a short pulse [59].

The oscillators in this thesis produced soliton pulses using either SESAMs or carbon nanotubes (CNT) as absorbers. The soliton pulse is described in the temporal (and spectral) domain by a sekans-hyberbolicus function:

$$P(t) = \frac{P_p}{\cosh^2(t/\tau)} \tag{2.26}$$

Where the FWHM of the sech-pulse length is defined as $\tau_0 = \tau\ 1.76$. Hereby the soliton pulse with a pulse energy E_p maintains its temporal and spectral shape when following condition is given.

$$E_p = \frac{2\beta_2}{\gamma\tau} \tag{2.27}$$

Soliton pulses are formed in the presence of anormal dispersion ($\beta_2 < 0$). Dispersion only leads to a temporal broadening of the pulse along the propagation axis. However, self-phase modulation, represented by the nonlinear coefficient γ, counteracts this temporal broadening: As consequence the pulse maintains its pulse duration for a proper balance in dispersion and nonlinearity [60]. When the pulse energy is higher than E_p, higher order solitons are produced. The nonlinear coefficient is calculated from the intensity dependent nonlinear refractive index n_2 ($\approx 2.6 \cdot 10^{-20}\ \text{m}^2/\text{W}$ for a standard SMF28 fiber), the effective area of the light's mode field diameter A_{eff} and the angular frequency ω_0 ($= v_c \cdot 2\pi$) as:

$$\gamma = \frac{n_2\omega_0}{cA_{eff}} \tag{2.28}$$

The spectral width $\varDelta\lambda$ of soliton laser pulses is technically limited to about 20 nm by the relaxation time of the saturable absorber [61, 62] and the fiber dispersion. The pulse duration of a transform limited soliton pulse is estimated by the spectral bandwidth via the time-bandwidth product as:

$$\Delta\lambda \cdot \tau_0 = 0.315 \tag{2.29}$$

A low intensity noise pump diode paired with a low noise current helps to reduce the femtosecond laser's phase noise. The phase noise of a femtosecond oscillator depends on three important design criteria. On the one side, the oscillator's net dispersion shall be as low as possible, as the noise of the oscillator is converted into timing jitter via dispersion as it is described by the Gordon-Haus jitter [63, 42]. Further, the intra cavity pulses shall be as short as possible (↑spectral width) as the quantum-limited timing jitter PSD scales proportional to the pulse duration squared. A high pulse energy helps to reduce the contribution of the shot noise [64, 61, 34].

2.5.2 Carbon Nanotube and SESAM Absorbers

A scheme of a SESAM based absorber and a tapered fiber carbon nanotube absorber is illustrated in Figure 2-13. In the case of the SESAM, a semiconductor absorber (one or several layers of InGaAs quantum well(s)) is embedded on a Bragg mirror structure. Details on the structure of SESAM absorbers can be found here [58]. The tf-CNT absorber is built from a tapered fiber, which is covered by a carbon nanotube polymer composite. Due to the tapered design the carbon nanotubes interact with the evanescent field of the laser pulses within the fiber. This means only a part of the light is interacting with the CNTs, which makes the CNT absorber more resistant against laser light induced damage.

Figure 2-13: Scheme of (a) a SESAM absorber and (b) a tapered fiber carbon nanotube absorber.

SESAM absorbers show a relaxation time in picosecond domain, while CNTs have a relaxation time in the sub-fs level. Due to the relative long relaxation time of SESAM absorbers it is difficult to realize stable laser oscillators with a low cavity net dispersion [62]. On the

other hand (dispersion managed) stretched-pulsed lasers [65] with a near zero net cavity dispersion were demonstrated employing CNTs as absorbers leading to sub 100 fs pulses. Dispersion managed lasers have the lowest free running phase noise compared to other femtosecond lasers showing pulse shaping mechanisms types such as similariton, soliton or all normal dispersion propagation.

Saturable absorbers are specified by parameters as non-saturable losses ($\Delta R_{ns}/\Delta T_{ns}$), saturation fluence F_{sat}, modulation depth ($\Delta R, \Delta T$) and spectral transmission/reflection ($R(\lambda),T(\lambda)$). In Figure 2-14 a, the reflectivity of a SESAM absorber as function of the pulse's fluence is illustrated. The fluence F is the pulse energy divided trough the absorber's illuminated spot-size area:

$$F = \frac{P_{avg}}{f_{rep} \cdot A_{spot}} \tag{2.30}$$

The modulation depth is the maximum change in reflection (or transmission) of absorber, where the saturation fluence marks the fluence causing a change in 36.8% (e^{-1}) of the modulation depth. Mode-locked lasers are operated at a fluence of about 2-5 times of the saturation fluence. Single walled carbon nanotubes have a broadband spectral absorption (see Figure 2-14 b,) and are employed in pulsed lasers operating from 1 µm to 2 µm. In Figure 2-14 b, the SESAM has a local minimum at 1560 nm with a reflectivity of 55%, which increases to 80% when the absorber is fully saturated.
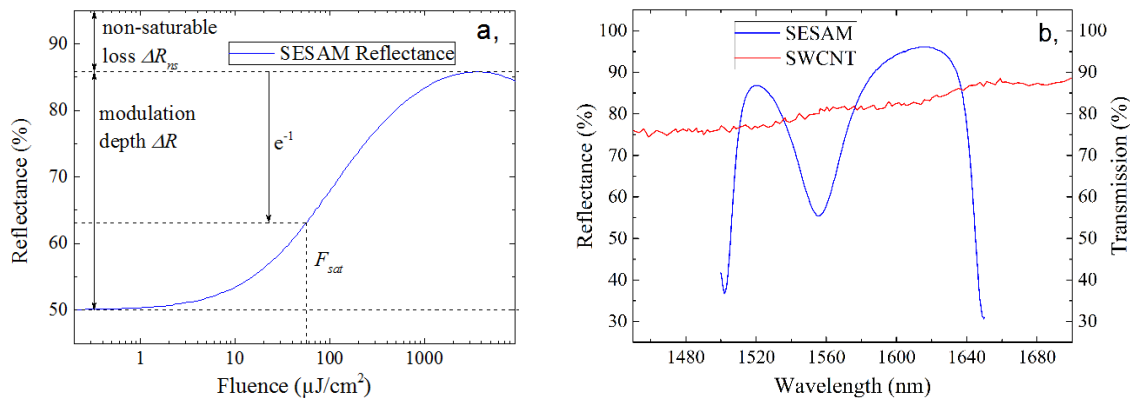
Figure 2-14: (a,) a SESAM's reflectance as function of the incident pulse fluence [66] as well as (b,) the reflection/transmission of a carbon nanotube and SESAM absorber [67].

2.6 Pulse Propagation in Optical Fibers

Simulations on the amplification of pulses, in-fiber pulse compression as well as on super-continuum generation were carried out. On the one hand these simulations helped to determine suitable fibers showing appropriate parameters such as gain, nonlinearity, dispersion. On the other side system parameters such as fiber length, pump power, pulse length and output power were estimated to design the optical interfaces properly.

The propagation of pulses in optical fibers is described via the nonlinear Schrödinger equation (NLSE). Since a commercial split-step solver [68] (Fiberdesk-Software) for the NLSW was used, just a brief overview of the pulse propagation in fiber is given. The NLSE depicts how a temporal short pulse with the amplitude *A* evolves over certain propagation distance *z* [69]:

$$\frac{\partial A}{\partial z} = \underbrace{\frac{g-\alpha}{2}A}_{gain/loss} + \underbrace{\sum_{n\geq 2}\beta_n \frac{i^{n+1}}{n!}\frac{\partial^n}{\partial t^n}A}_{dispersion} - \underbrace{i\gamma \cdot \left(1+\frac{i}{\omega_0}\frac{\partial}{\partial t}\right)\left(A(t)\int_{-\infty}^{\infty}R(\tau)\left|A(t-\tau_{RM})\right|^2 d\tau\right)}_{nonlinearity} \qquad (2.31)$$

The NLSE is subdivided into three sections representing gain/loss, dispersion and nonlinearity acting on the laser pulse. The gain coefficient *g* is derived from the rate equation for Erbium doped amplifiers [70]. Dispersion plays an important role for the pulse formation process in optical fibers. The second order dispersion[2] was measured by a home build white light interferometer based on a Michelson interferometer [71]. By means of this setup the dispersion of Erbium fibers with a short length and high absorption (up to 100 dB/m @1530 nm) was estimated. In Figure 2-15 the dispersion of a standard PM fiber (PM 15-U25D), two different Erbium fibers (IXF-EDF-FGL-PM-S013, OFS EDF50-PM) and a highly nonlinear fiber HNF (Sumitomo PM) is depicted. Each of this fiber type was integrated within the frequency comb lasers. Higher order dispersion coefficients were derived by fitting a Taylor series function to the second order dispersion data [73]:

$$\beta_2(\omega) = \beta_2 + \beta_3(\omega-\omega_0) + \frac{1}{2}\beta_4(\omega-\omega_0)^2 + \frac{1}{6}\beta_5(\omega-\omega_0)^3 ... \qquad (2.32)$$

Where the Taylor series is developed around the angular frequency ω_0. In particular the dispersion of HNF fibers needs to be known within a wide wavelength range of about 900 nm to 2200 nm. The use of dispersion coefficient up to the 6th order helps to portray the dispersion precisely in this wavelength range. In Figure 2-15 the HNF dispersion was estimated in a narrow wavelength area, but sufficient to determine the HNF's zero dispersion wavelength (ZDW) at 1492 nm, which indicates how far the SC's dispersive pulse can be shifted towards

---

[2] The zero (phase velocity) and first order (group velocity) dispersion are not relevant for our simulations.

lower wavelength values. In general the dispersive wave pulse shifts towards shorter wavelength values when the ZDW decreases [72].
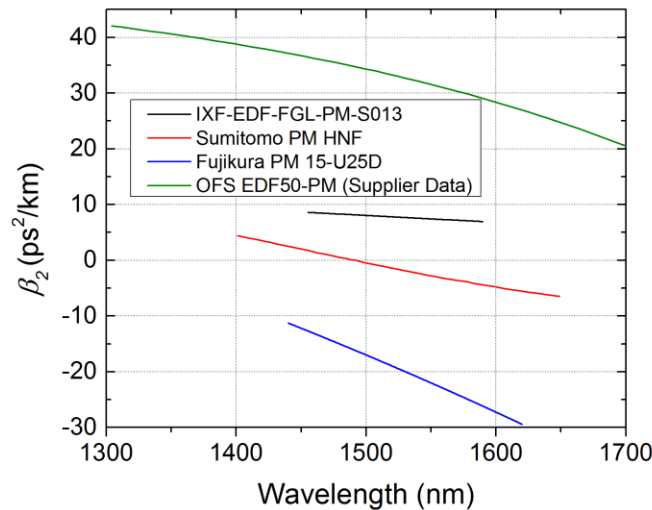
Figure 2-15: Dispersion curves for two different Erbium doped fibers (green and black line), a standard PM fiber (blue line) and a highly nonlinear fiber (red line).

Optical fiber manufacturer in the telecommunication branch define the dispersion as [73]:

$$D(\lambda) = \frac{S_0}{4}\left[\lambda - \frac{\lambda_0^4}{\lambda^3}\right]; \qquad \left[D(\lambda)\right] = \frac{ps}{nm \cdot km} \qquad (2.33)$$

Where S_0 ($dD/d\lambda$) is the dispersion slope and λ_0 is the zero dispersion wavelength. The dispersion and dispersion slope relates to the physical unit of dispersion as [73]:

$$D = -\frac{2\pi c}{\lambda^2}\beta_2 \quad ; \quad S = -\frac{2\omega^3}{(2\pi c)^2}\beta_2 + \frac{\omega^4}{(2\pi c)^2}\beta_3 \qquad (2.34)$$

The last section of the NLSE considers nonlinear effects such as self-phase modulation [74], self-steepening, Raman scattering [75] and four wave mixing [76]. Self-phase modulation leads to an intensity dependent phase velocity given by the intensity dependent (Kerr-Effect) nonlinear refractive index n_2. Phase modulation influences the spectral domain by shifting and/or generating of frequency components around the carrier frequency. Self-steepening also originates from the Kerr effect, which leads to an intensity dependent group velocity. This results in an asymmetric balanced spectrum and pulse shape. Due to Raman induced inelastic scattering, the pulse loses energy (Δv_{max}=13.5 THz) and so shifts towards higher wavelength values, where the response time τ_{RM} is taken from [75]. Four wave mixing occurs within HNF fibers, whereas new frequencies are generated around the fiber's zero dispersion wavelength.

A pulse duration in the sub 100 fs domain and a pulse energy of some nJs was required to achieve a SC for *f-2f* interferometry. However, the pulses from the femtosecond oscillators were a few 100 fs long and had an energy of about 12 pJ. Due to this reason the pulses were amplified and spectrally broadened in normal dispersive Erbium doped fiber amplifiers. Erbium doped fibers with anormal dispersion are not suited for this purpose, since the pulse breaks up into multiple solitons during amplification.

If the Erbium amplifier shows a proper balance between gain, dispersion and nonlinearity a parabolic (self-similar) pulse evolves during the amplification process [77]. For the following condition the input pulse converges fastest from a sech- to a parabolic pulse [78].

$$U_{in} = \frac{2\tau_0^3 g^2}{27\gamma\beta_2} \tag{2.35}$$

Where U_{in} is the energy of the input pulses. In Figure 2-16 the simulation results of the temporal and spectral pulse evolving in a 3.5 m long Erbium fiber (OFS EDF50-PM, 50 dB/m gain at 1530 nm) are shown.
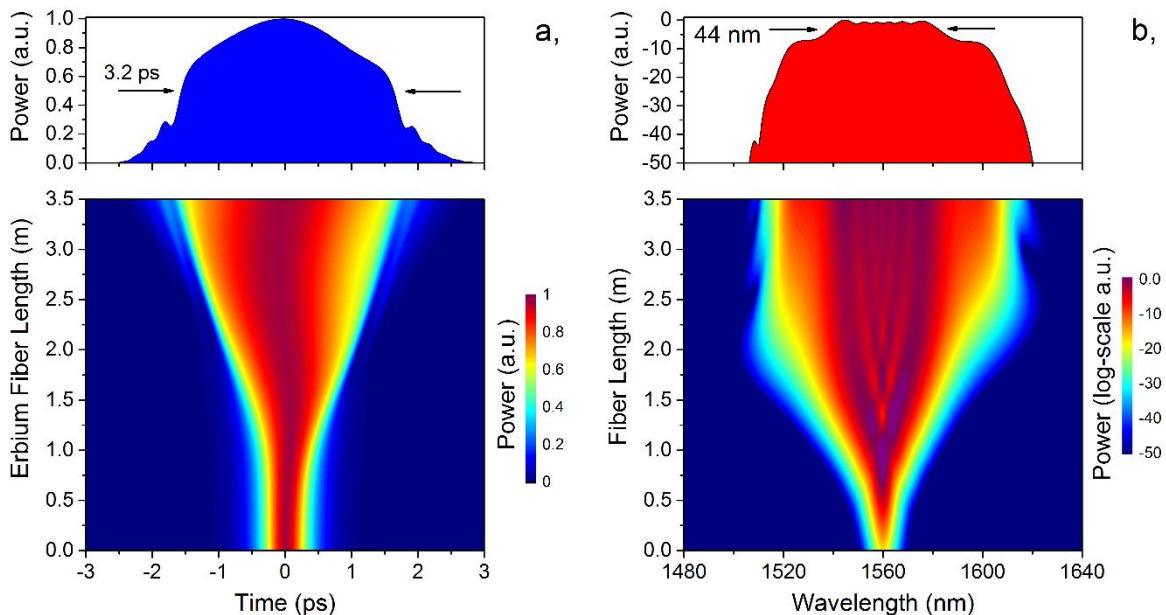
Figure 2-16: Temporal a, and spectral b, pulse propagation in a 3.5 m long Erbium fiber amplifier.

The EDF was pumped with a power of 700 mW from each side. A 400 fs sech pulse with an average power of 500 µW and a repetition rate of 80 MHz is injected into the fiber. The spectral width increases from initially 6.5 nm to 44 nm. Farther the 3.2 ps long output pulses have a linear chirp in the central region enabling a near bandwidth limiting pulse compression down to the sub 100 fs region [79]. The output pulses show an average power of 280 mW and so have an energy of 3.5 nJ, sufficient for supercontinuum generation.

3   Setup of Oscillators and Optical Interfaces

3.1   All in Fiber Femtosecond Laser Oscillators

Figure 3-1 shows the three in-fiber femtosecond oscillators, which were studied in this work. The PM SESAM EOM prototype oscillator (Figure 3-1 a,) was developed by Toptica Photonics and the tapered-fiber carbon nanotube opto-optical modulator (tf-CNT OOM) laser (Figure 3-1 b,) was realized by Professor Khanh Kieu (College of Optics, Arizona, USA). The PM tf-CNT EOM laser (Figure 3-1 c,) was built together with Professor Khanh Kieu and the author of this thesis.
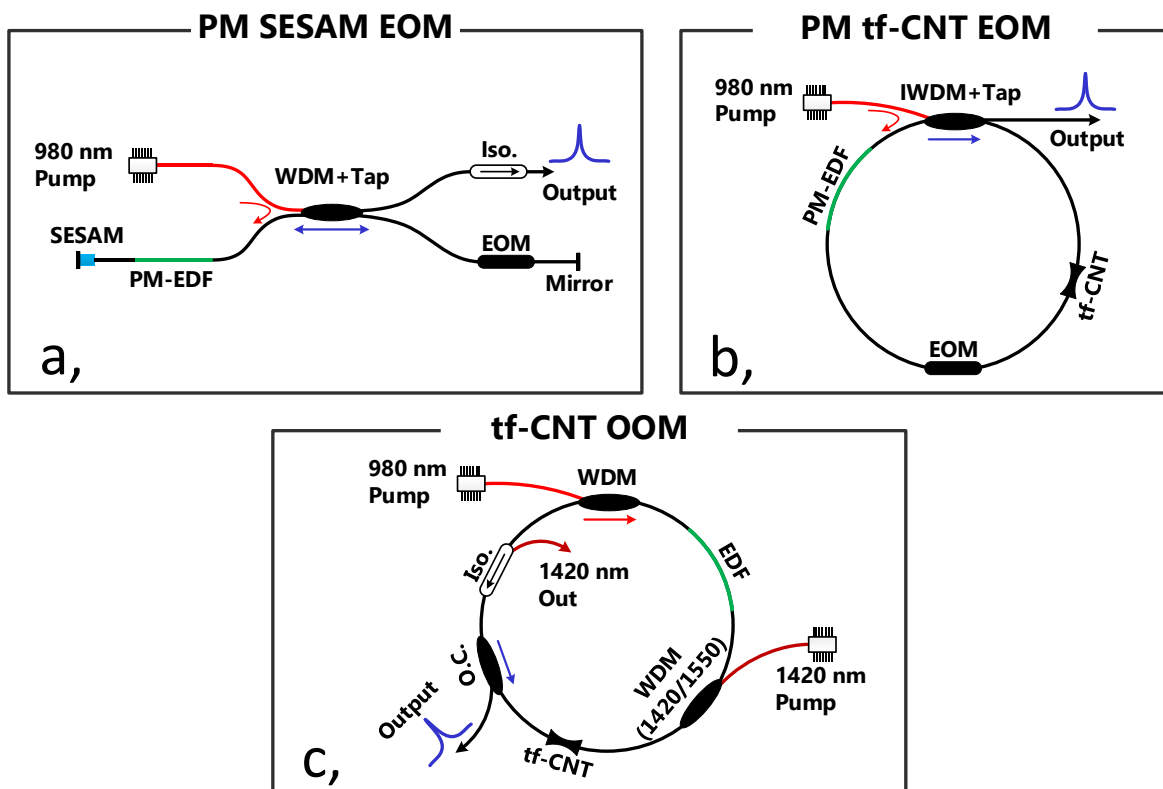
Figure 3-1: Femtosecond laser oscillator prototypes based whether on a SESAM or tf-CNT as saturable absorber.

Blue arrows indicate the direction of the pulse propagation. Red arrows indicate the direction of the pump laser light. WDM, wavelength division multiplexing coupler; WDM+Tap, WDM with tap output coupler: IWDM, WDM with integrated isolator; PM-EDF, polarization maintaining Erbium doped fiber; SAM, saturable absorber mirror; EOM, electro-optic phase modulator, O. C., optical coupler; Iso., optical isolator; tf-CNT, tapered fiber carbon nanotube absorber.

The CNT based oscillators promise a lower level of free running noise compared to the SESAM based laser due to the sub-ps relaxation time of the CNT absorber. Non-polarization maintaining tf-CNT femtosecond lasers with low timing jitter and a sub 100 kHz f_{CEO} linewidth [80] were demonstrated in literature. This suggests that femtosecond lasers based

on tf-CNT absorbers have a high potential to outperform conventional SESAM based comb oscillators.

Oscillator a, and b, were both equipped with a waveguide EOM for high bandwidth comb stabilization. The optical insertion loss of the EOM was about 3 dB resulting in an intra-cavity loss of 75% and 50% per round trip for the SESAM oscillator and tf-CNT laser, re-spectively. Furthermore, the WDMs and the absorbers show additional losses. Hereby the CNT absorber has a non-saturable loss in the range of 40%. Nevertheless, a 80 cm long high gain erbium doped fiber (80 dB/m absorption at 1530 nm) helps to compensate for these losses. About 10% and about 20% of the SESAM and CNT laser intra-cavity light is directed to the output via the tap coupler integrated within the WDM. The output light of these oscil-lators is linear polarized with a polarization extinction ratio better than 20 dB. A long-term stable linear polarized output was achieved due to the utilization of a polarization filter and polarization maintaining components with the oscillator.

The tf-CNT OOM laser (see Figure 3-1) was developed to demonstrate the opto-optical mod-ulator principle applied to a CNT absorber. The oscillator was built from non-PM compo-nents, since standard single mode fiber components are 5-10 times cheaper and non-PM tf-CNT absorbers are well exploited within industrial available lasers. The tf-CNT OOM laser has a ring cavity such as the tf-CNT EOM laser. However, an additional WDM (1420 nm/1560 nm) was integrated to seed light from a FBG stabilized pump diode at 1420 nm into the cavity. With this light the CNT absorber is pre-saturated yielding to a change in the absorber transmission. This in turn leads to a change in the net cavity loss and so into a variation in the CEO frequency and repetition rate. As result the CEO frequency or repetition rate can be controlled by changing the power of the OOM laser at 1420 nm. An isolator and coupler prevents that light at 1420 nm propagates to the active erbium fiber. A seed source with a wavelength of 1420 nm was selected due to availability of commercial of the shelf components. Furthermore, the Erbium fiber shows almost no absorption at this wavelength.

3.2 Optical interface for Optical beat and CEO-beat detection.

A generic setup was established to generate and measure the oscillators' CEO beat as well as an optical beat $f_{opt(633\,nm)}$ between a narrow linewidth HeNe laser and a comb mode. By characterization of f_{CEO} and f_{opt} the free running linewidth as well as the actuators' fixed point frequency and modulation bandwidth were estimated. This is essential information to develop an optimized feedback loop for comb stabilization. Furthermore the optical interfaces were developed to demonstrate the hybrid stabilization of the ring laser gyroscope in section 6.
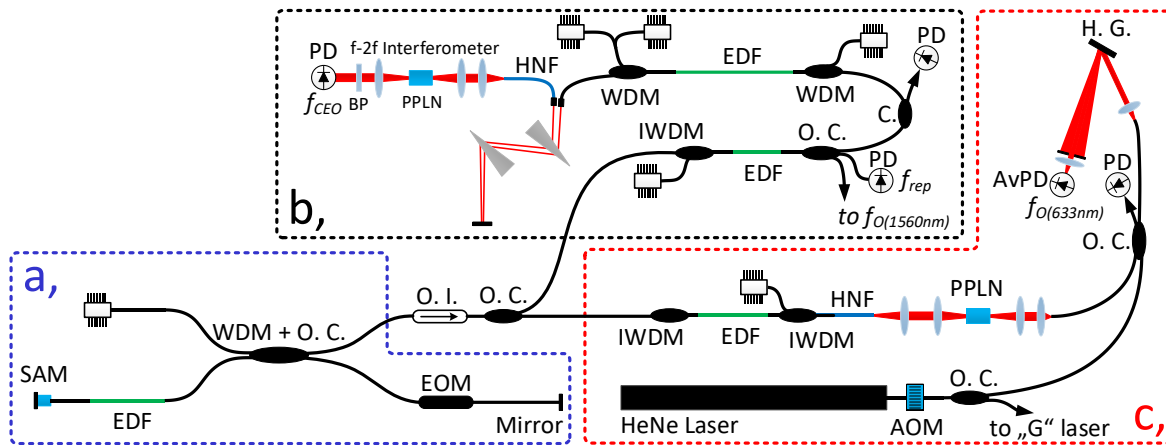
Figure 3-2: Optical setup of the SESAM EOM comb including (a) a femtosecond fiber oscillator, (b) an f-2f interferometer for CEO beat detection and (c) a 633 nm interface for optical beating with a HeNe laser.

WDM, wavelength division multiplexing coupler; IWDM, WDM with integrated isolator; EDF, Erbium doped fiber; SAM, saturable absorber mirror; EOM, electro-optic phase modulator, O. C., optical coupler; O. I., optical isolator; C., optical circulator; BP, band pass filter; HNF, highly nonlinear fiber; PPLN, periodically-poled lithium niobate; H. G., holographic grating; AvPD, avalanche photo diode; PD, pin photo diode; AOM, acousto optic modulator. Black solid lines indicate polarization maintaining single mode fiber.

The setup is subdivided into three modules a, b and c, (see Figure 3-2). The setup was designed so that any of the oscillators from Figure 3-1 could be placed as module a, to perform characterization and stabilization measurements.

In section b, the f_{CEO} beat of the femtosecond laser is detected. Within section c, the comb light is converted to 633 nm to generate an optical beat signal $f_{opt(633\,nm)}$ against the HeNe laser. The optical interfaces b, and c, are discussed in detail within the following sub-sections.

3.2.1 Interface for CEO Beat Detection

The interface for f_{CEO} detection (see Figure 3-2 b,) consists of a self-build pre-amplifier, a commercial module (Toptica FFPro) for supercontinuum generation [29] including a bi-directional parabolic amplifier, prism compressor and HNF as well as a self-build *f-2f* interferometer.

The pre-amplifier was implemented to adjust the chirp and pulse energy of the femtosecond laser pulses for the main amplifier. Without pre-amplification, the pulse energy and chirp was not sufficient to realize a converging parabolic amplification process within the main amplifier. Hereby the normal dispersion of the pre-amplifier ($\beta > 0$) was slightly compensating the pulse negative chirp, introduced by the (anormal dispersive, $\beta < 0$) standard PM fiber. The oscillators' output power was typically below one mW, which was increased to about 10-20 mW within the pre-amplification stage. Hereby only 30% of the output light was used to seed the main amplifier. The other 70% were used for monitoring e.g. measuring of f_{rep} and/or generating an optical beat with a laser at 1560 nm.
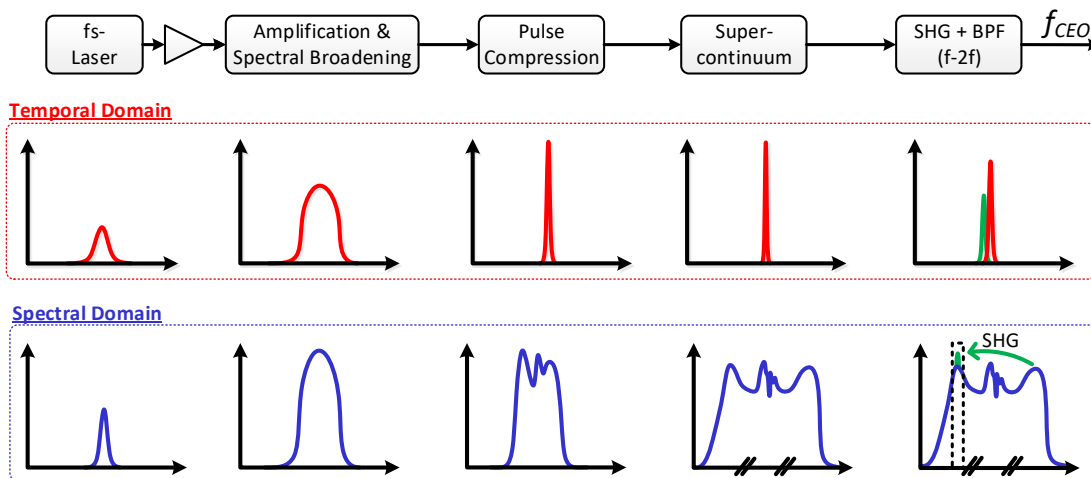
Figure 3-3: Laser pulse manipulation stages to generate a CEO-beat as well as the associated pulse evolution in the temporal and spectral domain.

SHG, second harmonic generation; BPF, optical bandpass filter at 1 µm

The principle of operation for the f_{CEO} interface is depicted in Figure 3-3. The oscillator pulses were fed into the main amplifier, after passing the pre-amplifier. The output power of the amplifier was about 300 mW resulting in a pulse energy of more than 3.7 nJ (for f_{rep}= 80 MHz). This was sufficient pulse energy to generate a supercontinuum in the highly nonlinear fiber. Due to the parabolic amplification, the pulses show no break up and were broadened in the spectral and temporal domain to more than 50 nm and 2 ps, respectively. Afterwards, the pulses are temporally compressed by a Si-prism pair to a pulse duration less

than 70 fs. The free space prism compressor removes the negative linear chirp of the pulses without introducing significant non-linearity in terms of self-phase modulation. A further advantage over in-fiber pulse compression was, that the pulse chirp and pulse length could be controlled by adjusting the amount of Si-class introduced within the free space section. This helped to fine-tune the pulse compression for each femtosecond oscillator individually. A supercontinuum from about 950 nm to 2200 nm was generated within the 10 cm long HNF fiber. For the detection of f_{CEO} a common *f-2f* interferometer was set-up consisting of a 10 mm long PPLN for second harmonic generation (SHG) from 2000 nm to 1000 nm.
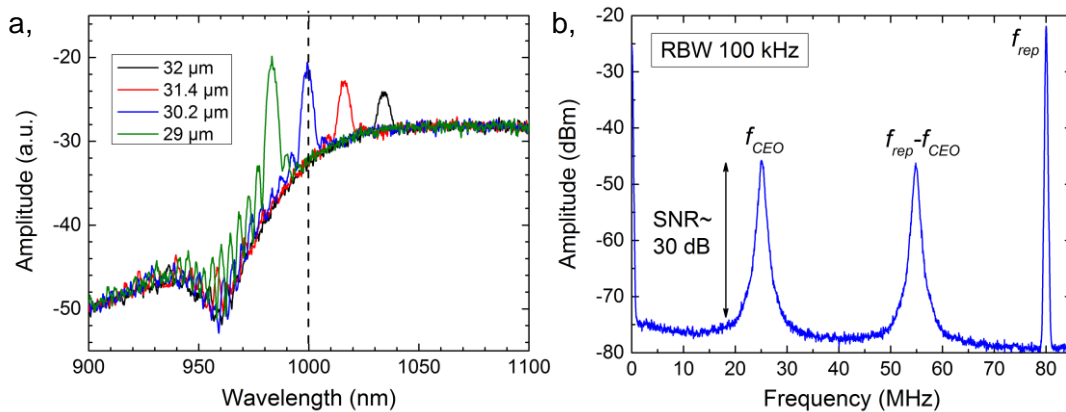
Figure 3-4: a, optical spectrum of the superontinuum and second harmonic signal in wavelength range from 0.9 µm to 1.1 µm and b, frequency spectrum of the measured CEO-beat.

Figure 3-4 a, shows a part of the supercontinuum and SHG for different PPLN gratings. The optical spectra were measured by coupling some light after the PPLN into a multimode fiber, which itself was connected to an optical spectrum analyzer (OSA). An optimum SNR for the f_{CEO} beat was estimated for a PLLN grating with a 30.2 µm period.

The f_{CEO} signal was detected by measuring the bandpass filtered light at 1µm via a Si-PIN diode. In Figure 3-4 b, the electrical frequency spectrum of the f_{CEO} signal for the SESAM EOM is shown. The spectrum was taken with an electrical spectrum analyzer (Rohde&Schwarz, FSU). A SNR of 30 dB for the CEO beat in a 100 kHz resolution band-width was obtained. A SNR of at least 30 dB is required to guarantee a robust, phase slip free comb stabilization.

3.2.2 Interface for Measurements at 633 nm

With this interface the oscillator light at 1560 nm is shifted to 1266 nm with a highly nonlinear fiber and then converted to the HeNe laser wavelength at 633 nm via a second harmonic generation process. The setup for the 633 nm interface is illustrated in Figure 3-2 c,. In detail, a part of the femtosecond oscillator is feed into the self-build backward pumped normal dispersive amplifier [81]. WDMs with integrated isolators were selected for the amplifier to avoid q-switching or other instabilities by blocking light, which potentially could propagate back into the amplifier or oscillator. An output power up to 230 mW was reached, resulting in an overall gain of 28 dB.

The pulses from the amplifier were temporally compressed within a standard PM fiber before entering the HNF. A cut-back method was applied to optimize the fiber length so that the shortest pulses were obtained at a maximum pump power. In this way, short pulses with tens of kilowatt peak power and a pulse energy of more than 2 nJ were generated.
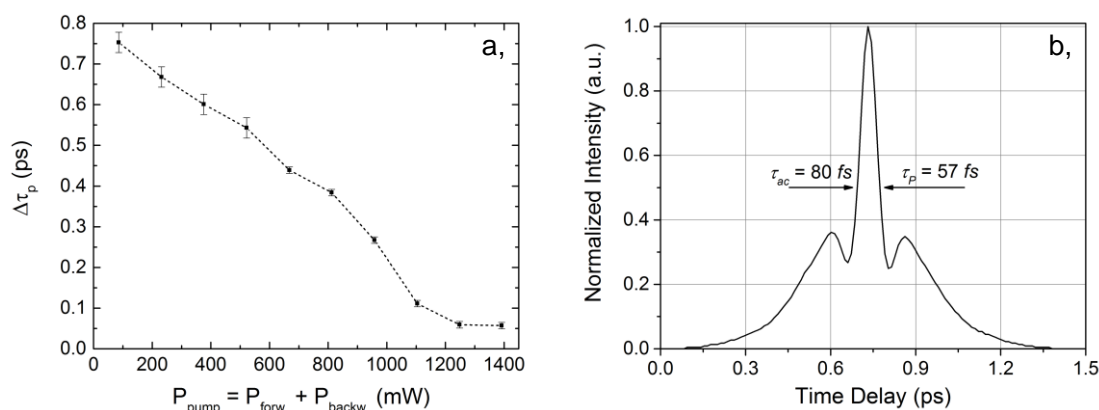
Figure 3-5 a, pulse duration as function of the amplifier's pump power and b, corresponding autocorrelation measurement of the pulse at a pump power of 1300 mW.

The pulse duration as a function of the amplifier's pump power at the standard PM fiber's output is depicted in Figure 3-5 a). The pulse duration was measured with an intensity autocorrelator (APE Mini). A pulse length of approximately 57 fs was reached above a total pump power of 1200 mW. The amplifier was pumped bi-directional with two pump diodes for this measurement. However, similar results were obtained with a backward pumped configuration. Hereby the pump light was not attenuated by optical isolators at 976 nm, which were required for bi-directional pumped setup.

An autocorrelation trace of the pulses at a total pump power of 1300 mW is shown in Figure 3-5 b). A autocorrelation pulse length of 80 fs was estimated resulting in a pulse length of 57 fs for a sech-like pulse. The compressed pulse shows a higher soliton order, which is indicated by the side lobes in the autocorrelation. About 50% of the pulse's energy is located

in the side lobes. A more efficient pulse compression, with more than 80% of the pulse energy within its center is achievable with a prism compressor or a large mode area fiber.

The compressed pulses were injected into an elliptical core HNF to shift the spectrum towards 1266 nm. The dispersive wave pulse at 1266 nm was frequency doubled via a temperature stabilized 10 mm long PPLN to 633 nm. The waist beam diameter in the PPLN was calculated to about 52 µm for an optimum SHG efficiency according to [82].

Figure 3-6 a, shows the spectrum after frequency conversion, whereas a part of the light emerging from the PPLN was coupled into a multi-mode fiber for spectral measurements using an OSA. The "V" shaped section at 1560 nm originates from the HNF's seed pulse. The spectrum of the HNF's dispersive pulse is distinguished by the parabolic shape centered at a wavelength of 1266 nm. The spectrum from the SHG pulse is highlighted as a peak at 633 nm. The pulses at 633 nm reached an average power of about 1 mW in a 0.5 nm bandwidth. The red light from the comb and the HeNe laser (with a power of 40 µW) were superimposed in a fused fiber coupler. To achieve a perfect overlap between the transverse modes of both lasers a fiber-based solution was favored over a free space beam splitter. The optical beat f_{opt} between the HeNe laser and the frequency comb modes was detected by an avalanche photo diode. A beat signal with an SNR of more than 32 dB was achieved such as depicted in Figure 3-6 b).
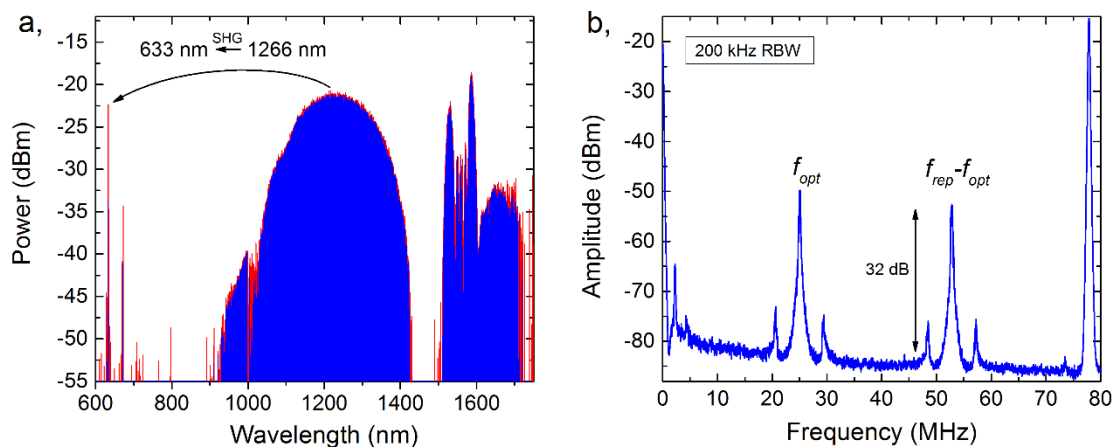
Figure 3-6: a, optical spectrum after frequency conversion to 1266 nm and SHG generation to 633 nm; b, electrical frequency spectrum of optical beat between HeNe laser and a comb mode.

4 Characterization of Femtosecond Oscillators

As described in section 3.1, the femtosecond laser oscillators shall have an all-in-fiber design without mechanical actuators for stabilization to prevent long-term damage to the optical fiber. Thereby, the actuators need to act on the femtosecond oscillator comb mode and/or CEO frequency with a sufficient modulation bandwidth to achieve a phase coherent stabilization. To ensure a phase coherent lock, a narrow CEO frequency and comb tooth (-3 dB) linewidth is required, which shall be well below 1 MHz (or even below 100 kHz).

Furthermore, the femtosecond oscillator shall show a repetition rate of more than 50 MHz in order to extract properly the CEO beat note and the optical beat note with a reference laser from the comb spectrum with RF filters. Another requirement was, that no degradation in the laser's optical output power and spectral bandwidth shall be observed. This is necessary to guarantee reliable and long-term laser operation.

In section 4.1 the oscillators' linewidth at 633 nm and the CEO beat note are characterized and compared against each other. Furthermore, the degradation of the PM tf-CNT absorber is pointed out in section 0. The actuators, which are necessary to stabilize the frequency comb oscillators are studied in detail in in section 4.3.

4.1 Linewidth of Femtosecond Oscillators

The CEO linewidth and the linewidth of a comb mode at a specific frequency gives an indication of the oscillator performance and helps to compare the comb oscillators against each other. Modern femtosecond fiber lasers have a free running CEO linewidth of less than 100 kHz, whereas the linewidth of the comb mode depends on the optical frequency itself.
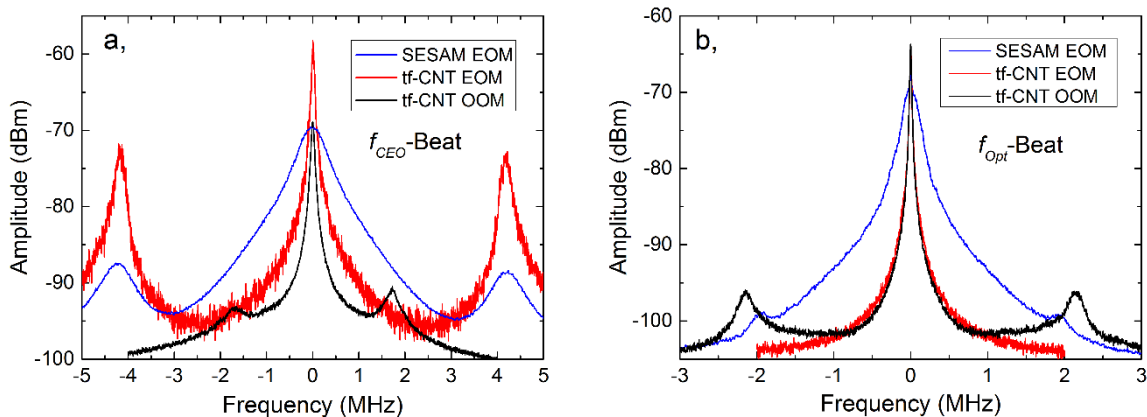
Figure 4-1: Frequency spectrum of a, the CEO beat and b, optical beat of the SESAM EOM, tf-CNT EOM and tf-CNT OOM laser.

Figure 4-1 shows the frequency spectrum of the CEO beat (left) and optical beat note at 633 nm of each femtosecond oscillator. The CEO and optical beats were measured with a spectrum analyzer in a 1 kHz resolution bandwidth.

Furthermore, the FWHM of the CEO and optical beat note, as well as the optical bandwidth and repetition rate of the oscillators are illustrated in Table 4-1. Hereby the oscillators' optical spectrum is centered at a wavelength of 1560 nm. The CEO linewidth and the optical beat note of the SESAM EOM laser is about 10 fold higher in comparison to the tf-CNT lasers. The lower noise of the tf-CNT lasers is given due to the higher spectral bandwidth of the intra-cavity pulses, a net cavity dispersion closer to zero and due to the sub-ps relaxation time of the CNT absorbers.

	-3dB Δf_{CEO}	-3dB Δf_{opt}	-3dB $\Delta\lambda$ (max)	f_{rep}
SESAM EOM	590 kHz	160 kHz	6.5 nm	80 MHz
tf-CNT EOM	51 kHz	16 kHz	10.5 nm	80 MHz
tf-CNT OOM	69 kHz	18 kHz	11 nm	70 MHz

Table 4-1: Oscillator parameters.

Strong side bumps are observed in the CEO beat at an offset frequency of about 4 MHz for the SESAM EOM and tf-CNT EOM lasers. These side bumps were also observed in the optical beat, but with lower amplitude. Furthermore, the offset frequency of the side-bumps increased, when increasing the pump power to the oscillator, similar as described for wake mode stabilities [62] and relaxation oscillations [83]. Hypothetical, these side-bumps might be induced due to the high loss of the intra-cavity EOMs leading to an underdamped oscillator.
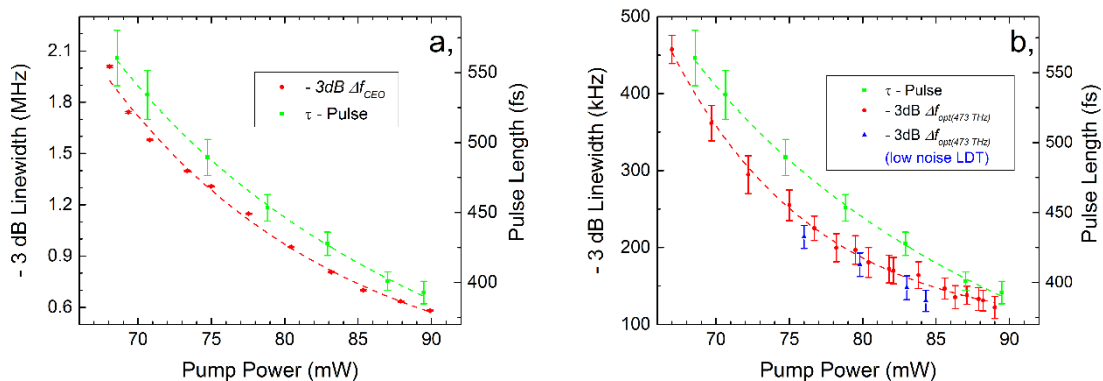
Figure 4-2: FWHM linewidth as a function of pump power for a, the f_{CEO} and b, optical beat note.

The beat notes were measured at about 80-90% of the oscillators' maximum pump power. The lasers switch to unstable or harmonic mode locked operation when the maximum pump

level is exceeded. As illustrated in Figure 4-2 the SESAM EOM's linewidth of the CEO and optical beat decreases as a function of pump power due to a decreasing intra-cavity pulse length.

4.2   Degradation of PM tf-CNT absorber

The spectral output bandwidth of the tf-CNT EOM oscillator decreased as a function of operation time. A similar behavior was observed for self-build CNT absorber femtosecond lasers, which were studied in the scope of a master thesis [52]. In particular, a decrease in spectral bandwidth was observed, when the oscillator was pumped near its maximum power maintaining mode-locked operation.

The reason for this was a degeneration of the tf-CNT PM absorber. Due to the degeneration of the CNTs, the absorber's modulation depth decreases and so only can support soliton pulses with a lower energy/spectral bandwidth. In this context the degeneration process is driven due to graphitization of the carbon nanotubes, whereas the carbon compounds break up. The degeneration process in CNT based femtosecond lasers is studied in [84]. Therefore, an average intra-cavity power of 30 mW is often sufficient to initiate degradation of the absorber. However, only the evanescent field interacts with the carbon nanotubes in the tapered fiber design, which in turns shall withstand an intra-cavity power > 30 mW. Out of this reason, no degeneration shall be observed for the tf-CNT absorbers. Furthermore, no degradation of tf-CNT OOM laser was observed despite bleaching the absorber with femtosecond pulses and light from the OOM laser, simultaneously. It is assumed, that the absorber of the tf-CNT EOM laser shows degradation due to its non-commercial prototype design and due to its polarization maintaining properties.
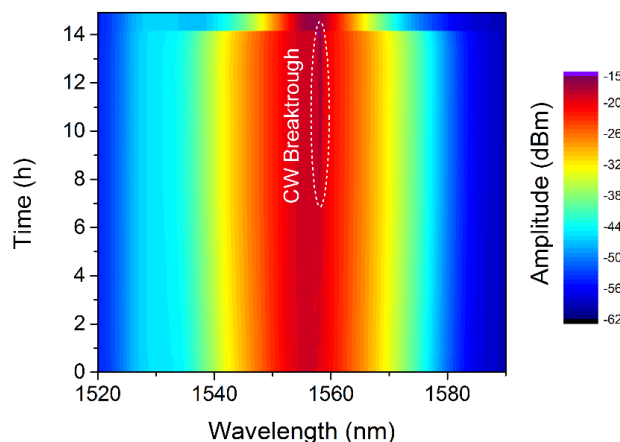
Figure 4-3: Optical output spectrum of the tf-CNT EOM laser as a function of time.

A detailed study of the degradation mechanism in the PM tf-CNT absorber would help to develop a highly reliable absorber such it is already demonstrated for the non-PM tf-CNT absorbers.

In Figure 4-3 the tf-CNT EOM laser output spectrum over a period of more than 14 h is illustrated. After an operation of 8 h a cw peak appears at a wavelength of 1559 nm. This peak indicated that the laser shows Q-switching, due to a degeneration of the absorber. Since the absorber could not support the broadband intra-cavity soliton pulse anymore, a new soliton pulse is formed after 14 h of operation.

4.3 Actuators and Phase Locked Loops for Laser Stabilization

The comb repetition rate and CEO frequency is each stabilized via a phase locked loop (PLL). A sketch of a PLL to synchronize the phase of the comb repetition rate, CEO frequency or optical beat to a reference frequency f_{ref} is shown in Figure 4-4. The femtosecond laser frequency (f_{rep}, f_{CEO} or f_{opt}) is detected via an optical interface (see chapter 3). This frequency is compared with f_{ref} in a phase detector. An error signal U_{error} which is proportional to the phase difference between f_{ref} and the laser frequency is generated by the phase detector. This error signal is fed into a PID servo controller to re-adjust the set-point of the laser actuator, which acts on the laser frequency itself. The overall PLL feedback bandwidth is determined by the sum of the frequency response functions of each element in the stabilization loop. In this context, the laser oscillator, the phase detector and the driver for the actuators show low pass like characteristics, which limits the overall the feedback bandwidth.
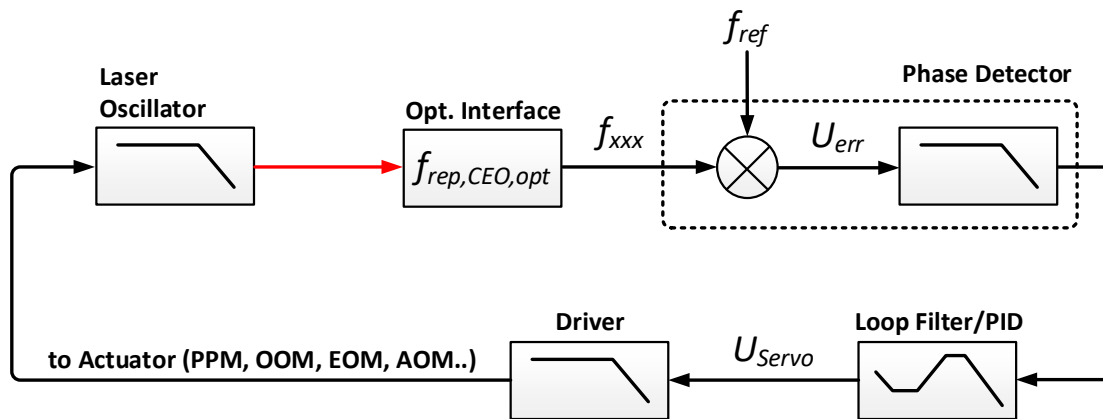
Figure 4-4: Principle of a phase locked loop and transfer function of each element within the PLL.

The optical interface and electrical cables might introduce a relevant dead time, due to long travel paths of light or electrons. This can limit the stabilization bandwidth down to the MHz

regime[3]. Different actuators such as EOMs, an AOM, pump power modulation (PPM), opto-optical modulation (OOM) and temperature tuning were used to stabilize the repetition rate and/or the f_{CEO} frequency of the femtosecond lasers. Each of this actuator has specific characteristics, which need to be adapted specifically to each phase locked loop. Therefore it is important to determine the parameters such as,

- the modulation depth, which determines by how much the laser repetition rate or CEO frequency changes, when the actuator set-point is varied,
- the fixed point frequency (see chapter 2.3)
- and the frequency and amplitude transfer functions of the oscillator, when the actuator set-point is modulated with a chirped sine signal.

A list on actuators for frequency stabilization as well as the corresponding fixed point frequency is depicted in Table 4-2. Actuators with a low value (0.1-10's THz) for the fixed point frequency are better suited for f_{rep} stabilization. Whereas actuators with a higher fixed point frequency are used to lock f_{CEO}. The bandwidth values in this table represent the maximum achieved stabilization bandwidth to f_{rep} or f_{CEO} in respect to the utilized actuator. These values do not represent the modulation bandwidth of the actuator itself.

	Fixed Point Frequency (THz)	Used for:		Bandwidth (Hz)	Ref.
		f_{rep}	f_{CEO}		
Piezo Fiber Stretcher	1-3	x		$1 \cdot 10^5$	[1]
Piezo Mirror	1-3	x		$3 \cdot 10^5$	[85]
Graphene Modulator	≈200	x	x	$2 \cdot 10^6$	[86]
EOM (Phase)	5-50	x		$3 \cdot 10^6$	[87]
EOM (polarization modulation)	≈200		x	$2 \cdot 10^6$	[88]
Pump Power Modulation (PPM)	150-230 (≈200)		x	$9 \cdot 10^5$	[89]
Opto-Optical Modulation (OOM)	system dependent	x	x	$2 \cdot 10^6$	[90]
Temperature	system dependent	x		< 0.1	-
Temperature Tuning via resistive gold coating	system dependent	x		< 1	[91]
Acousto-Optic Modulator (AOM)	∞		x	$4 \cdot 10^5$	[92]

Table 4-2: Actuators used for frequency comb stabilization.

---

[3] E.g. an optical interface with an effective optical path of 15 m leads to a dead time of 50 ns ~ 20 MHz

4.3.1 Pump Power and Electro-optic Modulation

In the following sub-sections the transfer function, fixed point frequency and modulation depth of the SESAM EOM and tf-CNT EOM laser for PPM and modulation of the intra-cavity EOMs voltage is presented. Furthermore, it is illustrated why PPM is not suitable to stabilize the tf-CNT EOM oscillator.

4.3.1.1 Amplitude Transfer Function for PPM

The CEO frequency was stabilized by adjusting the pump power to the oscillator. Hereby, fluctuations in the pump power lead to variations in the CEO frequency (AM to FM coupling) and to a change in the oscillator output power (AM to AM coupling). In this context, the AM to FM and AM to AM coupling show similar dynamics. The amplitude transfer function was measured instead of the frequency transfer function, since it is easier to measure. The amplitude transfer function was used to optimize the feedback bandwidth of the comb stabilization. Figure 4-5 shows the setup to measure the amplitude transfer function of the SESAM EOM laser for pump power modulation. A vector analyzer modulates the pump laser power with a chirped sinusoidal signal (U_{mod}). The output power is measured with a fast InGaAs photodiode. The (relative) amplitude transfer function is given by the ratio between the photo diode voltage and the modulation voltage:

$$H_{P,PPM} = 10\log\left(\frac{U_{PD}}{U_{Mod(Ref)}}\right)$$
(4.1)
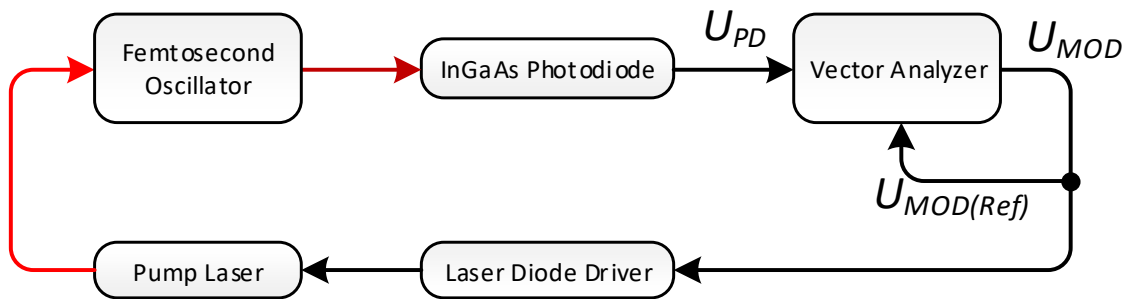
Figure 4-5: Measurement setup to measure the femtosecond transfer function via pump power modulation.

In Figure 4-6 the amplitude transfer function (red curve) for PPM and the transfer function of the laser diode driver (green curve) is shown. The amplitude transfer function was not corrected by the laser diode driver's response. The amplitude transfer function has a phase

margin of -45 degree at a modulation frequency of 3.1 kHz. The limit response bandwidth [93] PPM due to intra-cavity laser dynamics is described in detail in [32]. For the stabilization of f_{CEO} via PPM a bandwidth of more than 200 kHz is required to achieve a phase coherent lock.
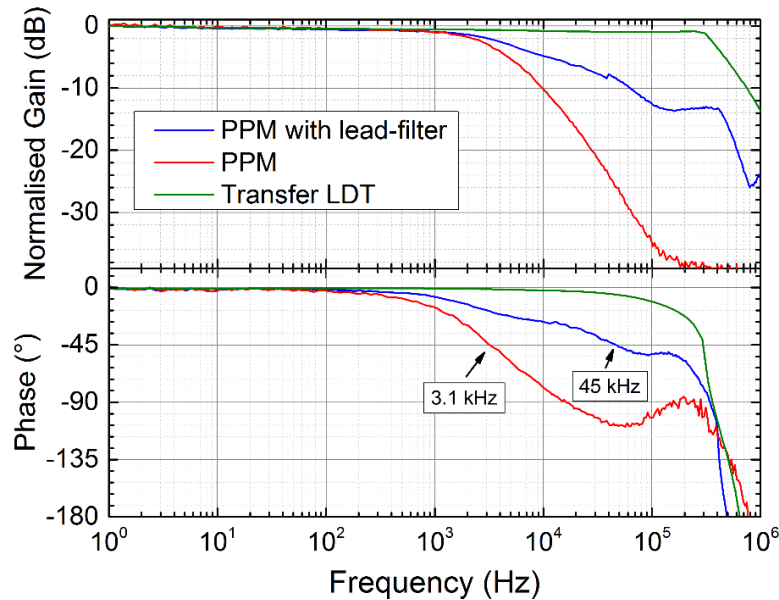
Figure 4-6: Normalized amplitude transfer function for PPM with and without lead-filter, as well as transfer function of laser diode driver.

To push the bandwidth for PPM towards higher values a lead filter (see Figure 4-7 left) was introduced within the PLL. Hereby the lead-filter was connected to the laser diode driver (LDT) modulation port. The lead filter has a high pass like transfer function (see Figure 4-7 right) to increase the gain and phase margin towards higher frequencies.
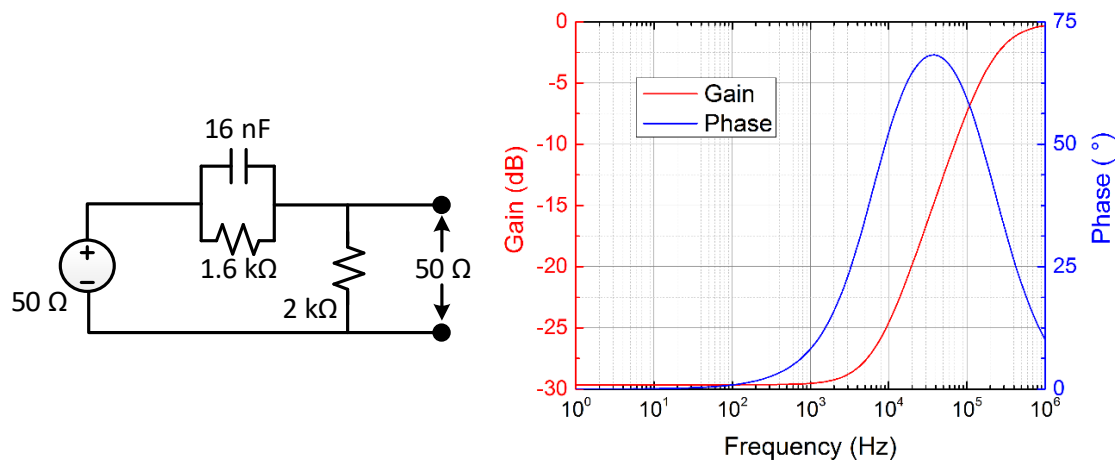
Figure 4-7: Lead-filter (left) and measured response function (right).

By introducing the phase lead filter, the amplitude transfer function (see blue curve in Figure 4-6) shows a -45 degree phase margin at a frequency of 45 kHz, which is more than a decade higher compared to the amplitude transfer function without a lead filter. Within the PLL the servo's active D-element was adjusted so that the in-loop -3 dB bandwidth was more than 200 kHz. However, the in-loop bandwidth was then limited by response of the laser diode driver's modulation bandwidth itself.

4.3.1.2 Reversal Point

A stabilization of the tf-CNT EOM laser CEO frequency was not achieved by means of pump power modulation. The reason for this was that a reversal point [94] was observed, where a change in pump power modulation did not affect the CEO frequency. Figure 4-8 shows the tf-CNT EOM repetition rate as a function of pump current. At a current of 147 mA the repetition rate has a reversal point where the repetition rate shows almost no change when the pump power is varied. Within this region it is not possible to stabilize whether f_{rep} or f_{CEO} of the comb. Nevertheless, the laser has its minimum in phase noise at the reversal point, due to a minimum conversion of pump power noise to frequency noise. However, a frequency stabilization of the CEO frequency was achieved at lower pump currents (115 mA-143 mA). Nevertheless, a tight sub-Hz phase coherent lock was not obtained due to the broad linewidth of the CEO beat at this pump current.
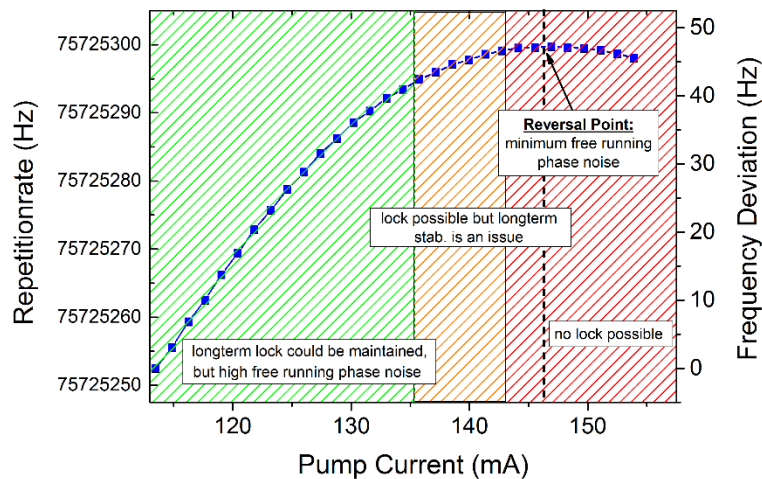
Figure 4-8: Tf-CNT EOM laser's repetition rate as a function of pump current.

Figure 4-9 illustrates the phase for the amplitude transfer function of the oscillator at three different pump current set-points. The phase margin approaches 180° at low frequencies

when the pump current is increased. At a phase margin of 180° the laser could not be sta-bilzed. This supports the observation from Figure 4-8.
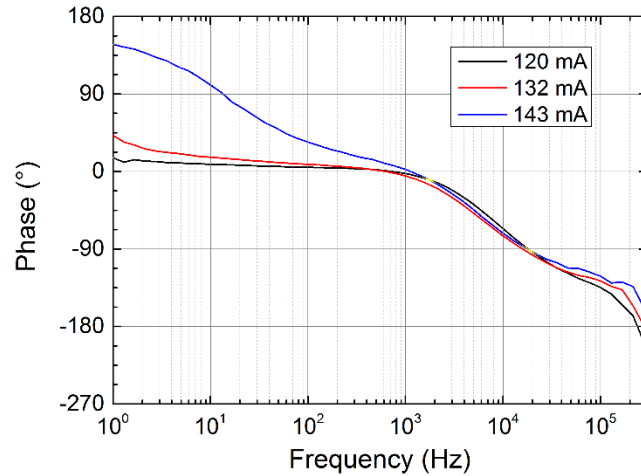
Figure 4-9: Phase function for the amplitude transfer function of the tf-CNT EOM when applying pump power modulation.

4.3.1.3 Frequency Transfer Function for EOM

The intra-cavity EOM in the tf-CNT EOM and the SESAM EOM laser was used to reference a comb mode to a HeNe laser. To obtain the response dynamics of the EOM to the comb mode at 633 nm, the response to the optical beat (f_{opt}=n·f_{rep}+2·f_{CEO}-v_{HeNe}) between the comb mode and the HeNe laser was determined. The response also includes the contribution of the CEO frequency. The setup to measure the transfer function for f_{opt} is illustrated in Figure 4-10. The EOM voltage is modulated with a chirped sinusoidal signal (U_{mod}) leading to a modulation in the comb mode frequency and so in f_{opt}. Frequency variations in f_{opt} are con-verted into voltage fluctuations by a frequency discriminator (MITEQ, FMDM-21.4/4-2B). These voltage variations were measured by the vector analyzer and compared to the EOM voltage to determine the transfer function:

$$H_{f_{opt},EOM} = 10 \log\left(\frac{U_{fopt}}{U_{EOM(Ref)}} \right) \tag{4.2}$$

In Figure 4-11 the transfer function (blue) $H_{fopt,EOM}$ of the tf-CNT EOM laser and the transfer function of the frequency discriminator (red) is illustrated. A -3 dB bandwidth of 2.5 MHz was estimated for the EOM. Hereby the measurement was limited by the response dynamics of the frequency discriminator itself. Out of this reason, a higher modulation bandwidth to f_{opt} is expected.
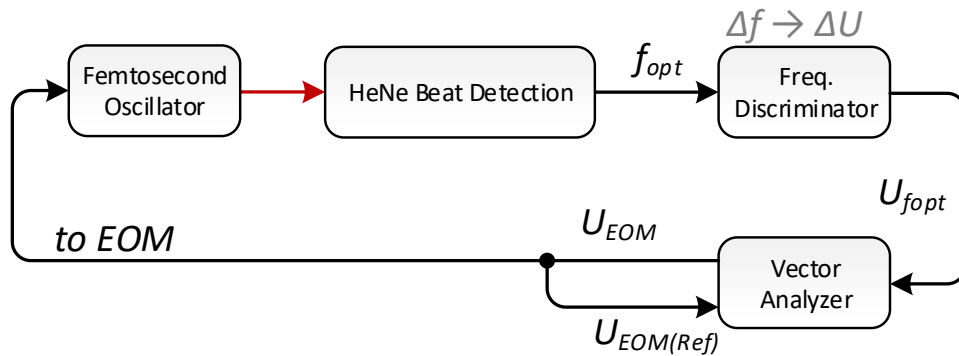
Figure 4-10: Setup to measure the response dynamics of the EOM actuator to *f*$_{opt}$.

The response dynamics of the EOM to *f*$_{opt}$ was not measured for the SESAM EOM laser, since no frequency discriminator was available. However, the response to the repetition rate was measured. Hereby side-bands were modulated to the repetition rate carrier [95]. The response function was estimated by measuring the difference in amplitude between the carrier and side bands. The results are depicted in [96]. Hereby, a resonance at a modulation frequency starting from 5 MHz occurred, which was caused by the RF-impedance mismatch of the signal generator output (50 Ω) and the EOM's input high impedance (10 kΩ). This resonance at 5 MHz limits the overall stabilization bandwidth of the laser. However, a bandwidth of some MHz for both EOMs promises a phase coherent stabilization of a comb mode to the HeNe laser frequency.
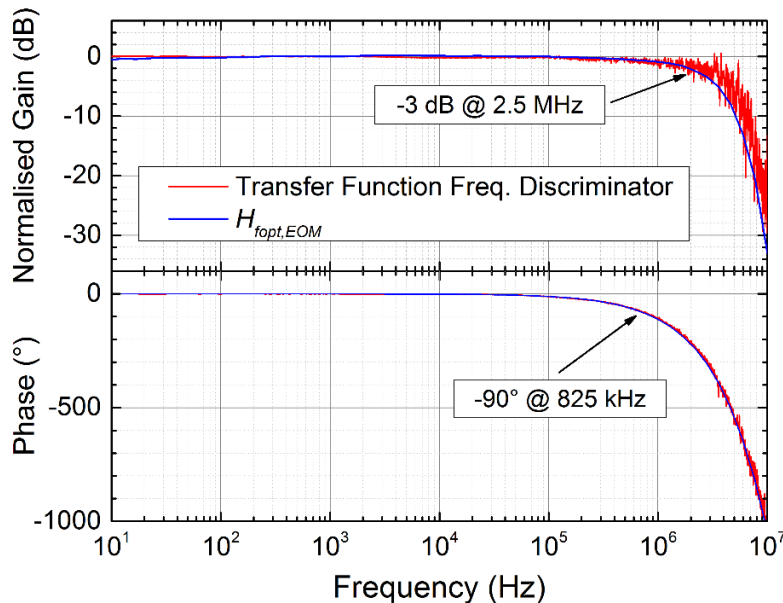
Figure 4-11: Transfer function of *n·f*$_{rep}$ for electro-optic modulation.

4.3.1.4 Fixed Point Frequency and Tuning Rate

The fixed point defines the spectral position, where no variation in the comb optical frequency is observed when changing the actuator set-point. The fixed point frequency [32] (see section 2.3) for PPM and the EOM was obtained by changing either the set-point of the pump power or the EOM bias voltage and simultaneously monitoring f_{rep} and f_{CEO} with a frequency counter. It is given by:

$$v_{fix(PPM,EOM)} = \left(-\Delta f_{CEO(PPM,EOM)} \Big/ \Delta f_{rep(PPM,EOM)} \right) \cdot f_{rep} + f_{CEO} \tag{4.3}$$

Figure 4-12 shows the change in CEO frequency and repetition rate at different pump power set-points for the SESAM EOM laser, measured at a laser temperature of 25.5°C, 27.7 C and 30.4°C. From this measurement a fixed point frequency from 150-170 THz was derived. Typically, the fixed point frequency for PPM is observed at the laser output frequency ($\approx$192 THz). However, the fixed point frequency might differ here due to integrated EOM.
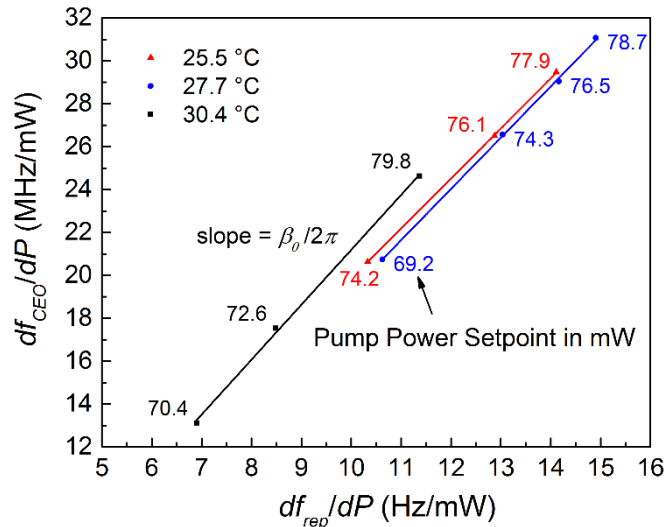
Figure 4-12: Change in the SESAM EOM laser repetition rate and CEO frequency for PPM at different pump power set-points and laser temperatures.

By taking equation (2.8) into account, the lumped propagation constant β_0 and the pump power induced self-phase modulation $d\varphi_{spm}/dP$ is derived from the measurement. The theoretical value for $\beta_0/2\pi = n_{eff} \cdot 2 \cdot L \cdot v_c/c = 1.44 \cdot 2 \cdot 1.3$ m$\cdot$192.1 THz/$3 \cdot 10^8$ m/s $= 2.39 \cdot 10^6$ agrees with the measurement data showing a slope of $2.33 \cdot 10^6$ @25.5°C, $2.38 \cdot 10^6$@27.7°C and $2.56 \cdot 10^6$@30.4°C, which underlines that the fixed point frequency was properly obtained.

Furthermore, the self-phase modulation term $f_{rep}/2\pi\cdot(\,d\varphi_{spm}/dP)$ is derived from the intersection of the fitted lines with the y-axis, which is here -3.5 MHz/mW @25.5°C, -4.6 MHz/mW @27.7°C and -4.4 MHz/mW @30.4°C.

The intra-cavity EOM of the SESAM EOM laser changes the repetition rate by about 11.86±0.3 Hz/V and the CEO-frequency by 3.65±0.67 MHz/V resulting into a fixed point frequency from 19 THz to 29 THz. The EOM fixed point frequency indicates that a change in the EOM bias voltage acts much stronger on f_{rep} than on f_{CEO} compared to the effect of the pump power. For this reason n·f_{rep} was optically locked to the HeNe laser via the EOM bias voltage, while f_{CEO} was stabilized via PPM. The EOM voltage has a total range of ±20 V allowing to change in the fundamental repetition rate by ±240 Hz, making a slow piezo fiber stretcher unnecessary to ensure the long-term stabilization of the repetition rate. A temperature sensitivity of 800 Hz/K was measured to the fundamental repetition rate. Subsequently, the oscillators were temperature stabilized 25±0.01°C with a thermo-electrical cooler (TEC).

	SESAM EOM laser	Tf-CNT EOM laser
v_{fix} PPM	150-172 THz	160 THz
Tuning rate to CEO via PPM	14-30 MHz/mW	tbc
v_{fix} EOM	19-29 THz	48 THz
Tuning rate to f_{rep} via EOM	11.86±0.3 Hz/V	5.88 Hz/V
Tuning rate to f_{rep} via temp.	800 Hz/K	800 Hz/K

Table 4-3: Fixed point frequency and tuning rates for the SESAM EOM and tf-CNT EOM laser.

The fixed point frequency as well as the tuning rate for the SESAM EOM and tf-CNT EOM laser are depicted in Table 4-3. In this context, the tf-CNT EOM laser fixed point frequency for PPM was about 160 THz, which is a similar value compared to the SESAM EOM laser. The tuning rate of the CNT laser EOM is about half compared to the tuning rate of the SESAM EOM laser's EOM, due to a shorter lithium niobate section.

4.3.2 Opto-Optical Modulator for Carbon Nanotube Laser

The opto-optical modulation method is based on the principle that the femtosecond laser intra-cavity loss is controlled by adjusting the saturation level of the absorber via an optical light source. As consequence the intra-cavity loss modulation results into a change in the laser's f_{rep} and f_{CEO}. The OOM principle was demonstrated to stabilize the CEO-frequency of femtosecond lasers based on SESAM absorbers [97, 90]. Here the OOM method is applied to a femtosecond laser with a tf-CNT absorber (see Figure 3-1 c).
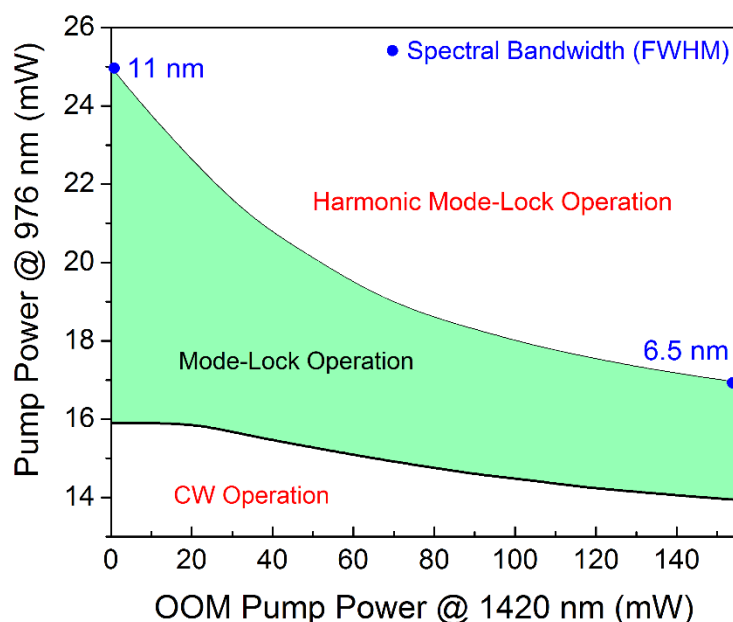
Figure 4-13: Area of mode locked operation depending on the oscillator's pump power and power from the OOM laser.

In Figure 4-13 the area of mode-locked operation for the tf-CNT opto-optical modulator laser as a function of pump power (PPM) and OOM power is shown. The pump power threshold as well as the oscillator's optical spectral pulse bandwidth for harmonic mode-locked operation decreases towards higher OOM powers. A bandwidth of 11 nm was achieved, when the CNT absorber was not illuminated by the OOM laser. Whereas a reduced bandwidth of 6.5 nm was obtained with a power of 155 mW from the OOM laser to the oscillator. The reduced bandwidth emerges from the pre-saturation of the CNT absorber by the OOM laser light. Due to the pre-saturation, the absorber's effective modulation depth decreases. Out of this reason the soliton pulse energy threshold (and so the spectral bandwidth) decreases, where the absorber supports mode locking. In summary, this measurement shows that the nonlinear transmission of the tf-CNT absorber and so the loss in the femtosecond laser cavity are controllable via the OOM laser at 1420 nm.

4.3.2.1 Fixed Point Frequency

The fixed point frequency (see equation (4.3)) for the OOM was measured similar as in section 4.3.1.4, by increasing the OOM pump power while simultaneously recording the CEO frequency and repetition rate. In addition the fixed point frequency for pump power modulation was measured. Figure 4-14 illustrates the change in the CEO-frequency and repetition rate for an increase in PPM and OOM. The change in both frequencies was determined for

OOM (PPM) as a function of different pump powers to the Erbium doped fiber (carbon nano-tube absorber).
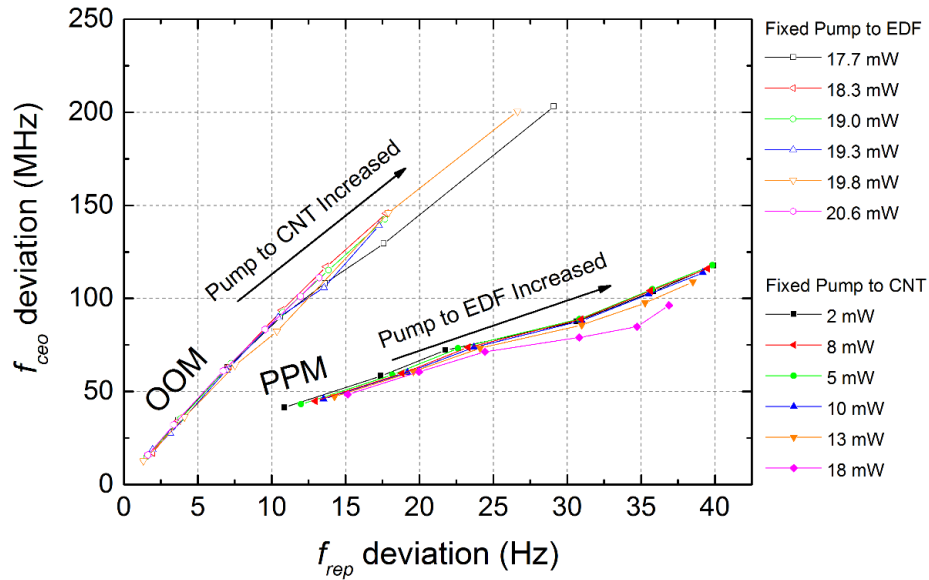
Figure 4-14: Simultaneous change in f_{rep} and f_{CEO} for PPM and OOM at different pump power set-points of the OOM and PPM laser, respectively.

A fixed point frequency of about 620 THz for OOM and 210 THz for PPM was determined (see Table 4-4). Thereby the fixed point for PPM is close to the carrier frequency (192 THz) of the laser. The high value for the OOM fixed point frequency indicates that the OOM method suits better for CEO stabilization than controlling the repetition rate.

Fixed Point Frequeny tf-CNT OOM Laser	
v_{fix} OOM	620 THz
v_{fix} PPM	210 THz
$v_{fix(OOM)}/v_{fix(PPM)}$	≈ 3:1

Table 4-4: Tf-CNT oscillator fixed point frequency for PPM and OOM.

A fixed point ratio of 3:1 is given between OOM and PPM. This means that the OOM and the PPM show a relatively strong crosstalk. Due to this a fully (low noise) stabilized comb via OOM and PPM is difficult to realize.

4.3.2.2 CEO Frequency Transfer Function

The tf-CNT EOM CEO-frequency transfer function was measured to compare the OOM and PPM against each other for CEO stabilization. Figure 4-15 shows the setup to measure the transfer function of f_{CEO} for OOM or PPM modulation. The pump power of the OOM/PPM laser is modulated via a chirped sinusoidal signal from a vector analyzer. This modulation leads to variations in the CEO frequency, which is converted into a voltage fluctuation via a frequency discriminator (MITEQ, FMDM-21.4/4-2B, sensitivity=1MHz/V) and were compared to modulation signal.
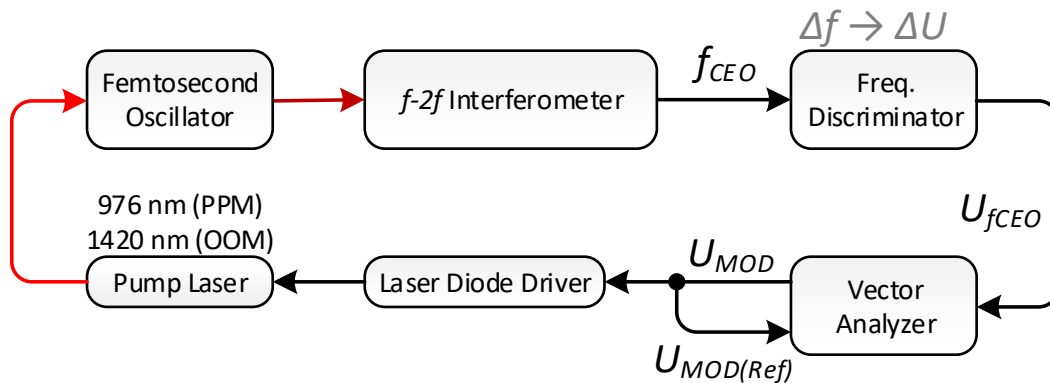
Figure 4-15: Transfer function to measure the f_{CEO}'s response for PPM or OOM.

The resulting transfer functions are depicted in Figure 4-16 and were corrected for the response of the frequency discriminator and laser diode driver. In Figure 4-16 a, the OOM transfer function has a similar characteristic such as the transfer function for PPM, but has a higher gain with respect to changes in f_{CEO}. In this context, the OOM has a tuning rate of 7.5 MHz/mA, where PPM has tuning rate of 1.1 MHz/mA at 1 Hz.
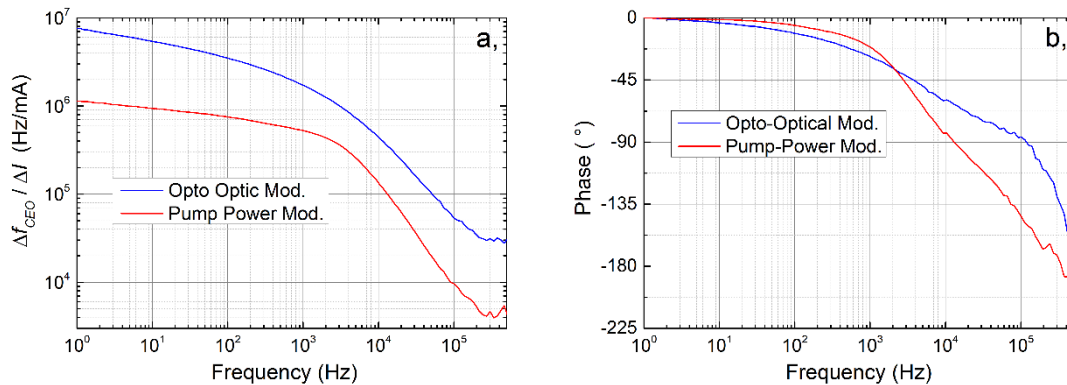
Figure 4-16: Transfer function of f_{CEO} for opto-optical and pump power modulation.

A flat response of CEO in respect to the OOM modulation frequency with a low pass filter like cut-off frequency limited by the LDTs bandwidth (≈300 kHz, see Figure 4-6) was expected for the measurement. The reason for this assumption is that the carbon nanotube absorber reacts almost instantaneously to intensity changes in the OOM laser. Hereby it is assumed that the loss modulation via OOM interacts with the low pass like intra-cavity laser dynamics.The key parameters derived from the transfer measurements are summarized in Table 4-5.

	OOM	PPM
CEO Tuning Rate (@ 1 Hz)	7.5 MHz/mA	1.1 MHz/mA
CEO Max. Tuning	±100 MHz	±10 MHz
Mod. Bandwidth @ -90° Phase Margin	120 kHz	10.3 kHz

Table 4-5: CEO frequency tuning rate, tuning range and modulation bandwidth for OOM and PPM.

A modulation bandwidth of 10.3 kHz and 120 kHz at a phase margin of -90°degrees (Figure 4-16 b,) was measured for PPM and OOM, respectively. Loss modulation has been demonstrated via a graphene based modulator achieving a feedback bandwidth of about 1 MHz for frequency comb stabilization [98,86,99,100]. A feedback bandwidth of 600 kHz was reached with the OOM method applied on a SESAM absorber [90].

4.3.2.3 CNT Absorber Extra-cavity Transfer Function

The tf-CNT absorber and WDMs were removed from the laser's cavity to characterize the tf-CNT absorber's response without taking the cavity's dynamics into account. Hereby pulses from a femtosecond oscillator were amplified and stretched to a pulse duration of about 1.5 ps and injected into the tf-CNT absorber (see Figure 4-17). On the other side, light from the OOM laser at 1420 nm was injected to the CNTs. Hereby no light at 1420 nm was guided whether to the Erbium amplifier or to the power meter.
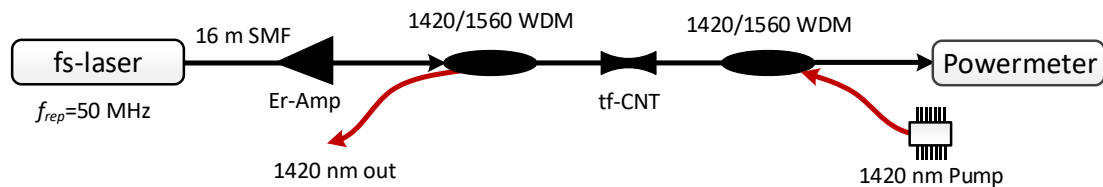
Figure 4-17: Optical setup to measure the tf-CNT absorbers transmission as function of pump power of the opto-optical modulator laser at 1420 nm.

By means of this setup, the change in transmission of the CNT absorber as a function of OOM power was estimated, which is illustrated in Figure 4-18. The signal light after the absorber increases from 43 mW to about 45.5 mW for a OOM laser power of 0 mW to 140 mW. This results into a change of 5.5 % yielding to a sensitivity in transmission of about 0.037 %/mW for opto-optical modulation. The resulting modulation depth and sensitivity is sufficient for controlling the femtosecond oscillator's frequency via intra-cavity loss modulation.
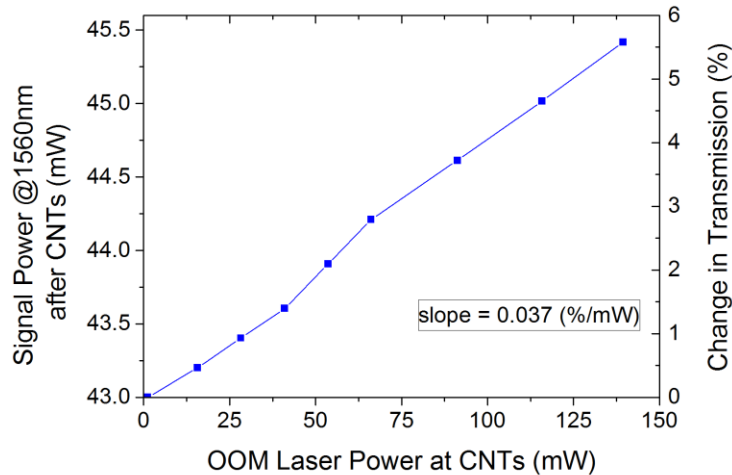
Figure 4-18: Change in the average power of the signal light at 1560 nm, when the power to the CNTs of the OOM laser is increased from 0 mW to about 140 mW.

In a next step the amplitude transfer function was measured to estimate how fast the transmission of the tf-CNT can be changed via OOM. Therefore the power meter in the setup was replaced with a fast InGaAs photodetector and the power of the 1420 nm laser was modulated via a vector analyzer (see Figure 4-19). The transfer function was then determined by the ratio between the frequency dependent change in the photodetector voltage and the modulation voltage from the vector analyzer.
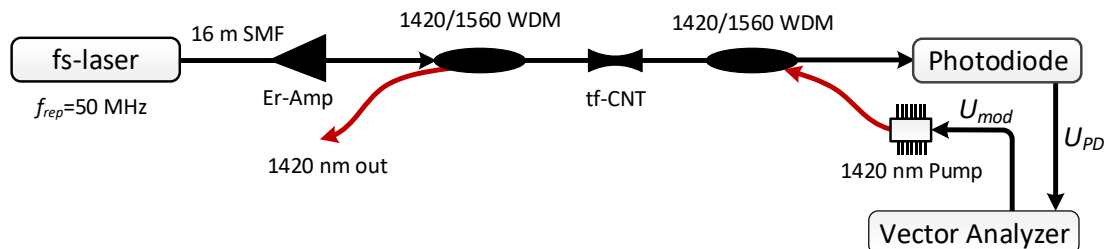
Figure 4-19: Setup to measure the tf-CNT absorber's extra-cavity response to opto-optical modulation.

The amplitude transfer function was measured for pump power set points of the OOM laser ranging from 7.5 mW to 91 mW. The gain and phase as function of modulation frequency is depicted in Figure 4-20 a, and b, respectively. Hereby the normalized gain decreases from 1 Hz to 30 Hz indicating temperature induced transmission changes of the CNT absorber. This observation is also supported by a drop in the phase margin. A resonance in the gain curve occurs at about 1 kHz, before the phase and so the gain of the laser drops further. The transfer function reveals a slow response of the CNT absorber, which highly probably is here dominated by temperature induced changes at the tapered fiber section. In this context the heat from the CNTs is dissipated into the tapered fiber. Tapered fibers itself are applied in the field of temperature sensing as their spectral transmission changes as function of temperature. However, a slight increase in phase margin is observed for frequencies higher than 10 kHz when the OOM power is increased. For frequencies > 1 kHz, the impact of temperature induced changes decreases, while the impact on the transmission due to saturation of the CNTs increases.
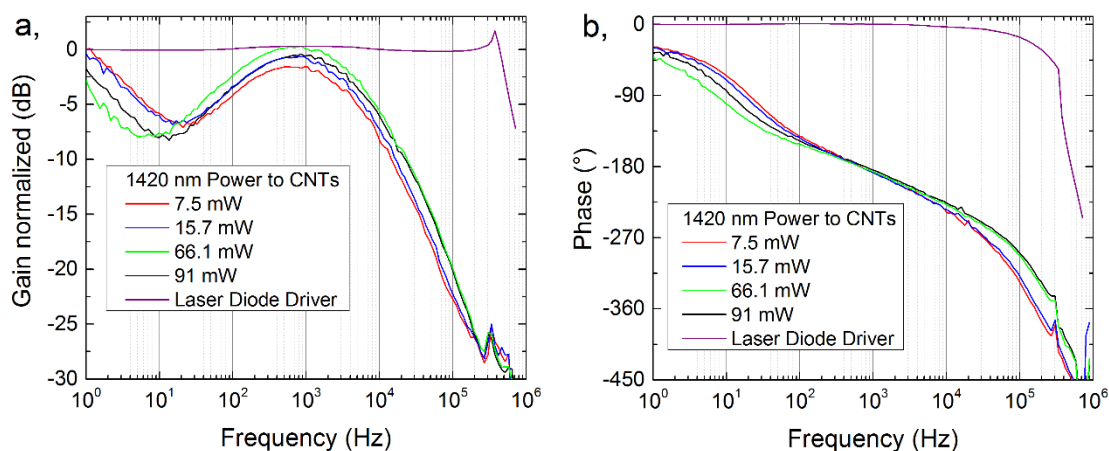
Figure 4-20: Normalized response in the tf-CNT absorber transmission within (a) the amplitude and (b) phase spac

For a proper measurement of the CNT absorber's response, temperature and "electrical" induced transmission fluctuations need to be separated. One method to reduce the temperature impact might be to seed the CNT absorber with ultra-short pulses for OOM.

Due to the short "adiabatic" interaction with the CNTs less heat would be generated. Nevertheless, this technique is complicated, since the pulses of the OOM seed laser and tf-CNT femtosecond laser need to be temporal synchronized. Another method would be to change the CNT's transmission by applying an external electrical field such as demonstrated for graphene- or electro-optic modulators.

However, both techniques would require extensive technological development to establish a measurement setup. An open question is still, why the amplitude transfer function (see Figure 4-20) and the CEO transfer function (see Figure 4-16) show a different behavior. Nevertheless, the CEO frequency transfer function shows that a stabilization via the OOM is possible, which is underlined by the results shown in chapter 5.3. Furthermore, the characterization results demonstrate the realization of an OOM modulator within a tf-CNT laser to vary its CEO-frequency and repetition rate.

5 Stabilization of Oscillators

In this chapter the stabilization of the SESAM EOM (section 5.1), tf-CNT OOM (section 5.3) and tf-CNT EOM (section 5.2) comb oscillator (see Figure 3-1) to a HeNe laser at 473 THz is studied.

Hereby, it shall be investigated if the SESAM EOM and tf-CNT EOM can be fully stabilized to the HeNe laser with a fractional in-loop Allan deviation better or equal than 10^{-16} at an integration time of 1 s. This performance is required for the in-fiber comb module to potentially transfer the stability of an optical clock to a frequency comb without significant loss. "Full" stabilized means that the repetition rate and the CEO frequency need to be locked at the same time. Furthermore, the femtosecond oscillators shall be locked to the HeNe lasers for a period of at least a day to show technical reliability.

Furthermore, the stabilization of the tf-CNT OOM oscillator shall show if a phase coherent lock to an optical reference is achieved, when applying the opto-optical modulation method to a femtosecond laser based on a tf-CNT absorber. Besides the demonstration of the proof of principle of the OOM method, information on the in-loop stabilization bandwidth and phase noise are gathered. By these information the performance of the OOM method is estimated.

The stabilization to an optical reference is more challenging in contrast to referencing the comb to a radio frequency standard such a H-maser or a RF-rubidium source. In the optical domain repetition rate variations are levered by $n \cdot f_{rep}$ yielding to a higher sensitivity in respect to environmental perturbations.

Phase locked loop and the actuators for frequency comb stabilization are discussed in section 0. In this context the response dynamics of actuators were measured to determine the system limits for comb stabilization. In section 5.3 the femtosecond laser results are discussed and compared against each other.

The stability of the comb lasers were measured with two different types of counters, depending on which counter was currently available. Hereby one counter from K&K (FXE) and counters from Keysight (53230a) were used. The K&K system is based on a time discrete measuring principle with a π (pi) or Λ (lambda) averaging window [48], which is favorable over the period based counting method from Keysight, since a "true" Allan deviation is obtained from the data. Due to the specific internal averaging algorithm of the Keysight counter, a modified like Allan deviation is determined from the measurement data, when applying a standard Allan deviation algorithm for evaluation.

5.1 SESAM EOM Comb Stabilization

The stabilization setup for the SESAM EOM comb is depicted in Figure 5-1.
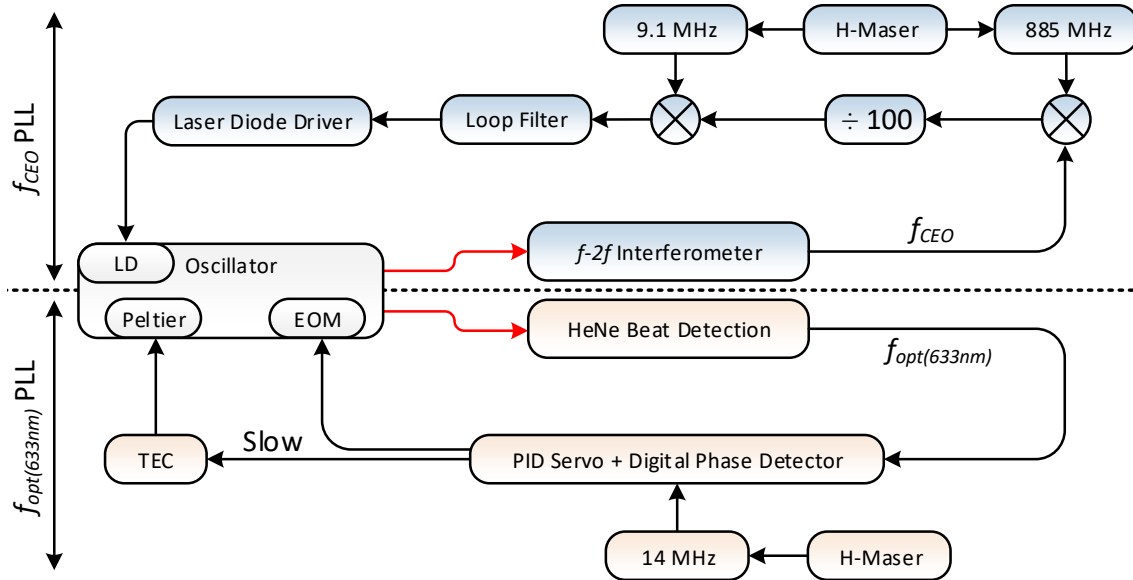
Figure 5-1: Phase locked loops for f_{CEO} and f_{opt} stabilization. Rf-filters and RF-amplifiers are not depicted.

Hereby the setup consists of two phase locked loops. Within one PLL the f_{CEO} frequency was stabilized to a H-maser. In the other PLL, f_{opt} was locked to the HeNe laser, whereas the same H-maser was also used as reference.

The f_{CEO} frequency was stabilized via pump power modulation. A long-term stable lock with an analogue PLL was ensured by dividing f_{CEO} with a frequency division factor of 100, virtually enhancing the capture range of the PLL from $\pi/2$ to $\pm$ 100 $\pi/2$. Without frequency division of f_{CEO} it was not possible to stabilize f_{CEO} with an analogue PLL. Due to the high frequency division factor it was necessary to up-convert f_{CEO} ($f_{CEO} \approx 25$ MHz) with a H-maser referenced synthesizer signal at 885 MHz to about 910 MHz. The up-converted f_{CEO} signal was bandpass filtered before being divided to about 9.1 MHz.

An error signal was generated by comparing the divided f_{CEO} signal to the 9.1 MHz of a synthesizer within an analogue phase detector (double balanced mixer). An active loop filter build from a lag (low pass filter/integrator) and lead element (high pass filter/derivator) as well as an passive lead filter (such as shows in Figure 4-7) was implemented in the PLL to achieve a locking bandwidth of more than 200 kHz. Since the free running CEO-beat has a linewidth of about 600 kHz a stabilization bandwidth of some 100 KHz was required to guarantee a phase locked operation.

A home build FPGA (Virtex 5 lx30, 250 MHz clock rate) based digital phase frequency detector (PFD) with an integrated PID controller was used to stabilize f_{opt} via the EOM. A PFD has the advantage that it is not sensitive to amplitude fluctuations and has a higher capture range with respect to the analogue phase detector. Further the digital servo was used to control the set-point of the comb temperature to obtain long-term operation.

5.1.1 CEO Beat Stabilization

Figure 5-2 shows the frequency spectrum of the CEO-beat, while being stabilized to the H-maser. The small coherent peak at 23.5 MHz with a SNR of about 5 dB (RBW=1kHz)/ 30 dB (RBW=10 Hz) with respect to the "non-coherent" part of the f_{CEO} beat indicates that a phase stabilization was obtained.
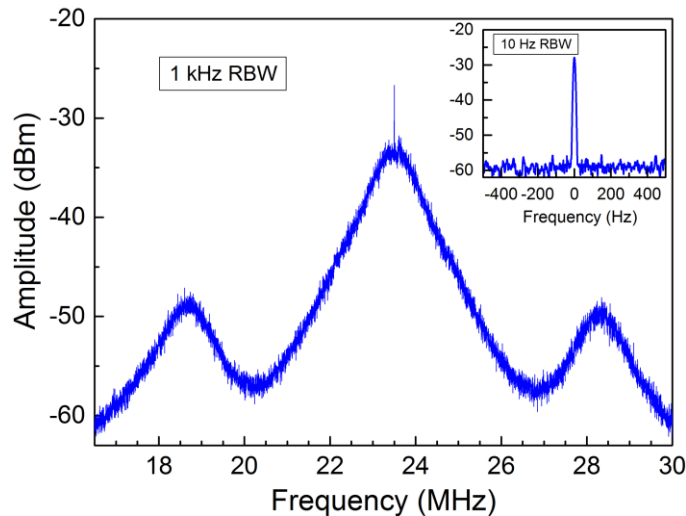
Figure 5-2: Frequency spectrum of the phase locked CEO beat.

The phase noise measurement of the phase and frequency (frequency) stabilized CEO beat is depicted in Figure 5-3. The frequency lock was realized by reducing the locking bandwidth of the PLL to some kHz. This was achieved by removing all lead filter elements within the PLL, so that the PLL is only adjusted via a proportional gain factor (P-element).
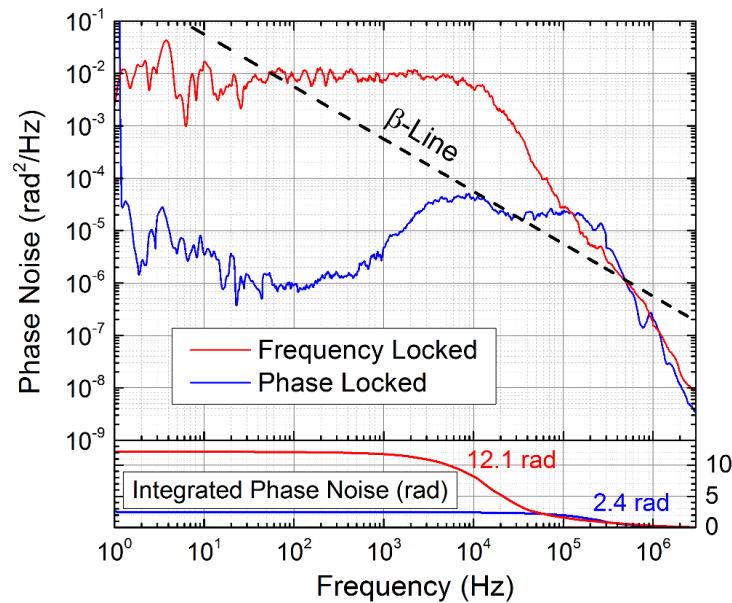
Figure 5-3: Phase noise measurement and integrated phase noise for frequency and phase locked f_{CEO} beat from 1 Hz to 3 MHz.

The frequency locked CEO-beat has an integrated phase noise of 12.1 rad (integrated from 3 MHz to 1 Hz), while the noise for the phase locked beat was reduced by a factor of 5 down to 2.4 rad. The servo loop bandwidth for f_{CEO} stabilization was about 260 kHz, which was estimated by the small bump within the phase noise spectrum. Hereby the overall stabilization bandwidth was mainly limited by the modulation bandwidth of the laser diode driver.

A coherent peak was observed despite showing high frequency noise above the β-separation line, which theoretically contributes to the linewidth of the laser. Nevertheless, a sub-Hz stability for f_{CEO} still was achieved with an integrated phase noise of a few rads [101].

A PLL bandwidth of more than 550 kHz would be required to maintain a sub-rad integrated phase noise for f_{CEO}. This was estimated from the intersection between the β-separation line and the phase noise of the frequency locked beat.

5.1.2 Stabilization to HeNe Laser

In Figure 5-4 the phase locked beat f_{opt} between the SESAM EOM comb HeNe is illustrated. The coherent delta peak at 14 MHz emerges from an u-shaped valley, which originates from the integral part of the servo loop. Hereby the integrators corner frequency was set to 100 kHz leading to robust lock. It was not possible to compensate for the bump occurring at about 270 kHz from the delta peak. This bump is introduced from the f_{CEO} stabilization due to the cross influence of both servo loops.
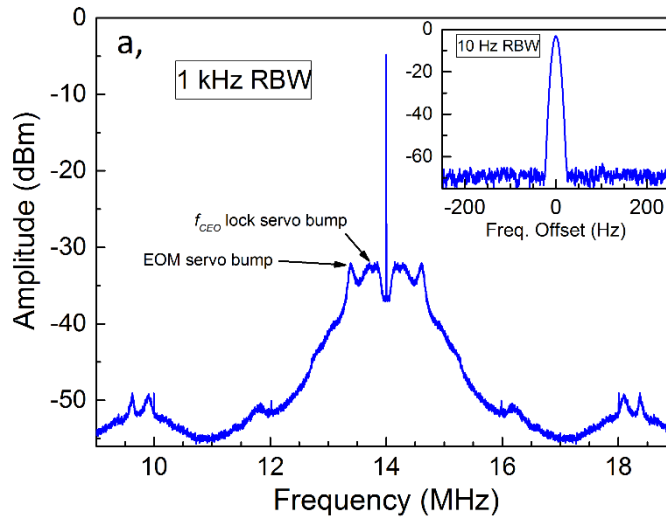
Figure 5-4: Spectrum of the phase locked optical beat note via the SESAM EOM's intra-cavity EOM.

Further the servo bump at 610 kHz from the carrier indicates the servo loop bandwidth of the for optical beat stabilization. The stabilization bandwidth is hereby limited by the FPGA based controller itself but not by the response of the integrated EOM (see section 4.3.1.3). The phase noise measurement of the phase and frequency locked optical beat note is depicted in Figure 5-5. Hereby an integrated phase noise of 2.7 rad and 1.1 rad was measured in a bandwidth from 3 MHz to 1 Hz, respectively.
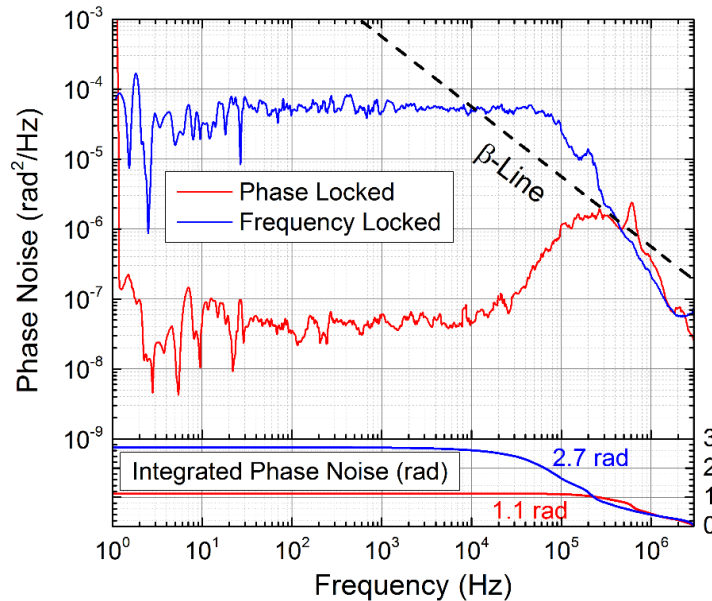
Figure 5-5: Phase noise measurement and integrated phase noise for frequency and phase locked fopt beat from 1 Hz to 3 MHz.

5.1.3 In-loop Stability

The frequency stability of f_{CEO} and f_{opt} (see Figure 5-4 and Figure 5-2) was measured with a frequency counter (K&K FXE) in a gate time of 1 s and is depicted in Figure 5-6. No phase slip was observed over a period than 46 h, which is indicated by the sub-Hz frequency stability. An in-loop stability of 7.6 mHz (τ = 1 s) and 21 mHz (τ = 1 s) was measured for f_{opt} and f_{CEO}, respectively. The fractional Allan deviation in respect to the HeNe laser frequency is below 10^{-16} @ τ= 1 s for f_{CEO} and f_{opt} (see Figure 5-7).
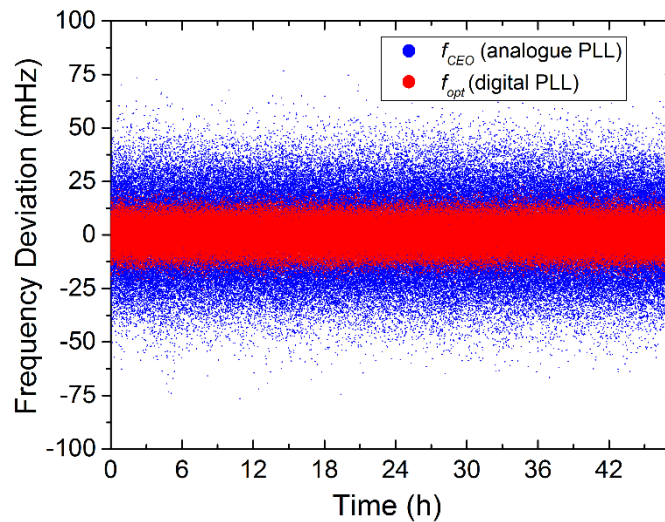
Figure 5-6: Frequency stability of f_{opt} and f_{CEO} measured (π-counter gate time = 1 s) over a period of 45 h.

The f_{CEO} beat was also stabilized with a digital PLL using the FPGA based controller. This PLL was later optimized for the All-in-fiber frequency comb system discussed in chapter 7. The Allan deviation for the digital phase locked f_{opt} and f_{CEO} beat decreases with a slope of τ^{-1}. Further the analogue locked f_{CEO} beat has a similar slope but shows a bump at an integration time of about 30 s. It is assumed that the analogue phase locked loop is sensitive to amplitude fluctuations of the f_{CEO} beat, which could be caused by temperature and/or pump power variations.
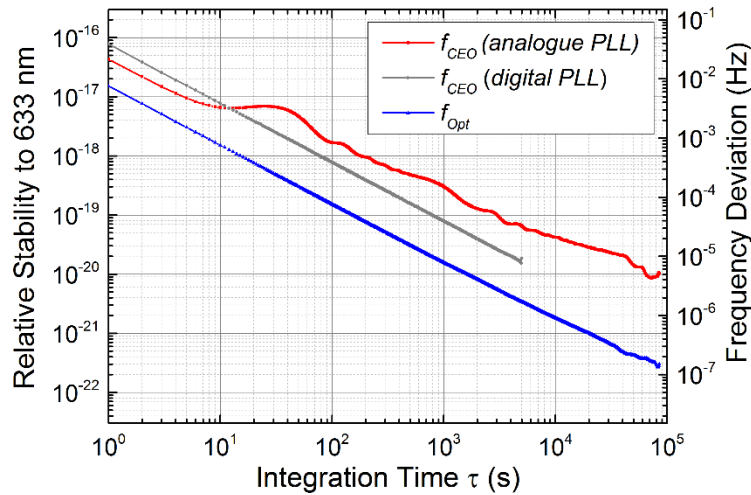
Figure 5-7: Overlapping Allan deviation of measurement shown in previous figure and for the f_{CEO} frequency stabilized with the FPGA based controller.

5.1.4 Stabilization via Balanced Optical Cross Correlator

By means of a balanced optical cross-correlator (BOC) [102] the timing jitter for femtosecond frequency comb oscillators down to the attosecond regime can be characterized. In this work the BOC was used to synchronize the pulse train of the SESAM EOM laser with a low noise femtosecond laser. Synchronization between femtosecond frequency combs is necessary in the field of frequency and time distribution/transfer to and between (optical) atomic standards.

Here we want to demonstrate the limit in optical stabilization of the SESAM EOM frequency comb to an optical reference laser, which is here the low noise femtosecond laser. The BOC measurement was done in cooperation with the company "Toptica Photonics" [103] at their facilities.

The principle of the BOC measurement is shown in Figure 5-8. Hereby two orthogonal polarized laser pulse trains, one from laser A (e.g. SESAM EOM laser) and one from laser B (e.g. Toptica low noise laser), are injected into a PPKTP (type II) crystal. At the output of the crystal only the light of the SHG pulses pass a dichroic mirror, whereas the fundamental pulses are reflected by this mirror. Hereby the reflected pulses generate another SHG pulse train, propagating into backward direction. This pulse train is again coupled out by another (45° tilted) dichroic mirror. The intensity of the forward and backward propagating SHG pulses is measured each with a photodetector.

The intensity of the SHG pulses depends on the temporal overlap between the orthogonal polarized fundamental pulse trains. The fundamental pulse trains experience a different group delay due to the birefringence of the PPKTP crystal. This means that the overlap between

both pulse trains varies as function of passed crystal length. The backward propagating pulse trains experience twice the relative group delay compared to the forward propagating ones. Due to this fact there is only one temporal offset between both fundamental input pulse trains which leads to the same intensity of the forward and backward propagating SHG pulses.
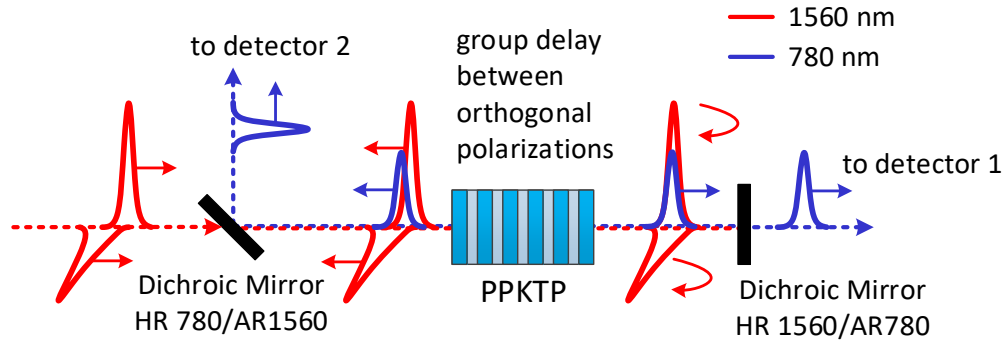
Figure 5-8: Principle of a balanced optical cross correlator [104].

Figure 5-9 shows the signal from the photo diodes when both femtosecond lasers show a slightly different repetition rate. Due to the slightly different repetition rate, a temporal cross correlation signal between both pulses is retrieved. The temporal distance between two consecutive correlated pulses is given by the difference in repetition rate.
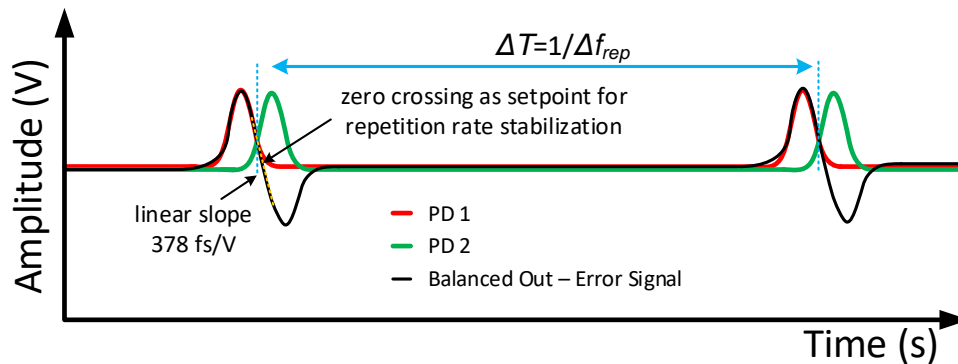
Figure 5-9: Signal of photodetector 1&2 as well as resulting balanced signal for laser stabilization.

By taking the difference between the two photodiode signals, an error signal is retrieved. This error signal has a zero crossing with a linear slope when both diode signals are equal at the same time. This zero crossing was used as set-point to stabilize the pulse train from the SESAM EOM laser to the low noise femtosecond laser. A sensitivity of 378 fs/V was measured for the error signal.
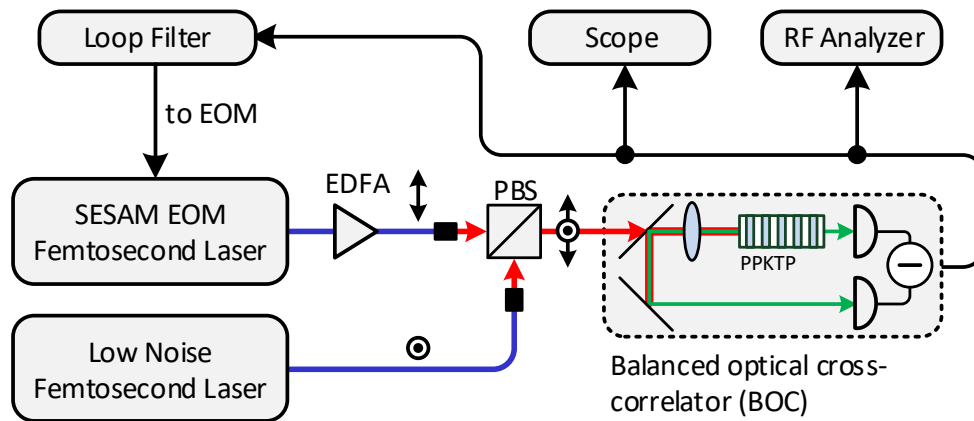
Figure 5-10: Setup to stabilize SESAM EOM laser on low noise comb laser via a balanced optical cross correlator.

The error signal was fed through a loop filter to synchronize the SESAM EOM laser to the femtosecond laser from Toptica (see Figure 5-10). Hereby the repetition rate was controlled via the intra-cavity EOM of the SESAM laser. The in-loop phase noise spectrum of the balanced photo diode signal was measured via a baseband RF-spectrum analyzer.

The in-loop timing jitter noise was obtained by multiplication of the phase noise by the error signal sensitivity (378 fs/V).
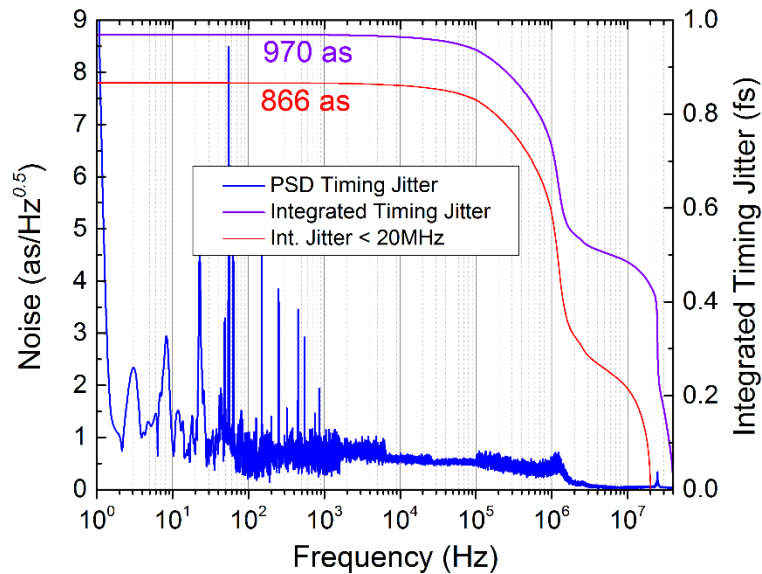
Figure 5-11: In-loop timing jitter of balanced photodetector signal from BOC.

Figure 5-11 shows the spectrum of the in-loop timing jitter noise as well as the integrated timing jitter. A integrated phase noise of 970 as in a bandwidth from 40 MHz (Nyquist) to 1 Hz was obtained. This means that the SESAM EOM oscillator is capable to transfer the

stability of oscillators with a pulse to pulse timing jitter down to the sub-fs range. Unfortunately, the impedance of the loop filter didn't matched to the EOM impedance. This resulted into a small resonance within the noise spectrum at 30 MHz adding some excessive noise of about 100 as. An integrated noise of 866 as was achieved in a bandwidth from 20 MHz to 1 Hz, which excludes the noise of the resonant peak at about 30 MHz.

5.1.5 In-fiber Graphene-Modulator

Graphene modulators were demonstrated as actuators whether to stabilize f_{CEO} or f_{rep} of a frequency comb with a 3 dB modulation bandwidth of up to 2.5 MHz [105]. The graphene modulator consists of a layer of graphene on top of a high reflective surface acting as mirror. The absolute modulation depth of the graphene layer is around 2%, whereas the transmission value of the absorber can be changed by a total maximum of 0.2% by applying an electric field ($\approx \pm 10$ V supply voltage) to the graphene layer. This change is small but has an impact on f_{CEO} and f_{rep}, when used as intra-cavity modulator. The reflective GM suits perfect for a femtosecond laser with a linear cavity such as the SESAM EOM laser. In this thesis an in-fiber graphene modulator was provided by C. C. Lee (University of Colorado, USA), which was implemented in a similar oscillator as the SESAM EOM laser but without an EOM (see Figure 5-12). The repetition rate of this oscillator was 50 MHz.
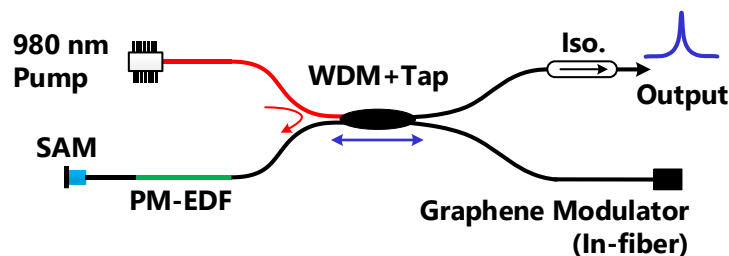
Figure 5-12: Linear cavity SESAM femtosecond oscillator with a graphene modulator for stabilization.

In particular the stabilization of f_{CEO} benefits from the high bandwidth GM to suppress the CEO beats broadband noise. Figure 5-13 shows the setup to stabilize the f_{CEO} via PPM and GM. It was necessary to support the stabilization via PPM, since the modulation depth of the GM is not sufficient to keep the CEO-frequency in lock for more than some seconds. The CEO beat was locked via the FPGA based controller to a signal generator with a frequency of 15.5 MHz. Unfortunately, just one PID element within the FPGA controller was available, which made it difficult to optimize the PLL for PPM and the GM.
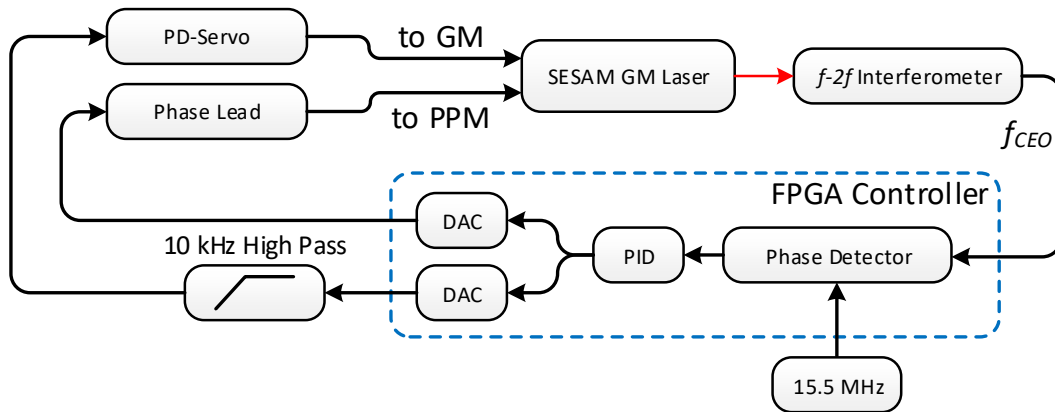
Figure 5-13: Setup to stabilize the CEO beat via PPM and the GM.

Figure 5-14 a, shows the frequency spectrum of the CEO beat when stabilized via PPM and when stabilized via PPM and the GM. A coherent peak was observed when both, PPM and the GM were applied for stabilization. Hereby a feedback bandwidth of 100 kHz for PPM was achieved. This bandwidth was enhanced to 425 kHz when the GM was added for stabilization, this was estimated from the divided CEO-beat in Figure 5-14 b,. Theoretically a five time higher bandwidth could be achieved with an optimized PLL. Nevertheless, here we demonstrate that an in-fiber GM has the potential to improve the performance of the linear cavity SESAM based femtosecond laser but would require development of the FPGA controller.
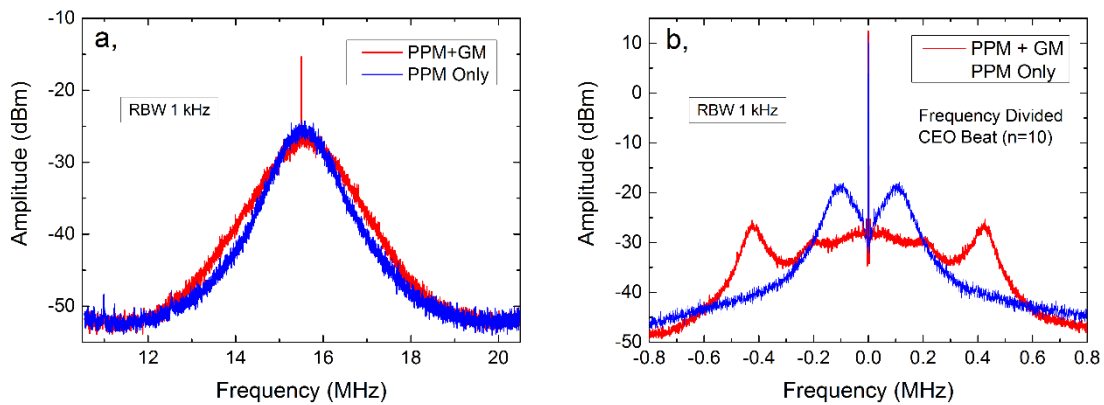
Figure 5-14: Frequency spectra of (a) the original and (b) divided CEO beats, when stabilized with PPM or stabilized via PPM and GM.

5.1.6 Summary

In Table 5-1 the results for the fully stabilized SESAM EOM laser are summarized. A sub-Hz stability for more than 42 hours was shown, while the comb was referenced to the HeNe laser. Hereby the frequency comb shows an in-loop stability better than $1 \cdot 10^{-16}$, which meets the requirements for OAC operation. In this context, a technical reliable, high stable, and long-term operating frequency comb oscillator was successfully demonstrated. These results verify that the SESAM EOM oscillator is a proper candidate for the in-fiber frequency comb module.

Furthermore, the stabilization of the SESAM EOM comb to an ultra-low noise femtosecond laser via a BOC yields to a pulse to pulse timing jitter below 1 fs. Within another SESAM based linear femtosecond laser cavity, the f_{CEO} stabilization via an in-fiber graphene modulator was presented. The GM has a high potential to enhance the feedback bandwidth from some hundreds of kHz to the MHz regime.

	f_{CEO}	f_{opt}
Integrated Phase Noise from 3 MHz – 1 Hz	2.4 rad	1.1 rad
Stabilization Bandwidth	260 kHz	610 kHz
Allan Deviation τ = 1 s (π-Counter)	21 mHz	7.6 mHz
Rel. Allan. Dev. to 473 THz τ = 1 s	$4.4 \cdot 10^{-17}$	$1.6 \cdot 10^{-17}$
Timing Jitter BOC measurement integrated from 40 MHz (20 MHz) to 1 Hz	970 as (866 as)	

Table 5-1: Overview on the stabilization results for the SESAM EOM frequency comb oscillator.

5.2 Tapered fiber CNT laser with integrated EOM

The setup for stabilization of f_{CEO} and f_{opt} is illustrated in Figure 5-15. For f_{CEO} stabilization an AOM (acousto-optic frequency shifter modulator) was selected, since CEO stabilization via PPM was difficult to realize due to a reversal point in f_{rep} and f_{CEO} (see section 4.3.1.2). A voltage controlled oscillator at 80±5 MHz was driving the AOM. The (two channel) home-build digital phase detector was implemented to stabilize f_{CEO} and f_{opt} each to a RF-synthesizer. The two RF-synthesizer were referenced to a rubidium clock. The optical beat note was locked to the HeNe-laser via the intra-cavity EOM.
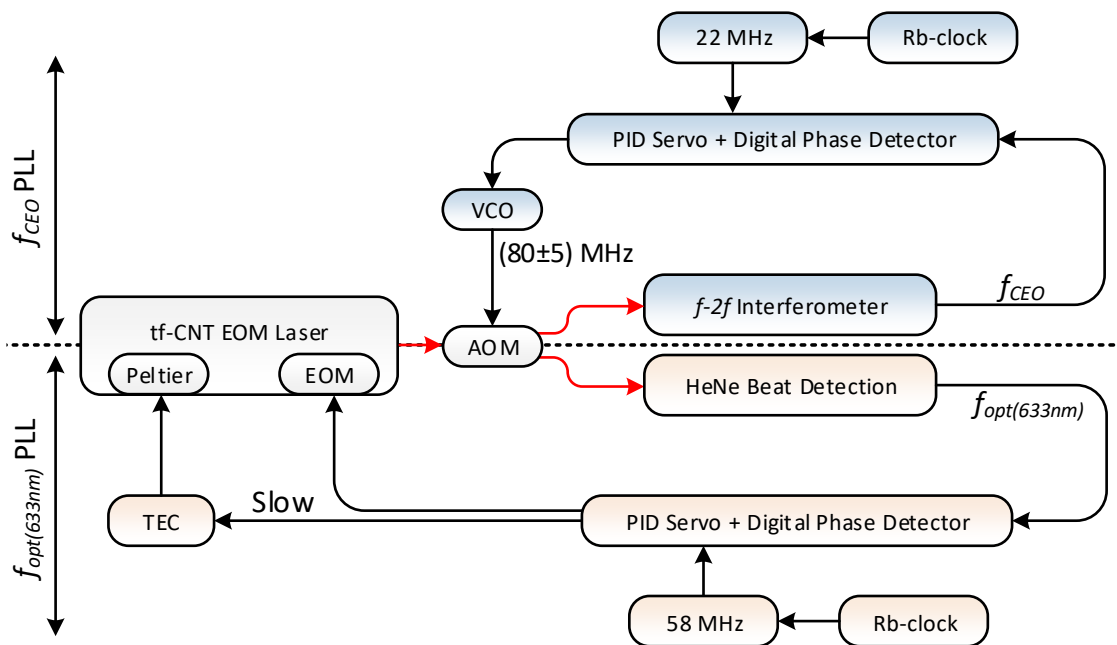
Figure 5-15: Phase locked loops to stabilize f_{CEO} and f_{opt} of the tf-CNT EOM laser.

5.2.1 CEO Beat Stabilization

The frequency spectrum of the CEO beat, while stabilized via the AOM is depicted in Figure 5-16. A coherent peak with a SNR of about 20 dB in a 1 kHz resolution bandwidth was observed. The CEO beat has an integrated phase noise of 1.71 rad (1.63 rad) within 10 MHz (3 MHz) to 1 Hz from the carrier frequency (see Figure 5-17). Further, an in-loop stabilization bandwidth of 121 kHz was estimated from the phase noise measurement.
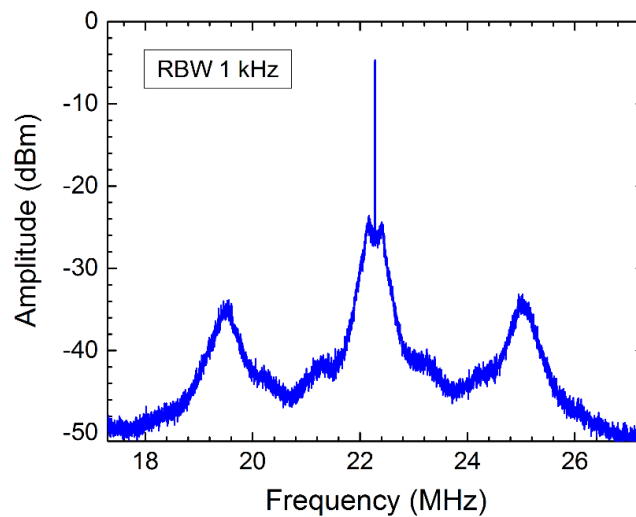
Figure 5-16: Frequency spectrum of phase locked CEO-beat.
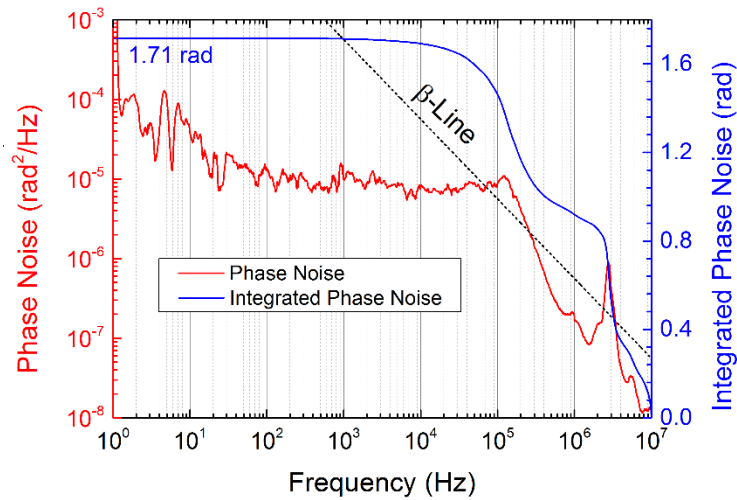
Figure 5-17: Phase noise spectrum and integrated phase noise of the phase locked CEO-beat.

5.2.2 Stabilization to HeNe Laser

In Figure 5-18 the frequency spectrum of the locked optical beat note is illustrated. The coherent optical lock shows a SNR of more than 30 dB in respect to its carrier frequency at 58 MHz.
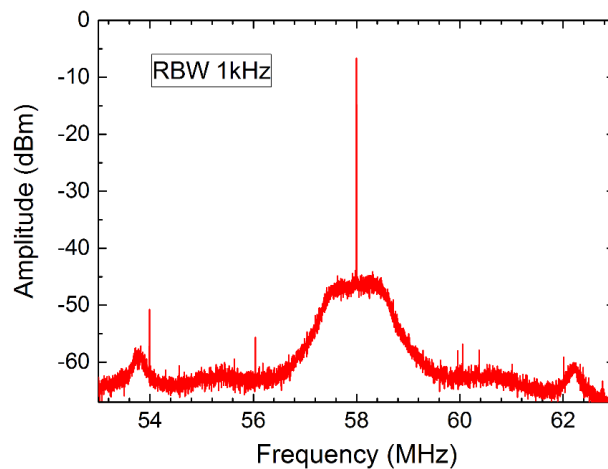
Figure 5-18: Frequency spectrum of phase stabilized f_{opt} beat.

An integrated phase noise of 287 mrad (197 mrad) was determined for the optical beat note in a bandwidth from 10 MHz (3 MHz) to 1 Hz (see Figure 5-19). This is the lowest in-loop phase noise measured within this thesis, which underlies the potential of the tf-CNT laser technology combined with a fast actuator such as an EOM for frequency stabilization. A stabilization bandwidth of 423 kHz via the EOM was reached.
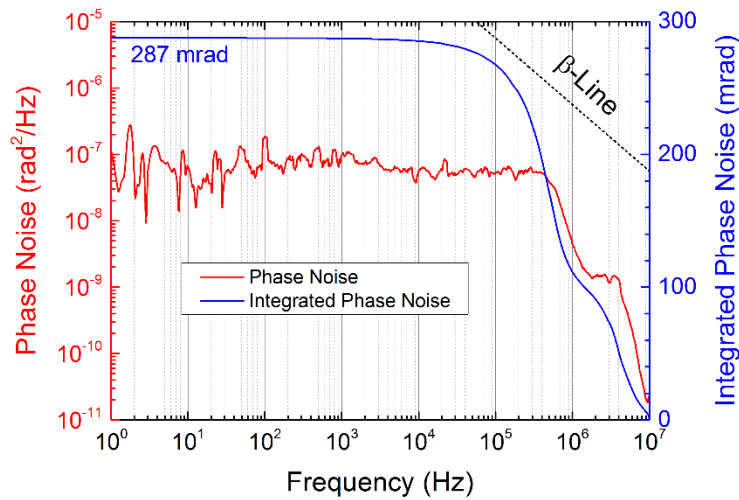
Figure 5-19: Phase noise and integrated phase noise of the optical beat from Figure 5-19.

In Figure 5-20 The optical beat note shows a peak to peak stability better than ±10 mHz for more than 10 hours. Farther, no phase slips were observed during this measurement time. After 10 hours of operation, the stabilization was switched off, since the comb was used for other experiments.
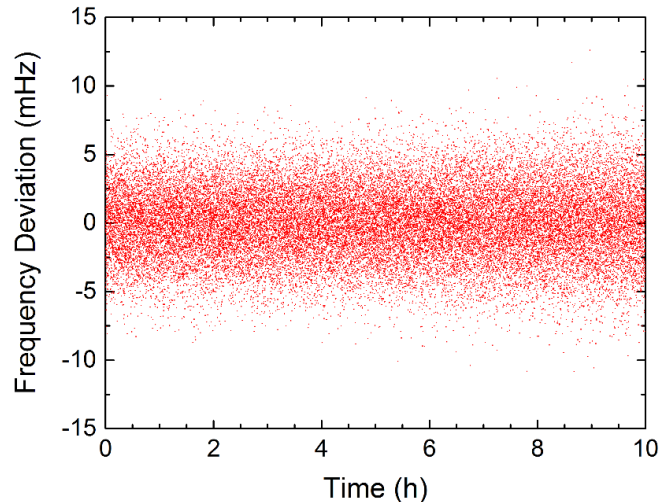
Figure 5-20: Frequency deviation of f_{opt} measured in a gate time of 1 s over an interval of 10 hours.

An Allan deviation of 3.3 mHz (K&K FXE counter) in a gate time of 1 s was estimated from the frequency stability measurements. This is a relative in-loop stability better than 10^{-17} at 1 s in respect to the HeNe lasers frequency. The in-loop Allan deviation decreases with a slope proportional to τ^{-1}.
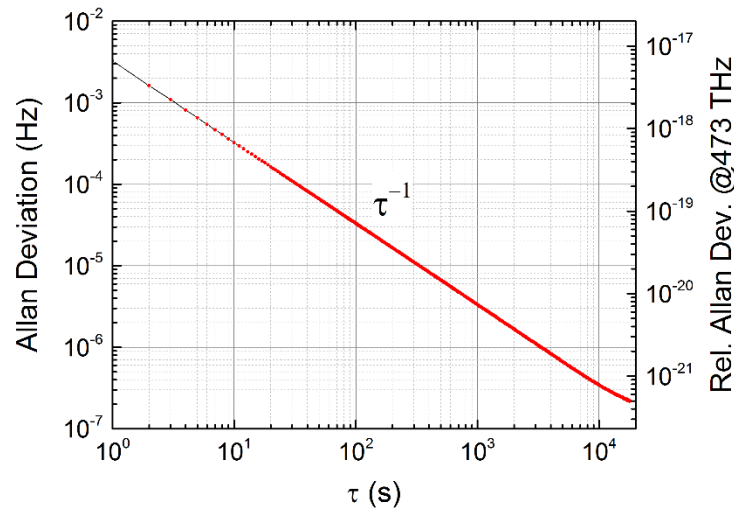
Figure 5-21: Overlapping Allan deviation of the stabilized optical beat.

5.2.3 Summary

An overview on the stabilization results is given in Table 5-2. The stabilization of f_{CEO} and f_{opt} was successfully shown. No frequency stability measurements for f_{CEO} were applied. Due to the small locking range of the EOM (± 5 MHz) it was not possible to maintain a stabilized CEO beat for more than some seconds. It has to be noted that f_{opt} and the CEO-beat were not stabilized simultaneously. Due to the laser degradation no more work was invested to demonstrate a fully stabilized tf-CNT EOM laser. Out of this reason, the goal was not achieved to demonstrate a reliable tf-CNT EOM laser suitable for integration within an in-fiber frequency comb module. Nevertheless, the phase coherent stabilization and phase noise measurement of the CEO- and optical beat indicate a performance, which is sufficient for OAC operation.

	f_{CEO}	f_{opt}
Integrated Phase Noise from 10 MHz (3 MHz) – 1 Hz	1.71 rad (1.63 rad)	287 mrad (197 mrad)
Stabilization Bandwidth	121 kHz	423 kHz
Allan Deviation $\tau = 1$ s (π-Counter)	not measured	3.3 mHz
Rel. Allan. Dev. to 473 THz $\tau = 1$ s	not measured	$6.5 \cdot 10^{-18}$

Table 5-2: Summary of the tf-CNT EOM femtosecond laser stabilization results.

5.3   Tapered fiber CNT laser with Opto-Optical Modulator

The OOM method for frequency comb stabilization was demonstrated for SESAM mode-locked laser systems in the past. Here we investigate the stabilization of f_{CEO} and f_{opt} via the OOM technique applied to a carbon nanotube absorber. Furthermore, the OOM technique is compared to the PPM method for comb stabilization. The setup to stabilize f_{CEO} or f_{opt} via the OOM or PPM method is sketched in Figure 5-22.
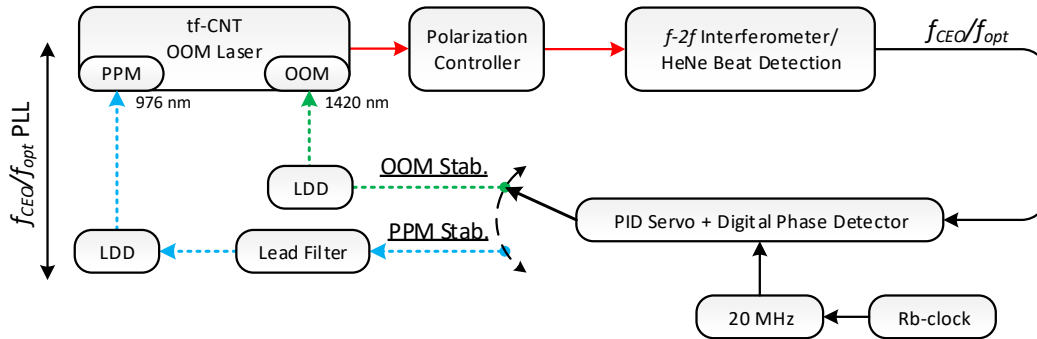
Figure 5-22: Stabilization setup to stabilize the fCEO or fopt beat whether with OOM or PPM, respectively.

A manual polarization controller was required to guarantee a linear input polarization (along the PM fiber's slow axis) for the *f-2f* interferometer and the optical interface at 633 nm (HeNe beat Detection).

Either the f_{CEO} or the CEO beat note was fed into the FPGA based phase detector. Hereby a synthesizer at 20 MHz, which was locked to a rubidium clock, served as a reference. For PPM the servo's output voltage was feed through a lead filter, which was connected to the modulation port of the laser diode driver.

5.3.1   CEO Beat Stabilization

Figure 5-23 a, and b, shows the spectrum of the CEO beat note when stabilized via OOM and PPM, respectively. A phase coherent lock was achieved for both stabilization methods. Hereby, a coherent peak with a SNR of 20 dB for OOM and 15 dB for PPM in a 1 kHz resolution bandwidth was observed. A stabilization bandwidth of approximately 200 kHz was reached for the OOM method, which is about twice as high as the bandwidth for the PPM technique. As consequence the CEO beat showed a lower phase noise when stabilized via OOM.
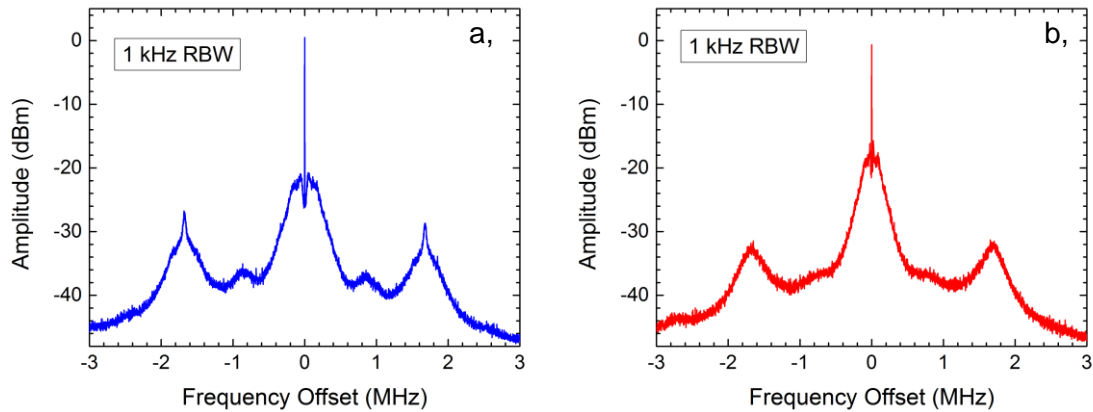
Figure 5-23: Frequency spectrum of the stabilized CEO beat via OOM (a) and PPM (b).

The CEO beat for the OOM method has an integrated phase noise of 1.06 rad (1.04 rad) integrated in a bandwidth from 10 MHz (3 MHz) to 1 Hz (see Figure 5-24). An integrated phase noise of 1.45 rad (1.42 rad) integrated from 10 MHz (3 MHz) to 1 Hz was estimated for the CEO beat, when stabilized via PPM.
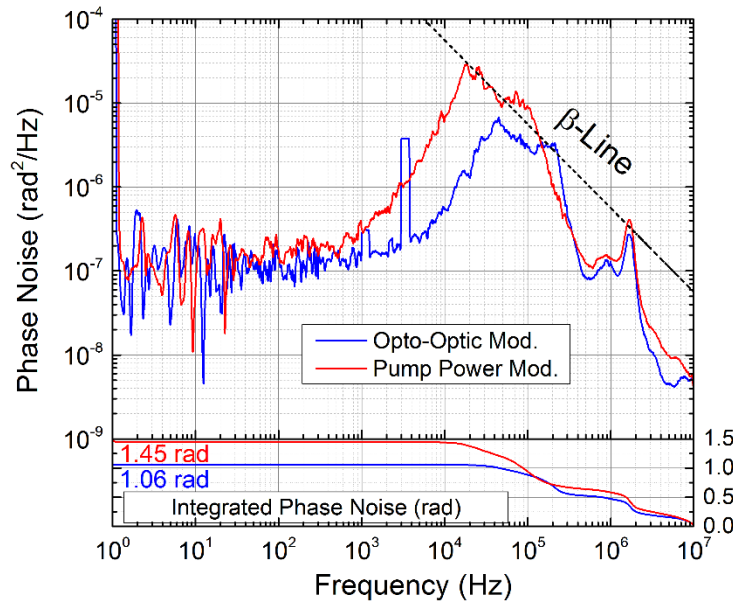
Figure 5-24: Phase noise and integrated phase noise of the phase stabilized fCEO beat via PPM and OOM.

The frequency stability of the CEO beat notes from Figure 5-23 were measured with a Λ-counter (Keysight 53230a) and are illustrated in Figure 5-25. Unfortunately, it was not possible to maintain a phase slip free f_{CEO} lock via PPM for more than one minute. The cause for

this was the limited tuning range of the CEO via PPM, which was just a few MHz (see Table 4-3).
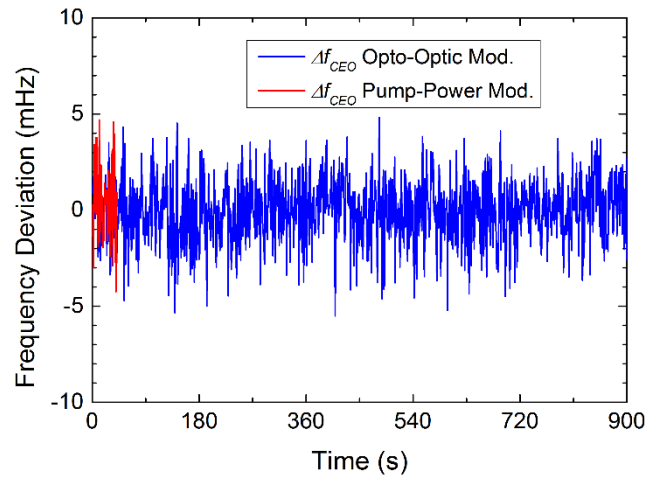
Figure 5-25: Frequency deviation of the CEO beat stabilized via OOM or PPM.

The peak to peak stability for both stabilized f_{CEO} beat notes was below ±5 mHz. Also a similar Allan deviation with about 2 mHz at $\tau = 1$ s for the OOM and PPM locked CEO beat was estimated (see Figure 5-26). The in-loop (modified) Allan deviation decreases with a slope of $\tau^{-0.5}$, which is typical for in-loop stability measurements based on a Λ-type counter.
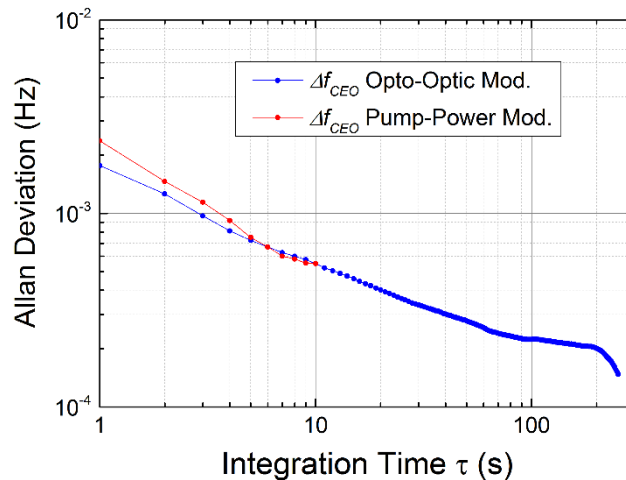
Figure 5-26:Overlapping Allan deviation of the counter measurements presented in Figure 5-25.

5.3.2 Stabilization to HeNe Laser

Despite that the tf-CNT OOM femtosecond oscillator was not actively temperature stabilized nor had any slow actuator such as a fiber stretcher to compensate for a drift in repetition rate, it was possible to stabilize a comb mode to the HeNe laser frequency for some seconds.
In Figure 5-27 a, and b, the frequency spectrum of the optical beat note when, stabilized via OOM and PPM is depicted. A coherent lock with a SNR of about 30 dB (RBW = 1 kHz) in the carrier was obtained for both, the PPM and the OOM lock.
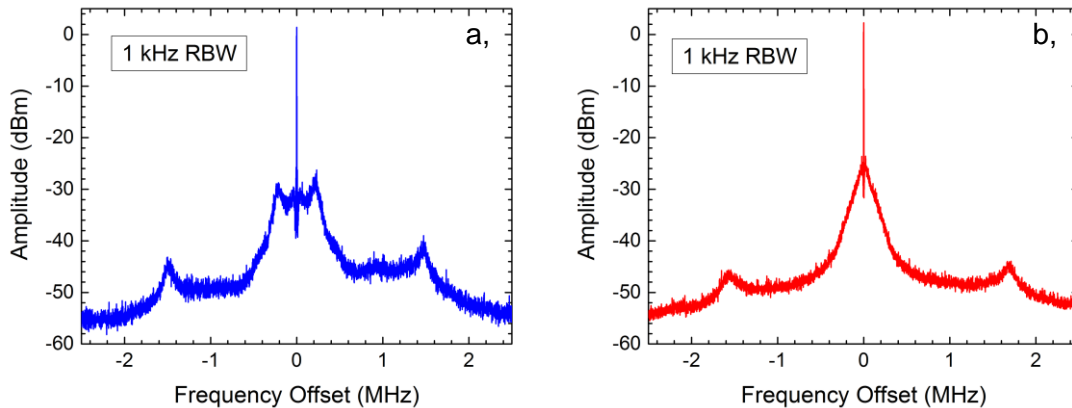
Figure 5-27; Frequency spectrum of the stabilized optical beat note via (a) OOM and (b) PPM.

A sub-rad in-loop integrated phase noise with 467 mrad (449 mrad) and 549 mrad (528 mrad) in a bandwidth from 10 MHz (3 MHz) to 1 Hz was measured for the OOM and PPM stabilized optical beat (see Figure 5-28), respectively.
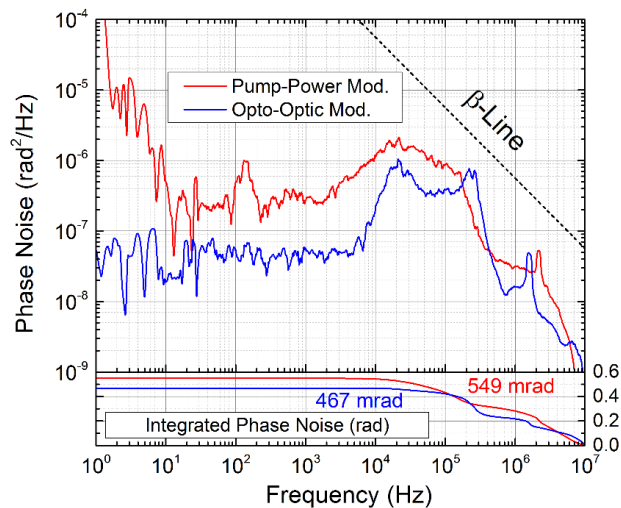
Figure 5-28: Phase noise and integrated phase noise of the phase stabilized fopt beat via PPM and OOM.

Hereby neither the noise spectrum of the OOM or PPM locked f_{opt} frequency exhibits the β-separation line, which is an indication for a sub-rad stability. An overlapping Allan deviation of about 3 mHz (K&K π-counter) at τ = 1 s was observed both for the OOM and the PPM stabilized f_{opt} frequency.

5.3.3 Summary

It was demonstrated that it is possible to stabilize either the optical beat or the CEO frequency of a tf-CNT laser oscillator via the OOM method. A higher feedback bandwidth and lower in-loop phase noise of f_{opt}/f_{CEO} was reached via OOM compared to the PPM approach. Another benefit is, that the OOM shows a wide tuning range for f_{CEO}, showing a high potential for reliable long term stabilization measurements. In conclusion the OOM method for phase coherent stabilization of tf-CNT laser was successfully demonstrated as a proof of principle. Hereby a sub-Hz phase noise and sub-rad stability for the referenced optical beat note and CEO beat depicts the tf-CNT OOM oscillator's potential for OAC applications. The results for the PPM and OOM stabilization are summarized in Table 5-3.

A fully optical stabilized comb to lock f_{opt} and f_{CEO} simultaneously via OOM and PPM could not demonstrated. Hereby, the comb's fixed point measurement indicates a strong crosstalk of about 3:2 between the OOM and PPM method (see section 4.3.2.1). This makes a simultaneous high bandwidth stabilization difficult. A controller would be required to orthogonalize the OOM and PPM feedback loops. The orthogonalization reduces the crosstalk between the OOM and PPM. Furthermore, the utilization of the OOM method for a polarization maintaining CNT based laser would be further step to realize a robust and long-term stabilization.

	f_{CEO}	f_{opt}
Integrated Phase Noise PPM from 10 MHz (3 MHz) – 1 Hz	1.45 rad (1.42 rad)	549 mrad (528 mrad)
Integrated Phase Noise OOM from 10 MHz (3 MHz) – 1 Hz	1.06 rad (1.04 rad)	467 mrad (449 mrad)
Stabilization Bandwidth PPM	102 kHz	162 kHz
Stabilization Bandwidth OOM	210 kHz	266 kHz
OOM/PPM Allan Deviation τ = 1 s	≈ 3 mHz (Λ-Counter)	≈ 3 mHz (π-Counter)

Table 5-3: Overview on the stabilization results for the tf-CNT OOM frequency comb oscillator.

5.4 Laser Comparison and Trade-Off

The stabilization results of the tf-CNT OOM, SESAM EOM and tf-CNT EOM oscillator are summarized in Table 5-4. All these oscillators show a potential for a robust comb system due to their in-fiber design. Nevertheless, only the SESAM EOM femtosecond oscillator fulfilled all requirements for the development of a reliable and compact in-fiber comb module. Thereby the SESAM EOM laser was fully phase locked to the HeNe laser reference for several days, while showing an in-loop stability of some mHz, sufficient to read out a clock laser.

A fully phase locked operation of the tf-CNT OOM and tf-CNT EOM laser could not be realized. Furthermore a degeneration of the tf-CNT EOM laser absorber was observed and a stable long-term linear polarization of tf-CNT OOM was not maintained due to its non-PM design.

	tf-CNT OOM		SESAM EOM	tf-CNT EOM	
Degeneration	No		No	Yes	→ no go
Fully Phase Locked (f_{CEO}+ f_{opt})	No	→ no go	Yes	No	→ no go
Polarization Maintaining	No	→ no go	Yes	Yes	
f_{CEO} integrated phase noise from 1Hz-3MHz (rad)	1.04 OOM	1.42 PPM	2.4	1.63	
Stability f_{CEO} (mHz) @ τ=1 s	≈ 3 (Λ)		21	N/A	
f_{opt} integrated phase noise from 1Hz-3MHz (rad)	0.449 OOM	0.528 PPM	1.1	0.197	
Stability f_{opt} (mHz) @ τ=1 s	≈ 3		7.6	3.3	
Pulse to Pulse Timing Jitter (fs)	-		≈ 1	-	

Table 5-4: Comparison of femtosecond laser oscillators.

Nonetheless, the OOM principle was successfully demonstrated for the tf-CNT OOM laser. Hereby the OOM stabilized CEO-beat of the tf-CNT OOM laser shows the lowest phase noise in respect to the other two oscillators. Furthermore, the best performance for the optical stabilization of a comb mode to the HeNe laser was achieved via tf-CNT EOM laser resulting to an integrated phase noise of just 197 mrad. In comparison to the SESAM laser, a lower phase noise was achieved for the referenced CEO and optical beat notes of the CNT lasers. This points out, that CNT based femtosecond lasers have still a high potential to replace SESAM lasers while having a better performance. Technical issues such as the degradation of the absorber and the reversal point, which prohibit a fully phase locked long-term stabilization could highly probably be solved by an improved design.

6   Measurement Application – G-Laser Stabilization

In this chapter the characterization (section 6.1) and stabilization (section 6.2) of the gyro-scope laser at the Geodatic Observatory Wettzell is presented. In this context the SESAM EOM oscillator with the setup from section 5.1 was utilized as a measurement tool.

Until now, the big "G" ring laser is the most precise instrument to measure the Earth rotation inertial with a usable sensitivity of 12 prad/s/√Hz. With the G ring laser, measurements of the polar motion, solid Earth tides, the Annual and the Chandler wobble as well as local tilts have been successfully detected. These results are a fundamental input for applications and scientific studies within the field of seismology, geodesy and geophysics [21].

The goal in this work was to measure the ring laser's free running frequency stability and to stabilize the G laser to an active H-maser reference. With the help of a hybrid stabilization approach, drifts of the ring laser frequency shall be compensated, while the laser's stability and low frequency noise are transferred to the frequency comb. A compensation in the ring laser frequency drift leads to a reduction in the drift and so in the uncertainty in measurements of physical effects related to variations in the Earth rotation.
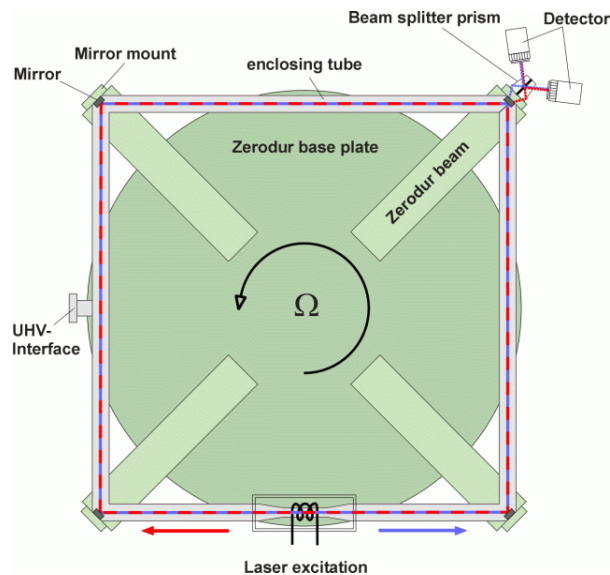
Figure 6-1: Ring laser setup [107].

In Figure 6-1 a sketch of the G laser is shown. Each side of the laser cavity has a length of 4 m which defines a free spectral range (FSR) of 18.75 MHz and an enclosed area of 16 m^2. The laser cavity is mounted on a massive Zerodur plate to provide a high mechanical stability and zero thermal expansion properties. Two laser beams propagate trough the laser cavity, one in clockwise (CW) and the other in counter clockwise (CCW) direction. Due to the earth rotation the laser frequency of both beams experience a Doppler shift. Hereby the sign of the

Doppler shift depends on whether the beam is propagating against or with the earth rotation. The frequency difference between the CW and CCW beam is called Sagnac frequency. By superimposing the CW and CCW laser with a beam splitter and a photo detector at the output of one of the four cavity mirrors the Sagnac frequency is estimated. The Sagnac frequency of the G is about 348.5 Hz and is given by [107]:

$$\sigma f = \frac{4A}{\lambda_G P} \vec{n} \cdot \overline{\Omega}$$

(6.1)

Where A is the enclosed area of the ring laser geometry, P is the optical beam path length, λ_G is the optical wavelength in vacuum (here 632.8 nm), $\vec{n}$ is the normal vector to A and $\overline{\Omega}$ is the rotation vector. The center frequency of the ring laser is estimated by an optical reference which is here a referenced optical frequency comb or an iodine stabilized HeNe laser.

6.1 Characterization Measurement

In this section the free running ring laser frequency is measured. Hereby, the stability of the ring laser is measured in the optical domain via a commercial frequency comb (Menlo-Systems FC1500) and simultaneously measured in the radio frequency domain by the SESAM EOM comb. By means of this measurements, the SESAM EOM comb property as an (optical) frequency divider is demonstrated.
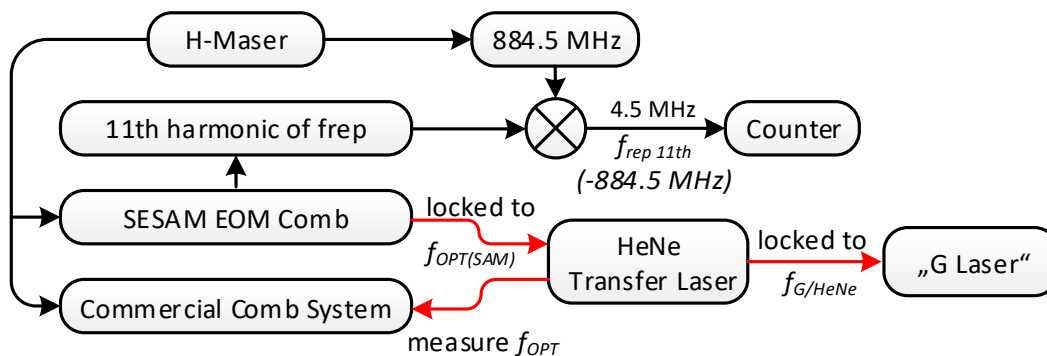
Figure 6-2: Setup to measure the G laser free running frequency stability.

The setup of the free running G's frequency stability is sketched in figure 6-2. The same HeNe laser, which is depicted in figure 3-2, was used as a transfer laser. As indicated by the name, the HeNe laser transfers the frequency of the ring laser to the SESAM EOM comb or further devices such as to the FC1500. The HeNe laser's output light is phase locked to the longitudinal mode of the ring laser's CCW beam by using an acousto-optic modulator. The

frequency offset lock had a fractional in-loop Allan deviation of $3 \cdot 10^{-18}$ @ $\tau = 1$ s, which is about 5 orders better compared to the stability of the H-maser and ring laser frequency. It was not possible to use the light directly from the ring laser for frequency comb measurements. This is because the output power of each G's cavity mirror is quite low (about 10 nW), to generate an optical beat between a comb line and the laser line with an adequate SNR.

A comb tooth of the SESAM EOM laser was optically locked to the HeNe transfer laser such as it is illustrated in section 5.1.2. Hence, the comb tooth follows the frequency drift of the G laser, also the comb repetition rate follows the ring laser frequency in a quasi-proportional manner. For this reason the ring laser frequency drift was estimated by measuring the comb repetition rate. The fundamental repetition rate is given as:

$$f_{rep} = \left(v_G - f_{opt} - 2f_{CEO} \right) / n_G \tag{6.2}$$

Where v_G is the ring laser frequency and n is the mode number of the referenced comb tooth. Hereby f_{opt}, f_{CEO}, n is fixed due to the comb stabilization to the ring laser. Here the 11th harmonic of the comb's repetition rate $f_{rep\,11}{}^{th}$ was measured in order to determine the change in the ring laser's frequency.

The 11th harmonic of the comb repetition rate $f_{rep\,11}{}^{th}$ was detected via an InGaAs photodiode and filtered by a SAW (Surface Acoustic Wave) bandpass filter at about 880 MHz. The harmonic signal was mixed down to about 4.5 MHz using a double balanced mixer and a local oscillator signal at 884.5 MHz. The sinusoidal signal at 884.5 MHz was generated by a synthesizer, which was referenced to the H-maser. It was necessary to mix down the frequency to 4.5 MHz, since the counter is only able to measure frequencies up to 350 MHz.

The 11th harmonic of the repetition rate instead of the fundamental was used for measurements, since it has a lever which is eleven times stronger to absolute changes in frequency compared to the fundamental repetition rate. Nevertheless, the fractional change in frequency is for all harmonics the same.

By the use of the down-mixing technique, the measurement resolution was enhanced. Let's assume that a relative stability of $1 \cdot 10^{-13}$ (@$\tau = 1$ s) needs to measured, which cannot be resolved by our frequency counter having a limit of about $1 \cdot 10^{-12}$ (@$\tau = 1$ s). A stability of 10^{-13} would mean that a frequency deviation less than 88 µHz needs to be determined at 880 MHz. However, the down mixed signal at 4.5 MHz experiences the same absolute shift in frequency. This results in a relative stability of 88 µHz/4.5 MHz = $\underline{1.96 \cdot 10^{-11}}$, which yet can be resolved by the counter itself.

On the other hand, the frequency stability was measured in the optical domain by the FC1500 comb. The FC1500's f_{rep} and f_{CEO} were referenced to the H-maser standard, leading to a fixed optical ruler. Hereby an optical beat $f_{opt(FC1500)}$ signal between a comb tooth and the HeNe transfer laser was generated. The change in frequency of the optical beat equals the drift in

the G's frequency. The optical beat was measured with a frequency counter (K&K FXE), which was included in the FC1500's hardware.
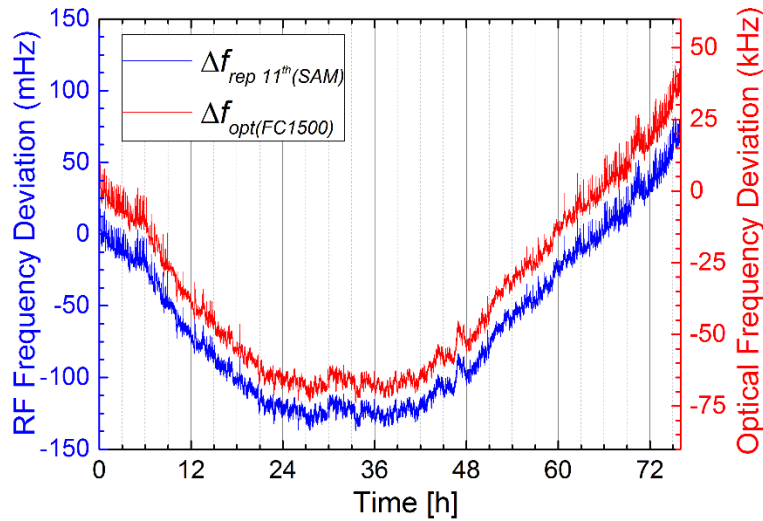
Figure 6-3: Change in the SESAM EOM's harmonic repetition rate (blue curve) and change in the G's frequency (red curve) as a function of time.

In figure 6-3 the change in the 11th harmonic of the SESAM EOM comb's repetition rate $\Delta f_{rep\ 11}{}^{th}$ and the change in the optical beat frequency $\Delta f_{opt(FC1500)}$ is shown as a function of time. The left and right y-axis were slightly offset, so $\Delta f_{opt(FC1500)}$ and $\Delta f_{rep\ 11}{}^{th}$ can be distinguished from each other. Hereby the change in $\Delta f_{opt(FC1500)}$ and $\Delta f_{rep\ 11}{}^{th}$ show a very similar behavior. The ring laser's frequency ($\Delta f_{opt(FC1500)}$) varies less than 75 kHz during an observation time of 75 h, whereas the repetition rate has a frequency excursion less than 150 mHz. The relation between $\Delta f_{rep\ 11}{}^{th}$ and $\Delta f_{opt(FC1500)}$ is given by:

$$n_G\!\!\Big/\!\!{}_{11} \cdot \Delta f_{rep11^{th}} = n_{11} \cdot \Delta f_{rep11^{th}} \approx \Delta f_{opt(FC1500)} \tag{6.3}$$

In Figure 6-4 n_{11} was calculated by the ratio between $\Delta f_{opt(FC1500)}$ and $\Delta f_{rep\ 11}{}^{th}$, whereas the measurement of $\Delta f_{opt(FC1500)}$ and $\Delta f_{rep\ 11}{}^{th}$ is depicted in figure 6-3. As result, a value of 540122 with a standard deviation of 3459 was determined for n_{11}. The relatively high standard deviation results from the fact that $f_{opt(FC1500)}$ and $f_{rep\ 11}{}^{th}$ were measured with two different frequency counter types, whereas each counter uses internally another algorithm to calculate the frequency. Further, both frequency counters were not synchronized and had a different time interval settings. Counter 1 (K&K FXE) measured the frequency within a gate time and time interval of 1 s. On the other hand counter two (Keysight 53230a) measured the frequency each 3 s with a gate time of 1 s.
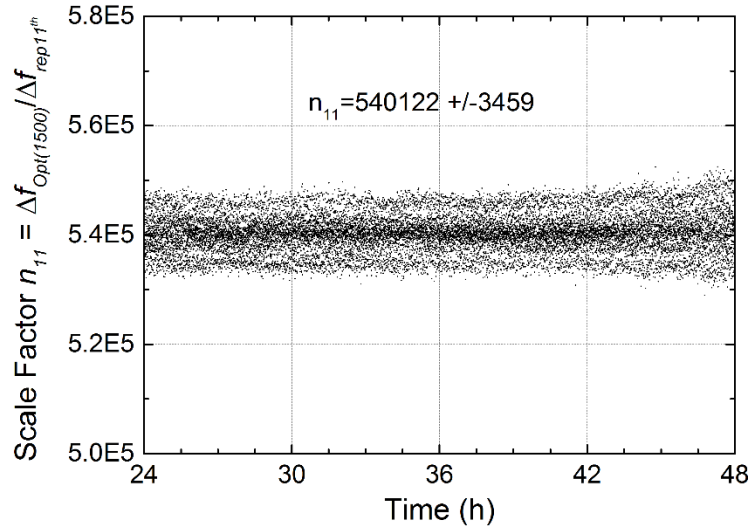
Figure 6-4: Divison factor n11 estimated from the ratio between $\Delta f_{opt(FC1500)}$ and $\Delta f_{rep11th}$ derived from Figure 6-3.

The division ratio n_{11}, which is the number of the SESAM EOM comb modes at the transfer laser's frequency divided by a factor of 11 was also estimated as follows:

$$
\begin{aligned}
n_{11(II)} &= \frac{v_G - f_{CEO(SAM)} - f_{OPT(SAM)} + f_{G/HeNe}}{11 \cdot f_{rep(SAM)}} \\
&= \frac{473.612701 THz - 21MHz - 14MHz + 15MHz}{11 \cdot 79.99985007 MHz} = 538197
\end{aligned}
\tag{6.4}
$$

With: $v_G = $ G laser's frequency, $f_{CEO(SAM)} = $ CEO frequency of SESAM EOM comb, $f_{OPT(SAM)}$ = optical beat frequency between HeNe transfer laser and comb, $f_{G/HeNe}$ = beat frequency between HeNe and G laser, $f_{rep(SAM)}$ = repetition rate of comb. The initial G's frequency was estimated by the FC1500 comb in another measurement. Since, all values in equation (6.4) were well known, the error in $n_{11(II)}$ is less than one comb mode. As result $n_{11(I)}$ agrees within one standard deviation with $n_{11(II)}$, which underlies the SESAM EOMs comb's basic function as a harmonic optical frequency divider.

6.2 Hybrid Stabilization

The stationary comb system FC1500 at the geodetic observatory Wettzell was used to reference the G ring laser to a H-maser. This technique helps to improve the ring laser's performance in the mid-term to long-term view due to the compensation of the laser's frequency drift [106].

One goal was to establish a hybrid stabilized comb system, which benefits from the short time stability ($\tau < 2$ s) of the ring laser as well as from the long term stability of the H-maser. Hereby the setup for the hybrid stabilization (see Figure 6-2) was very similar to the one shown in the section before (see Figure 6-2). The SESAM EOM comb is optically locked to the G laser via the HeNe transfer laser. As result, the SESAM EOM comb mode overtakes stability of the ring laser. In order to stabilize both, the comb and ring laser to the H-maser, an error signal was generated by comparing the 11th harmonic of the SESAM EOM comb against a synthesizer at 880 MHz using an analogue phase detector. The error signal voltage was fed into a slow servo controller to generate a feedback signal. This signal was applied to two of the piezo mounted mirrors of the G laser to control its frequency. Further, the ambient pressure of the ring laser was controlled to maintain long-term operation and keeping the piezos within working range. To achieve this, the ambient pressure set-point was changed after the voltage at the piezo reached a certain threshold. The servo itself was implemented within a LabView based software.
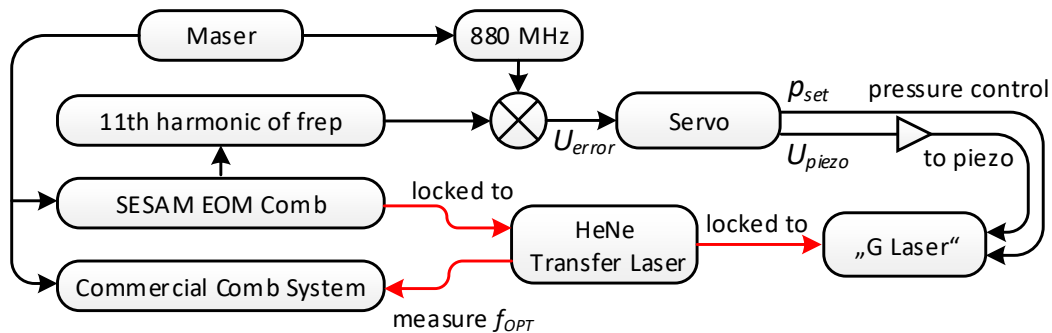
Figure 6-5: Hybrid stabilization of the ring laser and the SESAM comb laser.

The frequency stability of the ring laser was measured out-of-loop with the FC1500 comb and is illustrated in Figure 6-6 a. The ring laser showed a stability of 206 Hz ($\tau = 1$ s) during a period of about 18 h. No outlier were observed during this period. The Allan deviation of the hybrid stabilized and free running G-ring laser is depicted in Figure 6-6 b. Hereby, the Allan deviation of the free running laser was derived from the measurement of the optical beat between the FC1500 comb and the ring laser shown in Figure 6-3 (red curve). Further, the projected and specified Allan deviation of the H-maser reference is illustrated in Figure

6-6 b. The H-maser stability was estimated in another experiment, whereby the H-maser's signal was compared against a cryogenic sapphire oscillator [108].

The Allan deviation of the hybrid stabilized laser starts at 6 10^{-13} ($\tau = 1$ s), which is about twice the value of the free running ring laser at an integration time of 1 s. However after an integration time of 2.5 s the referenced ring laser starts to outperform the free running laser. The worse performance at integration times lower than 2.5 s is probably caused by the noise of the high voltage piezo amplifier. The bump at an integration time of 265 s was caused by the pressure stabilization. Towards a longer integration time a minimum fraction Allan stability of 5.4 10^{-16} ($\tau = 16384$ s) was reached. Hereby the ring laser's stability is limited by the H-maser's performance itself.
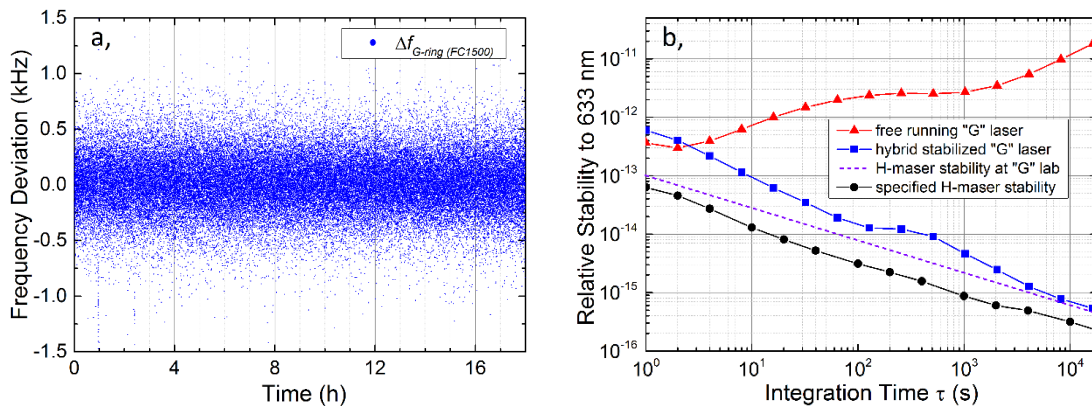
Figure 6-6: (a) Out-of-loop relative frequency stability of the hybrid stabilized "G" ring laser as well as (b) Allan deviation for the free-running and stabilized ring laser and for the H-maser.

The goal was to measure the ring laser free running stability and to reference the ring laser frequency to an active H-maser to improve its mid- to long-term measurement performance of physical effects related to earth rotation.

As result, the comb adopted the short-term stability of the ring laser while showing the stability of the H-maser by applying a hybrid stabilization approach. Hereby, the hybrid stabilization scheme leads to a significant reduction of the ring laser drift by more than four orders of magnitudes (see Figure 6-6 b, red vs blue curve), which yields to a potential improvement in the measurement of physical effects.

Furthermore, the optical lock to the narrow linewidth ring laser allows the comparison to an ultra-stable cavity referenced laser. By this comparison the short-term stability of the G-laser could be determined, which is expected to be below the stability of the H-maser.

7 In-Fiber Frequency Comb

The idea on the development of an-in fiber comb system was to reach a higher technical readiness level [109] towards future space borne payloads. Due to this, the SESAM EOM oscillator was equipped with an optical in-fiber module to detect the CEO beat frequency. The fiber optical setup was integrated within a compact and temperature controlled mechanical housing. Hereby, the in-fiber comb module was stabilized to an optical reference for several days to demonstrate its reliable operation with a performance sufficient for utilization in the field of optical atomic clocks. On the basis from this in-fiber design, the gained experience and knowledge builds a solid fundament for:

- work on system level basis in co-operation with potential partners in the photonics sector
- and subsequent development steps such as environmental tests (cosmic radiation, thermal-vacuum, mechanical vibrations, end of life tests) as well as critical component tests (Erbium doped fiber, optical isolators).

The all-in-fiber design is described in section 7.1. The characterization and insight on the optical interfaces is given in section 7.2 In section 7.3 the stabilization of the in-fiber comb is demonstrated.

7.1 Optical Setup

A scheme of the in-fiber optical setup is illustrated in Figure 7-1. The setup consists of the SESAM EOM femtosecond oscillator (see Figure 3-1 a,) and an optical interface (*f-2f* interferometer) to generate and detect the CEO beat signal.
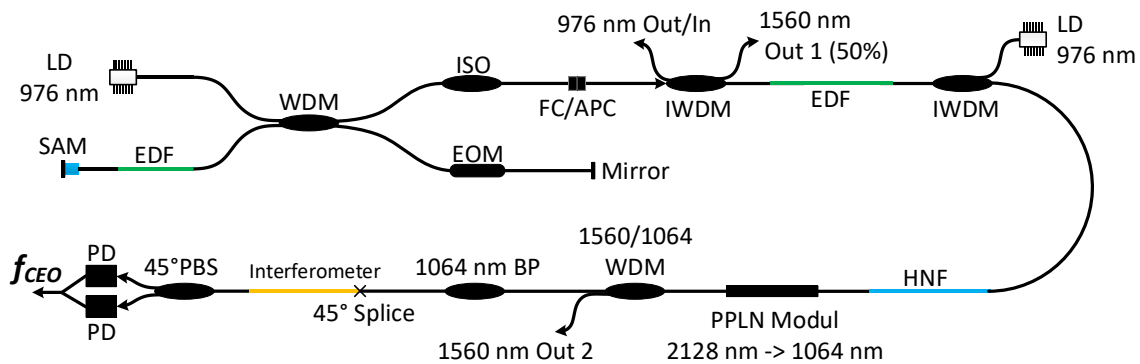
Figure 7-1: In-fiber frequency comb setup.

Hereby the *f-2f* interferometer is similar to the design from NIST [1, 101], which was demonstrated for the first time in-fiber frequency comb in the year 2014. The *f-2f* interferometer has the same functional configuration such as explained in Figure 3-3. The oscillator pulses are amplified within an Erbium doped fiber amplifier. After that, the pulses are temporally compressed in a standard PM fiber. Consequently, a highly nonlinear fiber (Sumitomo, λ_{ZDW} = 1492 nm) is seeded with the short femtosecond pulses to generate a supercontinuum with a dispersive wave pulse at 1064 nm and a soliton pulse located at 2128 nm. Hereby, the soliton pulse was frequency doubled in a fiber coupled waveguide PPLN (NTT, WH-1064-000-F-B-C). Space-environmental tests of this PPLN type promise reliable operation [110]. Most of the light above 1.7 µm is not transmitted by the PPLN towards the output. Further, light at 1560 nm (-200 nm/+100 nm) is coupled out via a WDM (1064/1560). The residual light is filtered by a 1064 nm (+/- 2 nm) bandpass filter. Within an inline interferometer the temporal delay of the fundamental dispersive wave pulse from the SC and SHG pulse at 1064 nm is compensated. Without an temporal overlap between the SHG and fundamental pulse no CEO beat would be observed. Hereby the delay is compensated by projecting the pulses to both, the slow (50%) and fast axis (50%) of a standard PM fiber. Due to the birefringence ($\Delta n_{ref} \approx 10^{-4}$) of the PM fiber, the pulses in the fast and slow axis experience a different group velocity, which allows for time delay compensation (please see [1] for a detailed description). At the inline interferometer's end a 45°degree polarization beam splitter is projecting the light from both axis whether on the slow axis (output port 1) or fast axis (output port 2).
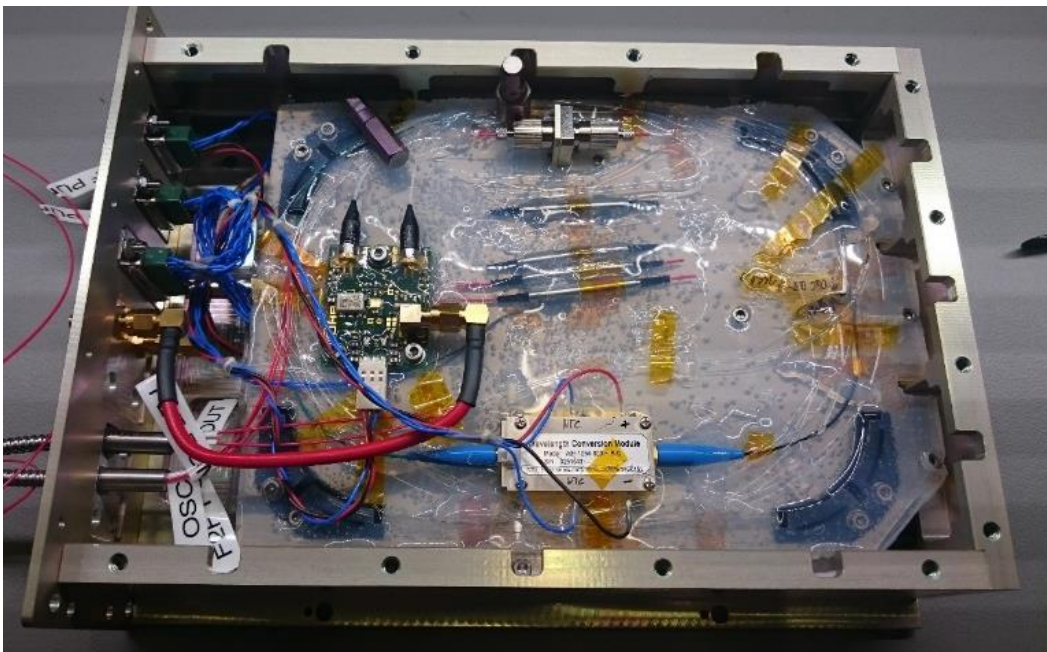
Figure 7-2: All-in-fiber frequency comb module.

The light from both output ports was measured via two balanced InGaAs photodiodes. The CEO beat frequency was obtained from the signal of both photodetectors. On the top, fiber optical components such as WDMs, the waveguide PPLN module can be distinguished from the *f-2f* assembly. Further a balanced photodetector board was integrated on the aluminum plate. The fiber optical components were covered by a 5 mm thick conformal coating (Dow Corning 3140) to enhance the setup's robustness against thermal fluctuations and mechanical vibrations such as acoustic noise. The module has several electrical connections (SMA or Sub-D connectors) for temperature sensors, Peltier elements (oscillator and PPLN), the EOM's modulation port as well as for the balanced photodetector board.

The optical module has a size of (69.9x251x189.6) mm and a weight of 2.8 kg (Figure 7-3). A modular approach was chosen to guarantee a high flexible setup, which could be customized depending on the application. The idea hereby was to integrate the optical module together with other electrical or optical modules in a hardware mainframe (see Figure 7-3). These modules could be laser diode drivers, temperature controllers, optical frequency conversion device or a FPGA based control unit for phase stabilization.
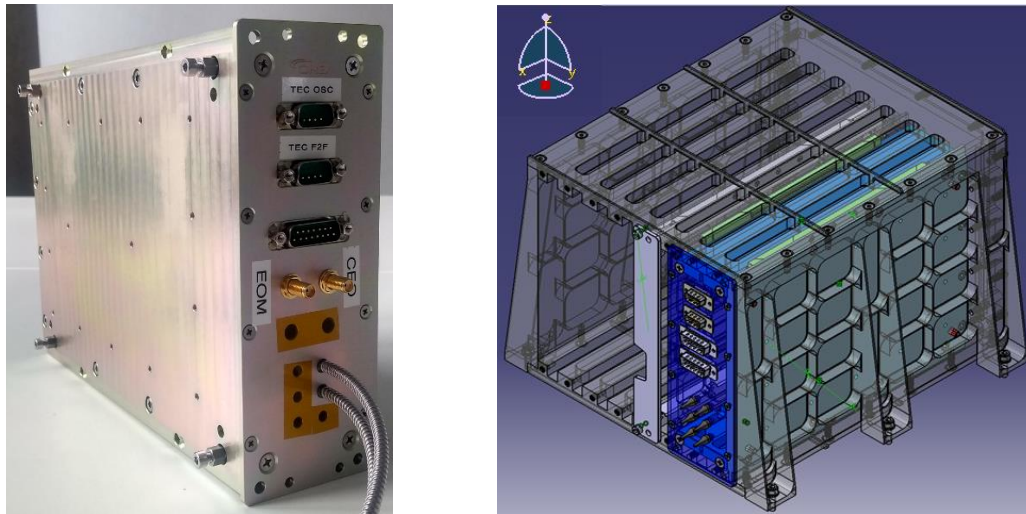
Figure 7-3: All-in-fiber frequency comb module (left) and mainframe for frequency comb module (right).

7.2 Interface for CEO-Beat Detection
7.2.1 Amplification and Pulse Compression

Two different PM Erbium doped fibers, with an peak absorption of 50 dB/m at 1530 nm (EDF50, D = -25 ps/(nm·km)) and 30 dB/m @1530 nm (EDF30: IXF-EDF-FGL-PM-S013, D = -7 ps/(nm·km)) were studied for the *f-2f* interferometer's amplifier. The EDF50 fiber has

a proper balance between gain, nonlinearity and dispersion to allow a fast asymptotic convergence towards parabolic pulse amplification such as shown in the simulation in Figure 2-16. However, due to the EDF50 fiber's elliptical core, low loss splicing to the standard PM fiber was difficult to achieve. Furthermore the high peak absorption required bi-directional pumping of the EDF50 (3.3 m fiber length) fiber to avoid a rapid depletion of the pump power along the Erbium fiber. In addition, high gain fibers tend to have a significant ASE level within the first centimeters of the gain fiber. This due that the weak input seed light only converts a part of the Erbium fiber excited population state into stimulated emission.

The balance between the EDF30's gain, nonlinearity and dispersion was not perfect to achieve parabolic amplification. In particular the dispersion of the EDF30 fiber is low and fringes in the simulated optical spectrum were observed, which probably were caused due to self-phase modulation. Nevertheless, due to the lower gain it was sufficient to pump the EDF30 fiber with just one pump diode at 976 nm in backward direction. Furthermore, due to the normal dispersive Erbium fiber, no pulse break up was observed during the amplification process. The EDF30 amplifier was used within the in-fiber comb design due to its lower power consumption, which is an important driver for spaceborne payload. An average output power of up to 293 mW was reached for the 4.5 m long EDF30 fiber (see Figure 7-4).
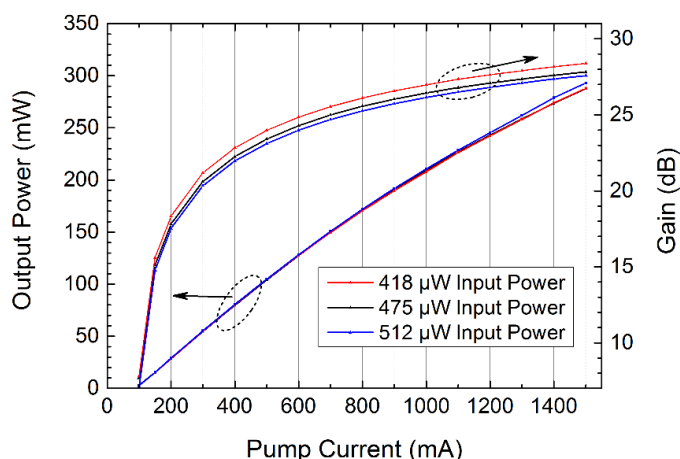
Figure 7-4: Output power and gain of the EDF30 amplifier as a function of the pump laser's current.

The 976 nm pump diodes, which were used for the amplifiers had a maximum output power of 1 W at a supply current of 1.5 A.

In Figure 7-5 the output spectrum for the EDF50 (a, b,) and EDF30 (c) amplifier is shown. The spectrum in a, was measured after the pulse propagated in about 50 cm of standard PM fiber (Fujikura, PM15-U25A) (including the WDM's fiber), which was spliced to the EDF. Through the self-similar amplification process, the seed pulse evolves from a sech-like spectral shape with a FWHM of 6 nm to a parabolic shaped spectral pulse with a FWHM of

40 nm. A bandwidth of 40 nm is sufficient to generate sub-100 fs pulses for supercontinuum generation.
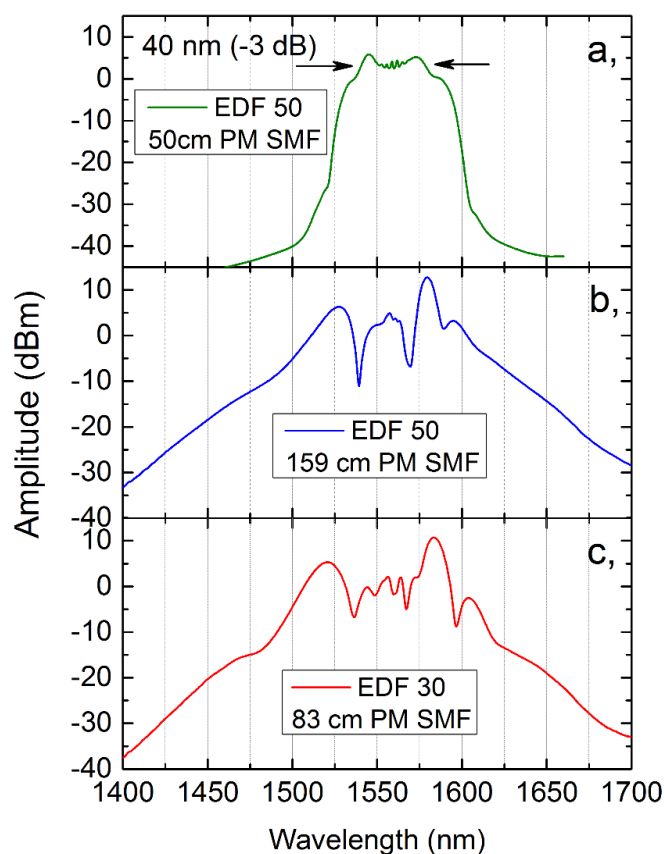
Figure 7-5: Pulse spectrum after (a, b) the EDF50 and (c) EDF 30 amplifier.

After a propagation of 159 cm in the standard PM fiber, the pulse was compressed down to 55 fs. The spectrum and associated autocorrelation measurement is depicted in Figure 7-5 b, and Figure 7-6 (blue curve).

Furthermore, the spectrum and autocorrelation for the compressed pulses from the EDF30 amplifier is shown in Figure 7-5 c, and Figure 7-6 (red curve). Hereby a pulse length of 42 fs was achieved. In comparison to the EDF50, the compressed pulses from the EDF30 have a worse ratio (~50%) between the pulse's energy located in the central part in respect to the energy, which is located in the higher order solitons (side-lobes). Nevertheless, the compressed pulses from the EDF30 amplifier show sufficient energy to generate a supercontinuum within the highly nonlinear fiber.
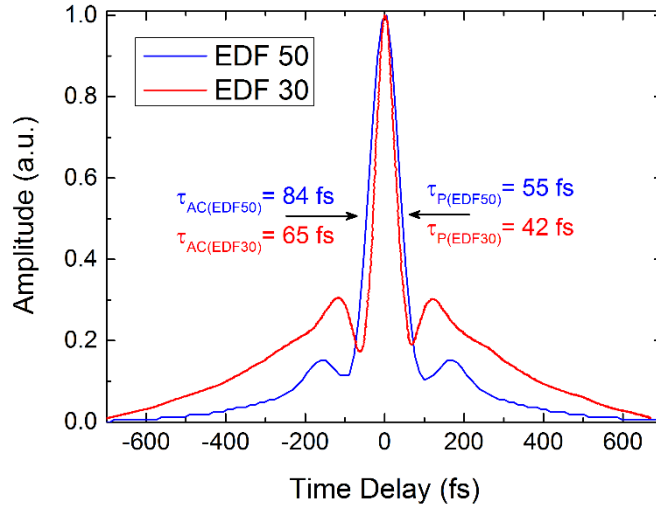
Figure 7-6: Intensity Autocorrelation of the temporal compressed pulses.

7.2.2 Supercontinuum Generation and CEO Beat Detection

In Figure 7-7 the supercontinuum generated within the HNF as a function of the EDF30 amplifier pump current is depicted. This supercontinuum was optimized so that the dispersive wave pulse and soliton pulse had it maximum spectral power at 1064 nm and 2128 nm, respectively.
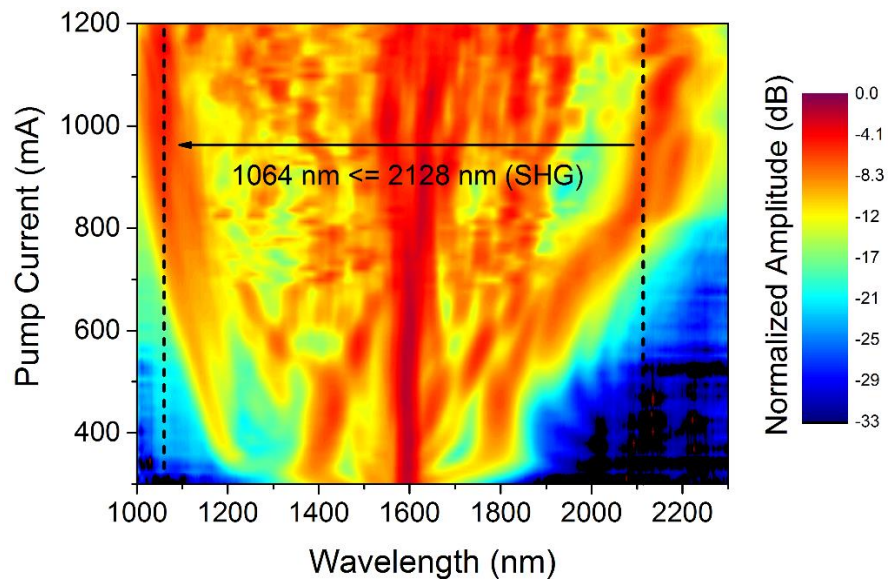
Figure 7-7: Optical spectrum after the highly nonlinear fiber as a function of pump current from the amplifier's pump laser.

In this context, the best results were obtained with a 313 mm long HNF fiber despite a supercontinuum was generated even with 5 centimeters of HNF. Within a pump current ranging

from 800 mA to 1000 mA the soliton and dispersive wave pulse were located at 2128 nm and 1064 nm. This means that the amplifier's pump power could vary in this range, while still maintaining a CEO beat signal. Same also accounted for the oscillator output power. The CEO beat signal kept stable in amplitude and SNR, while the oscillator's set-point was varied. About 50 µW of average power (at 1064 nm) reached each photodiode of the balanced detector board. A CEO beat with a SNR of about 33 dB was obtained from the balanced photodetector signal (see Figure 7-8).
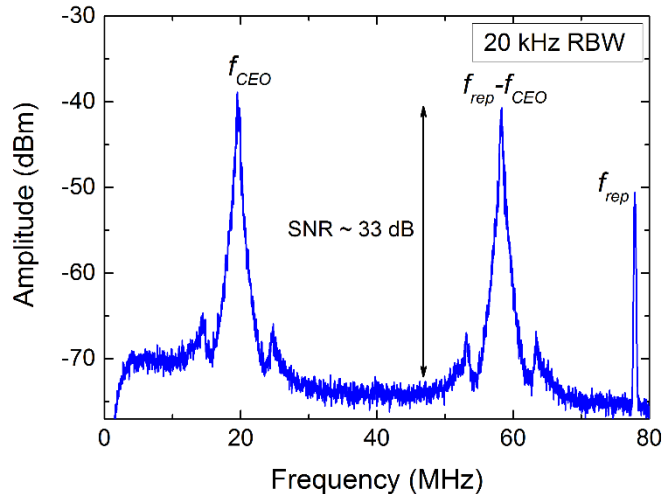
Figure 7-8: Frequency spectrum of the CEO beat note measured with the balanced photodetector board.

Despite using a balanced photodetector no improvement in the CEO's SNR was observed in comparison to a single photo detector. The same result was reached with a commercial balanced photodetector. By means of a balanced detector an improvement in the SNR for optical beats up to 6 dB was obtained, due to the cancellation of noise. It is not clear, why no improvement was observed here. A SNR better than 33 dB was not achieved, even when the inline interferometer's length and the PBS output fiber length was optimized. The limitation might origin from the oscillator performance itself (ASE limited quantum noise). However, the repetition rate was suppressed due to common mode rejection. In this context the amplitude of the repetition rate is about 10 dB lower with respect to the CEO beat amplitude. This leads to a suppression of the f_{rep}'s amplitude of more than -30 dB, when comparing this to a CEO-beat measurement with a single photo diode (see Figure 3-4). As a consequence, just one RF-band pass filter was required to extract and amplify the CEO beat note while suppressing a contribution of f_{rep}. Rf-filters can reduce the phase margin and so the locking bandwidth within the PLL for f_{CEO} stabilization.

7.3 Stabilization Results

To verify the comb's functionality it was fully optically stabilized to the HeNe laser. Hereby the FPGA based digital phase detector was integrated to lock both, the optical and CEO beat note. The setup for comb stabilization is illustrated in Figure 7-9. For f_{opt} beat generation the optical conversion interface from Figure 3-2 c, was used. Further, the out-of-loop CEO beat was measured via the free space from Figure 3-2 b,.
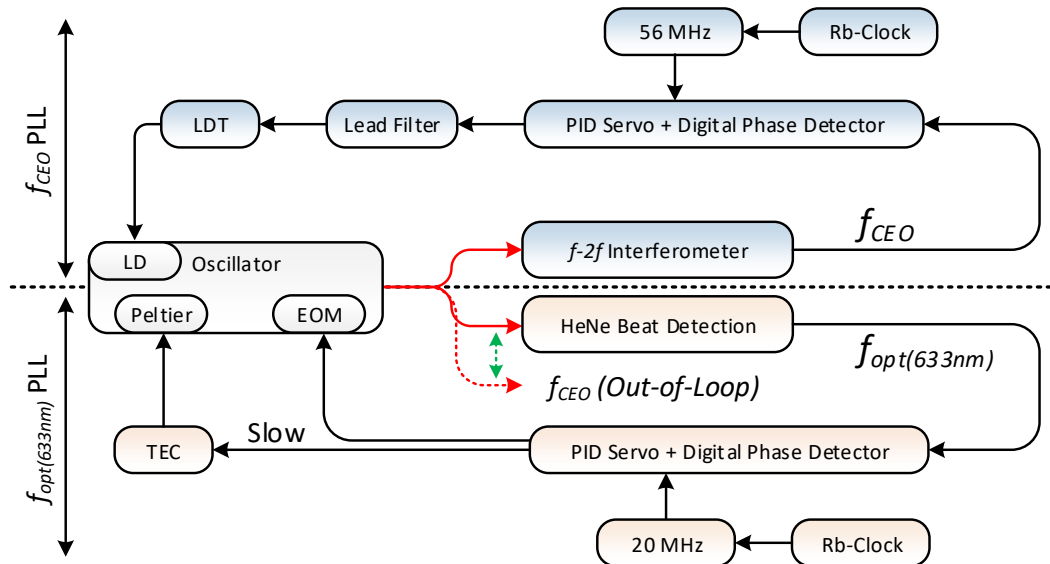
Figure 7-9: Phase locked loops to stabilize f_{CEO} and f_{opt} of the all-in-fiber comb.

The all-in-fiber comb was referenced to a Rb-clock, whereas f_{CEO} was stabilized via PPM and f_{opt} was locked via the EOM.

7.3.1 CEO- and Optical Beat Stabilization

Figure 7-10 shows the referenced in- and out-of-loop CEO beat. Both signals have a coherent peak at 56 MHz, which is an indication for a phase stabilized CEO frequency. Due to a better optimization of the in-fiber comb's *f-2f* interferometer, a higher SNR (about +10 dB) was achieved for the in-loop CEO beat in respect to the out-of-loop measurement. The phase noise measurement for the in-loop f_{CEO} and f_{opt} is depicted in Figure 7-11. Hereby an integrated phase noise of 2.01 rad and 809 rad was estimated in a bandwidth from 1 Hz to 3 MHz for the CEO- and optical beat, respectively. The integrated phase noise was slightly better in comparison to the stabilization measurements for SESAM EOM oscillator ($\phi_{CEO} = 2.4$ rad, $\phi_{opt} = 1.1$ rad) shown in section 5.1. This is due the fact, the PLL parameters were further

optimized for stabilization and to the use of the FPGA controller for CEO stabilization. Furthermore, the oscillator was less sensitive towards environmental fluctuations due to its packaging within the comb housing.
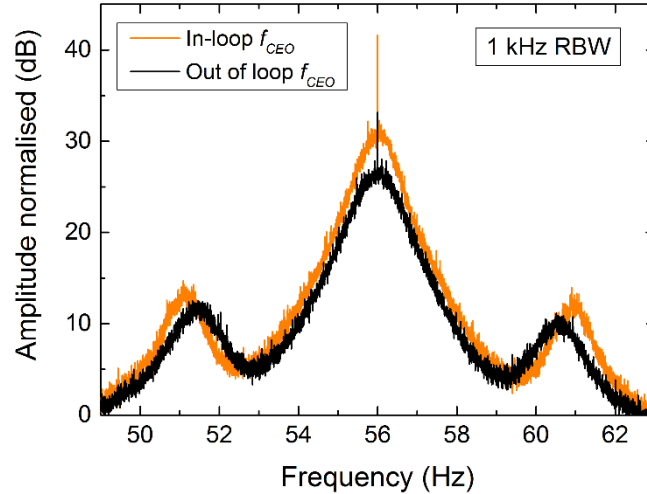
Figure 7-10: Frequency spectrum of the out-of-loop and in-loop phase stabilized CEO beat note.
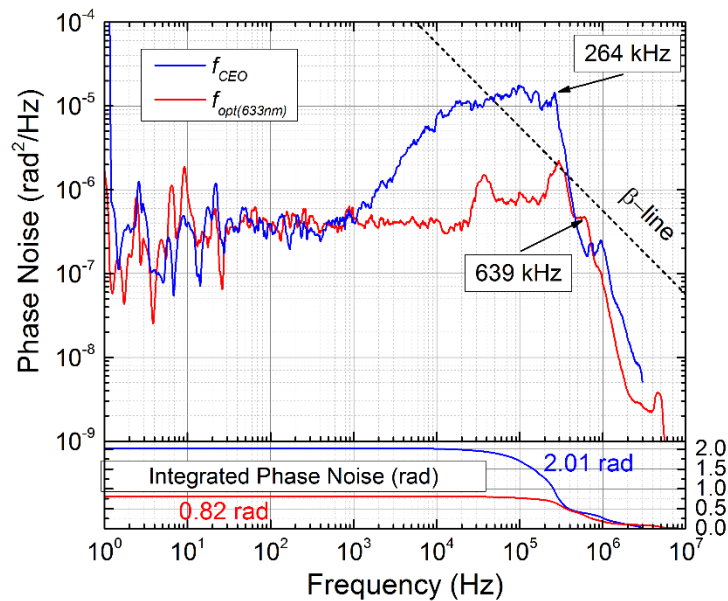
Figure 7-11: Phase noise spectrum and integrated phase noise for the stabilized f_{opt} and f_{CEO} signal

7.3.2 In-Loop Stability

The frequency stability of f_{CEO} and f_{opt} was measured with two Λ-counters (Keysight 53230a) and a multi-channel π-counter (K&K FXE) in a gate time of 1 s, consecutively. Figure 7-12 shows the frequency deviation (Λ-counter measurement) of f_{CEO} and f_{opt} over a period of more than 9 days of the fully stabilized comb.
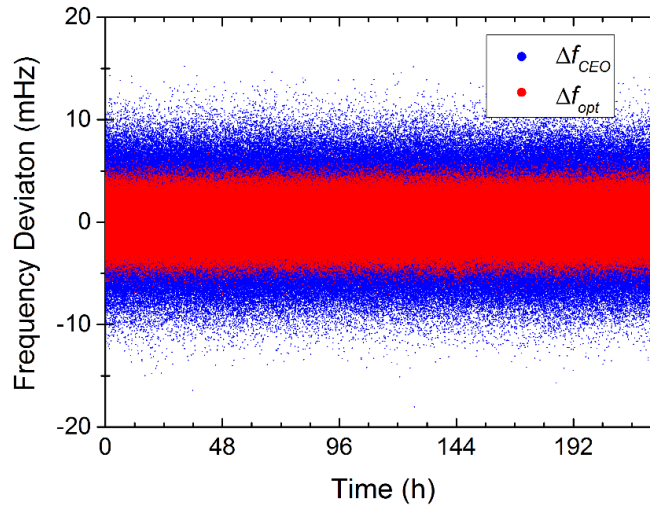
Figure 7-12: Frequency stability of f_{opt} and f_{CEO} (τ = 1 s) over a time period of more than 228 h.

Hereby, no phase slips were observed, while maintaining a stability better than ± 15 mHz. It has to be noted that the f_{CEO} frequency was divided by a factor of 10 before being fed to the frequency counter's input port. Without frequency division, no feasible measurement was obtained. In this context the frequency division was necessary to improve the signal's SNR. The measurement of the f_{CEO} frequency was later multiplied by 10 to compensate for the frequency division factor.

The Allan deviation for f_{CEO} and f_{opt} is illustrated in Figure 7-13. A modified Allan deviation with a slope of $\tau^{-0.5}$ and a stability of 3.4 mHz and 1.6 mHz (@ τ = 1 s) was determined for f_{CEO} and f_{opt} from the Λ-counter data, respectively. The overlapping Allan deviation determined from the π-counter data shows a worse stability with 18.9 mHz and 7.2 mHz (@ τ = 1 s). However, due to the τ^{-1} characteristics the overlapping Allan deviation shows lower values than the modified Allan deviation after a integration time of 30 s.

Furthermore, the in-loop Allan deviation of the Rb clock's 10 MHz signal is depicted in Figure 7-13. Hereby the comb stabilization is not limited by the Rb clock's stability (4.29 µHz @ τ =1 s) itself, which is more than two decades better than the comb's stability.
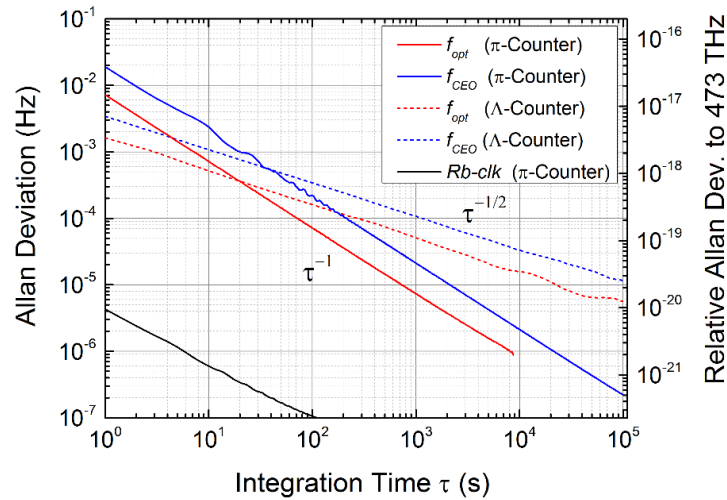
Figure 7-13: Overlapping Allan deviation of the stabilized fCEO and fopt beat note determined from π and Λ- counter measurements.

7.3.3 In-Fiber Comb Summary

An all-in-fiber frequency comb was developed, characterized and stabilized to a narrow linewidth laser to demonstrate its functionality. The stabilization results are summarized in Table 7-1. Hereby, no mechanical actuators were required for long-term stabilization hence the EOM's and temperature's modulation depth are sufficient to keep f_{rep} in lock. This shows a significant advantage over other comb systems requiring a fast and slow actuator e.g. based on a piezo stretcher, to stabilize a comb mode to an optical reference.

	f_{CEO}	f_{opt}
Integrated Phase Noise from 3 MHz (10 MHz) – 1 Hz	2.01 rad	0.809 rad (0.820 rad)
Stabilization Bandwidth	264 kHz	639 kHz
Allan Deviation τ = 1 s (π-Counter, Λ-Counter)	21 mHz 3.4 mHz	7.6 mHz 1.6 mHz
Rel. Allan. Dev. to 473 THz τ = 1 s (π-Counter)	$4.4 \cdot 10^{-17}$	$1.6 \cdot 10^{-17}$

Table 7-1: Summary of the all-in-fiber femtosecond laser's stabilization results.

The performance of the frequency comb system is similar to the in-fiber frequency comb system from NIST [1] (Phase Noise f_{CEO} = 2.9 rad, f_{opt}(192THz) = 0.22 rad) and is comparable to the performance of laboratory based setups. The resulting in-loop stability ($< 10^{16}$ @ τ=1 s) is sufficient for applications in the field of optical atomic clocks. The phase

slip free stabilization for over a period of 9 days proves the comb's reliable long-term operation.

8 Summary and Outlook

The goal of this work was to develop a robust frequency comb towards an engineering module for space applications. The performance of the frequency comb system shall be sufficient to transfer the stability of radio- and optical frequency standards without significant loss.

To achieve this goal a robust and compact in-fiber polarization maintaining Erbium frequency comb module was developed, characterized and stabilized. The engine of the comb module was a SESAM based femtosecond fiber laser with an integrated waveguide EOM. A fractional in-loop stability of less than 10^{-16} at an integration time of 1 s was demonstrated by phase-locking the comb to a HeNe laser over a period longer than 9 days. This stability is sufficient to cope with the performance of optical atomic clocks. The performance is comparable to (bulky) lab based comb systems, while having a ruggedized in-fiber design with a mass of just 2.8 kg and no need of mechanical actuators for stabilization.

As a measurement application the big ring laser gyroscope at the Geodetic Observatory Wettzell was stabilized with the SESAM EOM comb laser to a H-maser. Hereby the ring laser serves as a narrow linewidth passive stable optical resonator, which has similar properties as the interrogation laser of an optical atomic clock. Out of this reason, this application is adaptable to scenarios within the field of optical clocks.
A hybrid stabilization scheme was presented to reduce the drift of the ring laser by more than four orders of magnitudes leading to a potential improvement in the measurement of physical effects linked to earth rotation. A fractional Allan deviation of $5\cdot10^{-16}$ was reached at an integration time of 16384 s, limited by the H-maser stability.

Besides the SESAM EOM oscillator two femtosecond lasers with a tf-CNT absorber were studied. These lasers were also realized in an all-in-fiber design to fulfill the requirement on a compact and robust system. The linewidth of the free running tf-CNT lasers' comb tooth at 633 nm as well as the CEO beat was about 10 times narrower compared to the SESAM EOM laser. Hereby the low phase noise resulted from the sub-ps relaxation time of the tf-CNT absorbers.

One of the tf-CNT laser had an integrated waveguide EOM, such as the SESAM EOM laser. A phase coherent stabilization to the HeNe laser was realized via the EOM yielding to a sub-rad phase noise of 287 mrad (integrated from 1 Hz-10 MHz) for the optical beat note. Despite the better performance of the tf-CNT laser it was not a candidate for replacement of the SESAM EOM oscillator, since a degradation of the CNT absorber was observed.

The opto-optic modulator method has been applied to the other tf-CNT femtosecond laser as a proof of principle. Characterization measurements have shown that the CNT absorber is saturated by the OOM laser at 1420 nm and that the femtosecond oscillator has a fixed point at 600 THz for the OOM. Both, the phase stabilization of the CEO beat and a comb mode to the HeNe laser via the OOM were demonstrated. Hereby a lower integrated phase noise for the stabilization via OOM was achieved compared to a stabilization via pump power modulation. Hereby the feedback bandwidth of OOM was about 100 kHz higher in respect to PPM to suppress the phase noise of the stabilized beats.

In conclusion, optical interfaces have been built to measure and compare the CEO frequency and the comb tooth at 633 nm of different all-in-fiber Erbium femtosecond lasers . Phase locked loops with a non-commercial FPGA controller have been realized to study the high bandwidth stabilization of all-in-fiber frequency comb oscillators. Non-commercial electronics such as laser diode drivers, temperature controllers and balanced photodetectors were adapted to the characteristics of each femtosecond oscillator. The SESAM EOM oscillator was manufactured as a prototype by Toptica Photonics. The tf-CNT femtosecond lasers have been developed in cooperation with the College of Optics, Arizona (Professor Khanh Kieu). In summary the following contributions and outlook to research have been generated by this work:

- An all-in-fiber frequency comb module with a SESAM femtosecond oscillator (f_{rep}=80 MHz) with an integrated waveguide EOM was developed. A sub-fs pulse to pulse timing jitter and a stability below $1 \cdot 10^{-16}$ was demonstrated.
  For space-borne operation such a frequency comb module needs to be equipped with a PM radiation hard Erbium fiber and a proper shielding against cosmic radiation. Consequent development steps would be to realize a qualification module, which is tested in space environmental conditions in consideration of mechanical vibrations, cosmic radiation, vacuum and temperature. Furthermore the comb system power consumption could be reduced by silicon nitride technology and a fiber resistive modulator [111].

- The ring laser gyroscope at the Geodetic Observatory Wettzell was stabilized via hybrid stabilization approach to a H-maser with the SESAM EOM comb oscillator leading to a fractional Allan deviation of $5 \cdot 10^{-16}$ at an integration time of 16384 s.
  This setup could be used to reduce the frequency drift of other ring-lasers (such as the ROMY gyroscope located at Fürstenfeldbruck) significantly. Due to the active stabilization a performance might be achieved, which is similar to the high-end G laser even when the ring laser shows a worse passive stability.

- The optical phase stabilization of a tf-CNT femtosecond oscillator with an integrated waveguide EOM to a HeNe laser was demonstrated. This is a step forward towards a fully optical stabilized frequency comb based on a CNT absorber.

  To realize a full stabilization, the PM tf-CNT oscillator's reversal point in frequency tuning needs to be removed, which could be achieved by an optimized oscillator design. The PM tf-CNT absorber in this thesis was a prototype. In this context, the degradation of the PM tf-CNT absorber could highly probably be prevent (such as already shown by the non-PM CNT absorber) due to an improved manufacturing process under consideration of the optimization and purification of the PMMA CNT composite.

- The opto-optical modulator method was successfully demonstrated for the stabilization of a tf-CNT femtosecond oscillator.

  A following development step would be to demonstrate a fully stabilized comb oscillator based on a polarization maintaining design. Nevertheless, the heat dissipation within the tf-CNT absorber probably limits the stabilization performance. To circumvent this, other methods could be studied to change the CNT absorber transmission e.g. by applying an electric field to the CNT section.

Acknowledgment

- OHB System AG/ Kayser-Threde GmbH for giving me the possibility and the facilities to work on my PhD. In particular, I thank Norbert Lemke for granting me a high degree of flexibility from my day job at OHB.

- the engineers at OHB/Kayser-Threde GmbH for support in the field of electrical- and space engineering. Kudos to Philipp Putzer, Andreas Hurni, Martin Hutterer, Andreas Kölnberger, Tobias Lamour, Bastian Eder and Markus Plattner.

- the master students, working students and interns at OHB! Your work was a major support. It was a pleasure to introduce you to the world of fiber frequency combs and to learn from you as well in many aspects! Thanks are given to Sebastian Wick, Maximilian Breuer, Stefan Mayerhofer, Luna Dimitrio, Thomas Wheaterby, Maxime Delgrange and my sister Anna.

- the electrical engineering students Thomas Unterholzer, Johannes Obermaier and Markus Roner for the development of laser diode drivers, temperature controllers and the FPGA based phase detector.

- the AK Quantum at OHB for interesting talks/discussions on frequency comb technology for space applications.

- Armin Zach, Robert Herda and Christoph Skrobol from Toptica Photonics for fruitful discussions in the field of fiber optics, loan of laser equipment and the characterization of the SESAM EOM oscillator via a balanced optical cross cor- relator.

- Chien-Chung Lee (University of Colorado, USA) for the loan of the high-band- width graphene in-fiber modulator and the instruction in its use.

- Jochen Kuhnhenn (Fraunhofer INT) for exposing a highly nonlinear fiber with a high dose of γ-radiation.

- the excellent scientists Craig Benko (S2 Corporation, USA), Hajime Inaba (AIST,JP), Laura Sinclair (NIST, USA), Carsten Langrock (Stanford University, USA), Pavel Peterka (UFE Prague, CZ) and Steve Lecomte (CSEM, CH) for help- ful conversations via phone and/or mail.

Publications and Conference Contributions

Following publications were generated from this work and are not (all) cited formally:

<u>Journal publication:</u>

- S. Schweyer, B. Eder, P. Putzer, M. Mayerbacher, N. Lemke, K. U. Schreiber, U. Hugentobler, and R. Kienberger, "All-in-fiber SESAM based comb oscillator with an intra-cavity electro-optic modulator for coherent high bandwidth stabilization," Opt. Express **26**, 23798-23807 (2018)

<u>Conference contributions (first author):</u>

- S. Schweyer, K. Kieu, P. Putzer, M. Hutterer, T. Lamour, N. Lemke, R. Kienberger and U. Schreiber, "All-in-fiber polarization maintaining tapered fiber carbon nanotube erbium frequency comb with an integrated electro-optic modulator", Conference on Lasers and Electro-Optics Europe & European Quantum Electronics Conference (CLEO/Europe-EQEC), Munich, 2017
- S. Schweyer, P. Putzer, B. Eder, A. Kölnberger, M. Breuer, N. Lemke, A. Sell, A. Zach, R. Kienberger and U. Schreiber, "Stabilization of a SESAM Mode-Locked Erbium Laser Frequency Comb with an Integrated Electro-Optic Modulator to an Optical Reference", European Frequency and Time Forum (EFTF), York, 2016
- S. Schweyer, K. Kieu, P. Putzer, B. Eder, A. Kölnberger, N. Lemke, R. Kienberger and U. Schreiber, "First Results for the Offset Frequency Stabilization via Opto-Optical Modulation of an All-in Fiber Single Walled Carbon Nanotube Erbium Femtosecond Laser", European Frequency and Time Forum (EFTF), York, 2016
- S. Schweyer, B. Eder, P. Putzer, L. Pedrosa, J. Obermaier, T. Unterholzer, S. Wick, N. Lemke, R. Kienberger, and U. Hugentobler, "Fully Phase Stabilized SESAM Mode-locked Erbium Fiber Laser Frequency Comb Oscillator with an Integrated Electro-optic Modulator", 2017 Conference on Lasers and Electro-Optics Europe & European Quantum Electronics Conference (CLEO/Europe-EQEC), 2015
- S. Schweyer, R. Kienberger, B. Eder, P. Putzer, A. Kölnberger and N. Lemke, "Characterization of a SESAM mode-locked erbium fiber laser frequency comb with an integrated electro-optic modulator", European Frequency and Time Forum (EFTF), Neuchatel, 2014

Conference contributions (co-author):

- P. Putzer, S. Schweyer, N. Lemke, "Fiber based optical frequency comb: technical challenge for space applications", Proc. SPIE 10562, International Conference on Space Optics — ICSO 2016, 1056246, 25 September 2017
- B. Eder, M. Hutterer, T. Unterholzer, S. Lindner, A. Fischer, P. Putzer, S. Schweyer. N. Lemke. R. Kienberger, U. Schreiber and U. Hugentobler, "Highly Dynamic Distance Measurement for GNSS Using the Frequency Domain Distance Measurement, for Time and Frequency Transfer", 2014 European Frequency and Time Forum (EFTF), York, 2016
- B. Eder, M. Hutterer, L. Pedrosa, S. Schweyer, P. Putzer, N. Lemke, R. Kienberger, and U. Hugentobler, "Frequency Domain Distance Measurement for Formation Flights in Space", 2017 Conference on Lasers and Electro-Optics Europe & European Quantum Electronics Conference (CLEO/Europe-EQEC), 2015

Supervised Student Theses

Following theses were supervised by the author of this work and are not cited formally:

- Sebastian Wick, "Characterisation and Modelling of an in-fibre Ultra-Short Pulse Amplifier for a Frequency Comb Device," Master Thesis, University of Applied Sciences, (2015).
- Maximilian Breuer, "Setup of an all-in-fiber f-2f interferometer for the carrier-envelope offset detection of a fiber comb," Master Thesis, University of Applied Sciences Munich, (2016).
- Stefan Mayerhofer, "Development and Characterisation of an Erbium-Femtosecond-Fibrelaser based on Carbon Nanotubes," Master Thesis, University of Applied Sciences Munich, (2016).
- Maxime Delgrange, "Dispersion measurement using white light interferometry," Master Thesis, ENSSAT Graduate Engineering School in Lannion (France), (2017).

Theses which were not supervised by the author of this work (support only), but generated helpful output in terms of hardware for this work:

- Markus Roner: "Digital Temperature Stabilization of Laser Diodes," Bachelor Thesis, Technical University of Munich, 2013
- Johannes Obermaier, "Development and Evaluation of an FPGA-based digital phase-locked loop for stabilizing an Optical Frequency Comb," Advanced Seminar MST, Technical University of Munich, 2014.

A   Appendix

A.1   HeNe Laser Frequency Stability

This section describes the measurement of the HeNe laser free running frequency stability, which was performed with the measurement setup shown in chapter 7.3. Hereby the frequency stability was estimated by measuring the in-fiber comb repetition rate, while a comb mode was referenced to the HeNe laser (see Figure 7-3).

In Figure A-1 the comb's repetition rate drift and so the HeNe laser's frequency change Δf_{HeNe} is illustrated over a measurement period of 13 days (Λ-counter). The frequency counter gate time was 1 s. The repetition rate did not changed more than ± 0.6 Hz, which equals ± 3.6 MHz in the optical domain (at 473 THz).
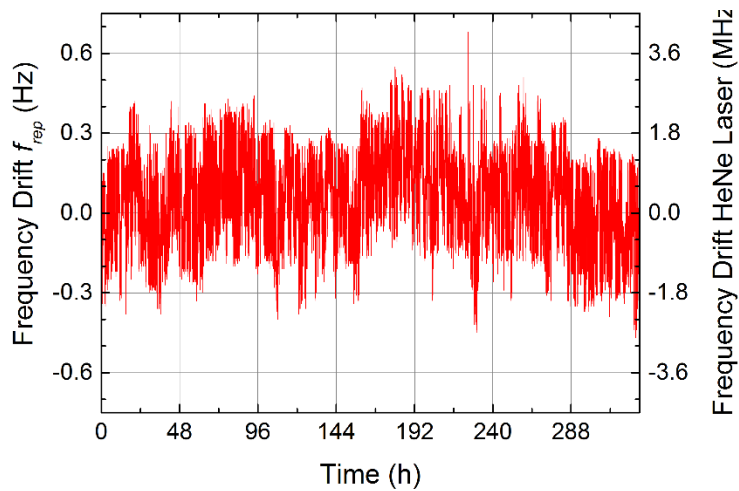
Figure A-1: Frequency drift of the free running HeNe laser measured against a rubidium clock.

The Allan deviation (see Figure A-2) is 20 mHz (40 mHz) for the Λ-counter (π-counter) at τ=1 s. This equals a relative stability of $2.5 \cdot 10^{-10}$ ($5.4 \cdot 10^{-10}$), which is a typical value for a two mode stabilized single mode HeNe laser.
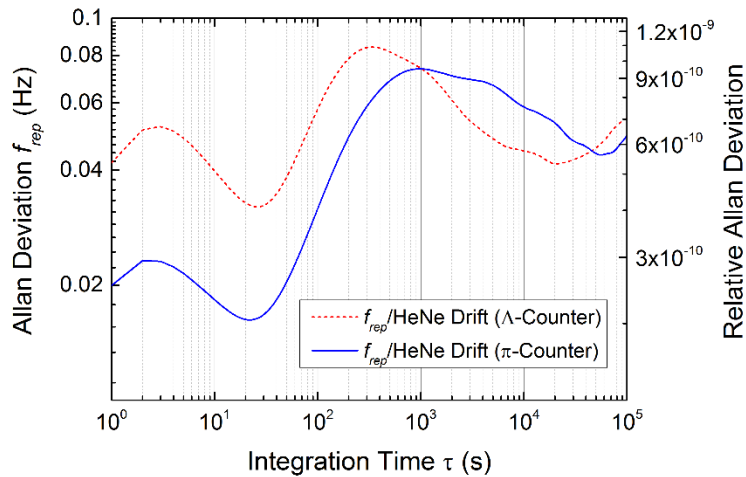
Figure A-2: Overlapping Allan Deviation of the free running HeNe laser.

A.2   Home-built Carbon Nanotube Lasers

Several femtosecond lasers were built with homemade CNT absorbers in the scope of a master thesis, which was supervised by the author of this thesis. The goal was here to use a home-built CNT femtosecond laser as frequency comb oscillators. However, a degradation of some of these lasers was observed. As consequence these lasers have not further been developed for frequency comb studies. Nevertheless, interesting results emerged from this master thesis, which are depicted here in the appendix.

A.2.1 Carbon Nanotube Absorber Types

Carbon nanotubes were discovered in 1952 by L.V. Radushkevich [112] and were studied in a multi-wall (MWCNT) structure in 1991 [113]. Farther graphene, which is basically an unfold CNT, gained a lot of attention in research [114] due to its outstanding electrical properties. The first CNT based mode-locked fiber laser was demonstrated in 2003 [115]. Since then femtosecond lasers with carbon based absorbers such as CNTs, MWCNT [116] and graphene [98] were developed. Carbon nanotubes are "rolled" from a 2d layer of graphene as illustrated in Figure A-3. Hereby the chiral vector $\vec{C}_h$ defines in which direction the layer is rolled, resulting into different CNT types such as zigzag, armchair or chiral. Depending on the CNT type, the CNT has conducting (armchair) or semiconducting (zigzag, chiral) properties.
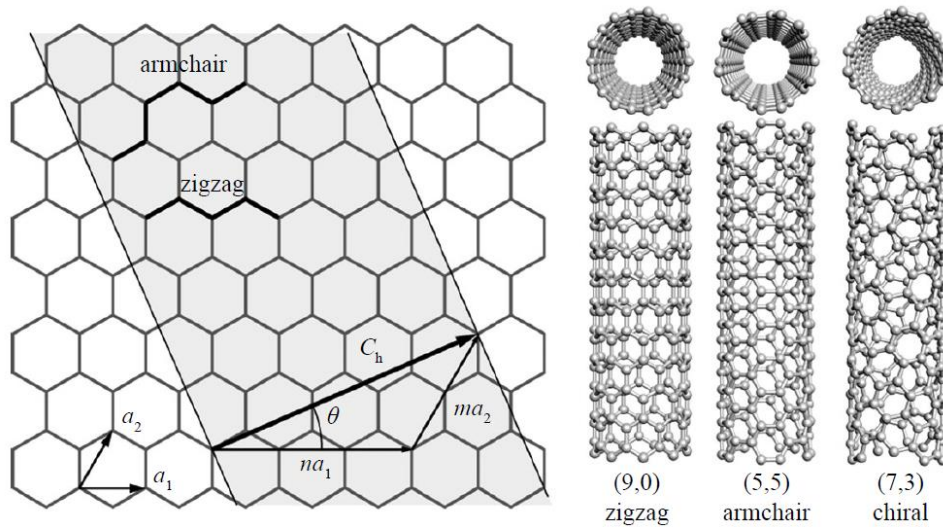
Figure A-3: On the left a layer of graphene is illustrated. On the right the graphene laser is rolled along three different chiral vectors C_h resulting into SWCNTs with a different structure (left) [117].

The bandgap and so the spectral absorption wavelength of the CNTs is defined by the diameter of the CNTs, which is here 0.8-1.2 nm. According to Figure A-4 this results into a bandgap of 0.7-1.0 eV, which lies within the photon energy $E=h·c/\lambda=0.785$ eV of the Erbium lasers wavelength at 1560 nm. Hereby only CNTs with semiconductor properties are suitable as absorber.
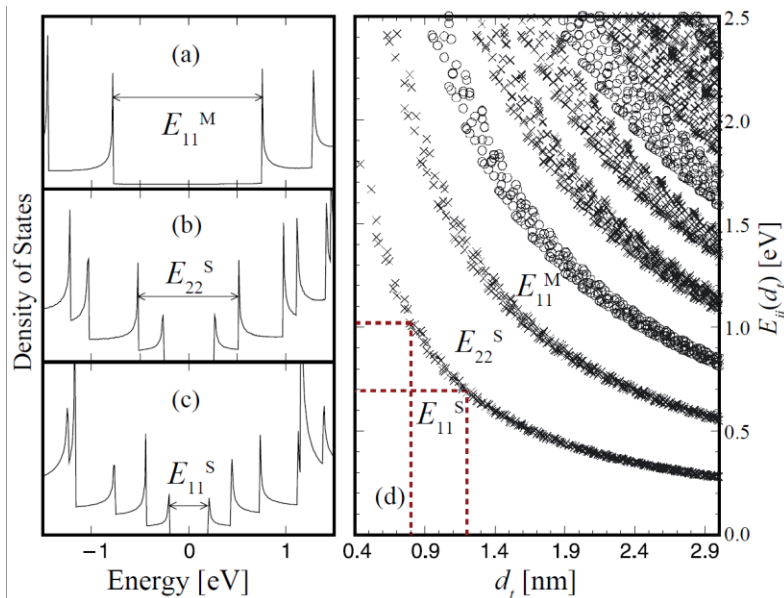
Figure A-4: Bandgap energy for (a) armchair (10,10), (b) chiral (11,9) and (c) zigzag (22,0) CNTs. In the right the transition energy as function of the CNT's tube diameter is illustrated [118].

There are four different ways to realize a saturable absorber based on carbon nanotubes (see Figure A-5) [112]. The "transmission type" and "reflection type" absorbers are used for optical free space applications. Out of this reason they are mostly implemented within solid state lasers [119]. Nevertheless, this two types show the benefit that the spot-size and so the fluence on the absorber is adjustable leading to an additional degree of freedom to optimize mode-locked operation.

The fiber end type architecture was selected for the self-build-CNT lasers, since it was the cheapest and simplest method to implement CNT absorbers. Hereby, the CNTs are placed in-between two fiber-end facets.

Evanescent field type absorbers require a tapered or D-shaped fiber as basis. In a D-shaped fiber, a part of the fiber's cladding is removed. CNTs are embedded into this section, which are exposed to the evanescent field of the light mode. The absorber's characteristics such as modulation depth is adjusted by the length and depth of the D-shape.

Tapered fiber CNTs were used two different femtosecond lasers in this thesis. Within the tapered area, a lot of the mode's light is located within the evanescent field. The tapered section is covered with the carbon nanotubes, which are bonded in a polymer composite. Parameters such as modulation depth, saturation fluence and non-saturable losses depend on the length and diameter of the taper. Evanescent field type absorbers have a higher damage threshold compared to the fiber end type absorbers. The reason is that the CNTs are exposed to a lower level of light intensity due to evanescent field interaction.
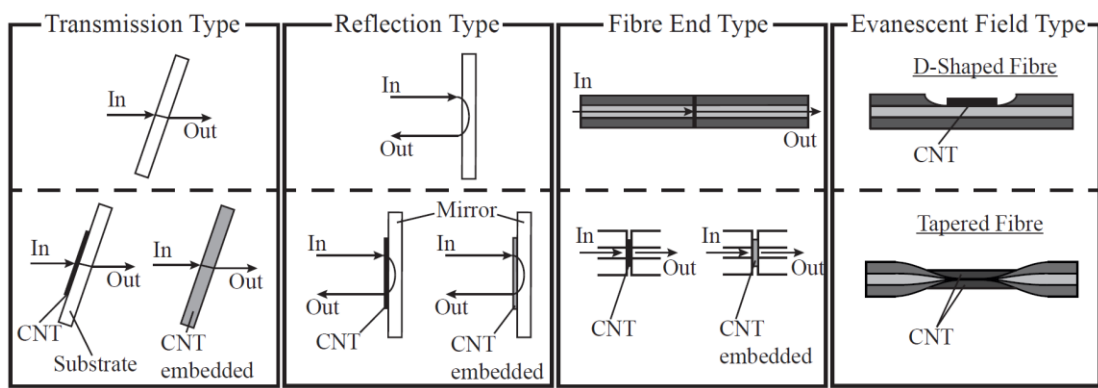
Figure A-5: Different CNT absorber types [112].

CNT absorbers with a fiber end type architecture can be produced by different methods such as optical deposition, thin coating or CNT layers. Within the optical deposition method, light at 1560 nm is injected into a fiber. Hereby the fiber end facet is located within a CNT solution. The CNT solution is heated locally at the fiber end facet leading to a thermodiffusion process. Due to this process, the CNTs deposit to the cold core surface of the fiber. By measuring the reflected light from the fiber end, the number of deposited CNTs is estimated. An

attempt was given to produce CNT absorbers via optical deposition. However, it was not possible to produce a proper absorber. The CNT coating was not thick enough to achieve a sufficient modulation depth for mode-locking.

Another approach is to place a flake of CNTs between two fiber end facets/connectors (CNT thin layer). Nevertheless, the thin coating method was used for this work, where CNT are directly coated on the fiber's surface. Thereby a fiber connector was dipped into a polymer CNT solution and was dried out. This process was repeated (20-30 times) until a certain coating thickness was achieved. With just one solution 10's to 100's of CNT absorbers could be manufactured, which makes it a cheap method to produce CNT absorbers.
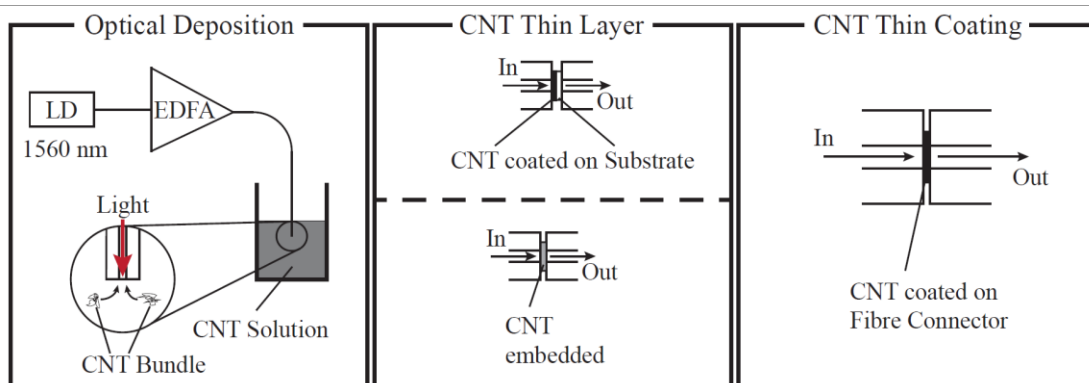
Figure A-6: Different methods to produce a fiber end type CNT absorber.

The CNT solution was fabricated by solving 5 mg of CNTs with 50 ml of chloroform in a small glass bottle. The solution was then ultra-sonicated for 30 minutes in an ultrasonic bath. Finally the polymer P3HT (poly3-hexylthiophen-2.5-diyl) was added to the solution and was ultra-sonicated for another 30 minutes.

The CNTs were produced by the company NanoIntegris by applying a high-pressure carbon monoxide (HIPCO) method [120]. The CNT powder had a residual iron (Fe) catalyst of < 15 wt% and a thermal stability (TGA) temperature of about 440°C. The polymer PH3T was selected as a compound for the CNTs since it has a relatively high meting point with 238°C compared to other polymers such as chitosan, polycarbonate (PC), polymethyl methacrylate (PMMA).

A.2.2 Carbon Nanotube Lasers

In total two CNT based femtosecond lasers (FSL,OOM) were setup and tested. The FSL laser was operated at a repetition rate of 48.9 MHz (FSL1) before the standard PM fiber in the oscillator was cut down to reach precisely a repetition rate of 79.1 MHz (FSL2). This oscillator was used for other experiments in the field of time and frequency transfer of femtosec-

ond lasers. The oscillator design is illustrated in Figure 3-1 b, and is similar to the laser studied in [67], whereas a high gain (90 dB/m @ 1530 nm) PM Erbium fiber (nLight ER80-4/125-HD-PM) was introduced into the laser cavity to compensate for the non-saturable losses of the CNTs. Mode-locking of the FSL2 is initiated at a pump power of 67 mW with a spectral output bandwidth of 5.7 nm (see Figure A-7). A maximum spectral bandwidth of 13.5 nm at a pump power of 143 mW was achieved resulting into 190 fs long soliton pulses. The autocorrelation measurement in Figure A-7 c, was done after the output pulse propagated in half a meter of fiber.

The side lobes in the output spectrum at 1537 nm and 1579.4 nm are called Kelly sidebands [121]. Kelly sidebands occur due to a periodic perturbation of the intra-cavity pulse shaping process. Hereby a part of the pulse light is dissipated into background radiation as dispersive wave. When the wave vector of the dispersive wave and soliton pulse matches 2π or n times 2π a periodic exchange of energy is given, resulting into narrow peaks in the optical spectrum. The wavelength-spacing between Kelly sidebands increases, when the cavity net dispersion decreases. Kelly sidebands have no technical use and are rather unpractical, when it comes to pulse amplification within active fibers.
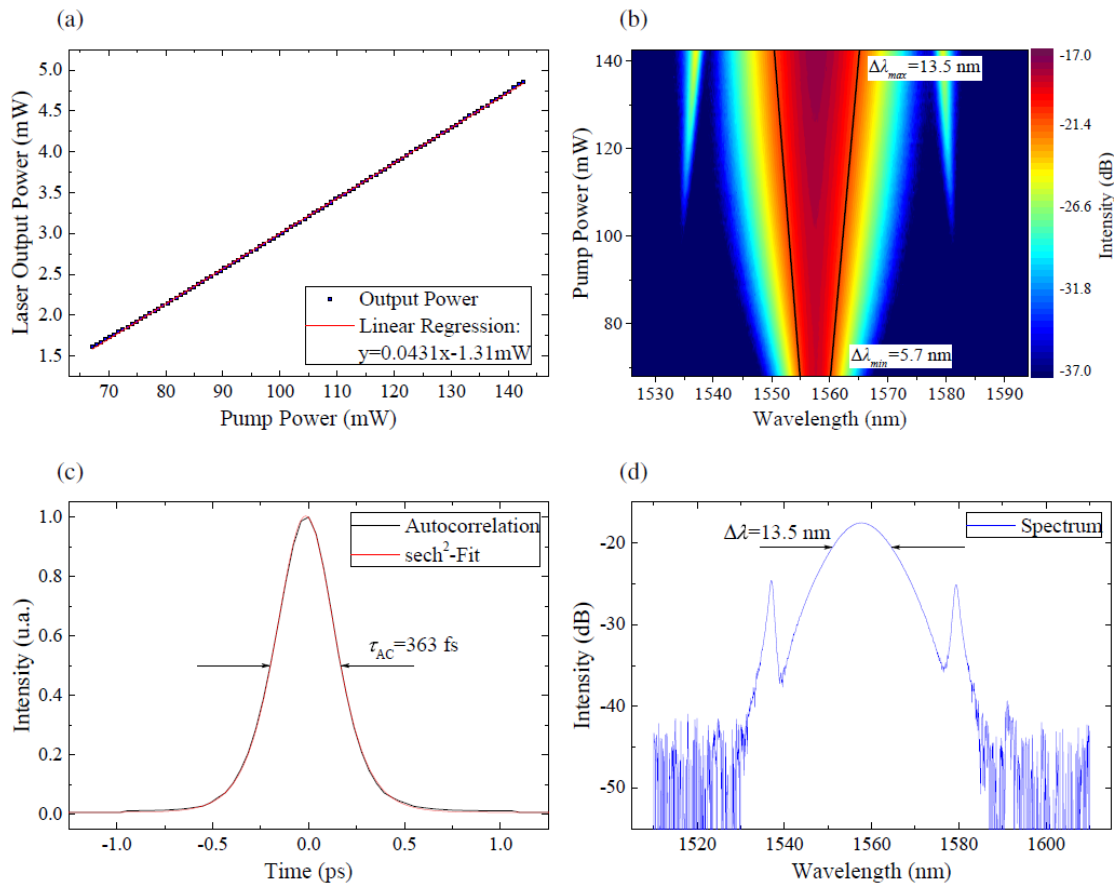
Figure A-7: (a) Output power, (b) spectrum as a function of pump power, (c) pulse autocorrelation and (d) spectrum at Ppump = 140 mW of the FSL2 laser

The OOM laser had a similar architecture like the FSL laser, but a further WDM was employed in the cavity to study the optical-optic modulation method. However, this method was later not investigated with this laser due to degradation issues of the CNT absorber. The results and specifications of the FSL and OOM laser are depicted in Table-A-1.

	FSL1	**FSL2**	**OOM1**	**OOM2**
f_{rep} (MHz)	48.9	79.1	71.8	62.8
EDF Length (m)	0.4	0.4	0.6	1
PMF Length (m)	3.82	2.35	2.29	2.29
Net dispersion (ps^2)	-0.0684	-0.0390	-0.0338	-0.0258
Δf_{CEO} (kHz)	-	-	380	125
$\Delta f_{opt(633\ nm)}$ (kHz)	-	-	125	52
$\Delta\lambda$ (nm)	5.3-9.2	5.7-13.5	~ 10.4	~ 10.4
$f_{3dB-Pump}$ (kHz)	-	-	11	4.7

Table-A-1: Measured parameters for the CNT femtosecond lasers.

The OOM's Erbium fiber was cut down from 1 m to 0.6 m increasing the net cavity dispersion from -0.0258 ps^2/m to -0.0338 ps^2/m. The optical comb linewidth at 633 nm (Δf_{opt}) and the f_{CEO} linewidth was measured to evaluate the impact of the net cavity dispersion on the laser's performance. As result the linewidth of the OOM2 laser is smaller compared to the OOM1 laser, since it shows a lower net cavity dispersion. Also the 3 dB frequency for coupling pump noise into amplitude fluctuations of the femtosecond oscillator decreases, which on the other side means that less amplitude noise is coupled into frequency noise resulting into a smaller linewidth. The free running linewidth of the self-build CNT oscillator probably could be further decreased by optimizing the net cavity dispersion towards zero. This would result into a sub-100 kHz linewidth for f_{CEO} such as was demonstrated for the tf-CNT lasers. However, this was not further studied due to degradation issues of the self-build CNT absorbers.

A.2.3 Characterization of Carbon Nanotube Absorbers

The absorber's spectral transmission as well as the absorber transmission as function of fluence are important information for building a femtosecond lasers. The transmission or rather loss of the absorber defines how much gain is needed to obtain laser operation. Furthermore,

parameter such as the saturation fluence and modulation depth determine the intra-cavity's soliton pulse energy and so the pulse length.

The spectral transmission was measured with a simple setup consisting of an Erbium amplifier source generating ASE, the absorber and an optical spectrum analyzer. The amplifier consisted of a 2 m long backward pumped PM Erbium fiber (Nufern PM-ESF-7/125).
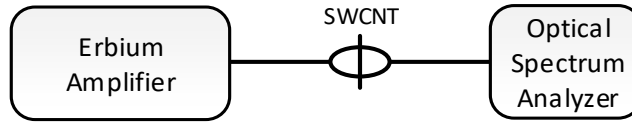
Figure A-8: Optical setup the measure the transmission of the single walled carbon nanotube absorbers.

The transmission of the absorber was estimated by taking a reference measurement of the ASE light with the uncoated FC/APC fiber connection. After that one connector was coated with CNTs. Hereby the ASE output level was kept low to omit saturation of the CNTs. The transmission is given as:

$$T = \frac{P_{coated}(\lambda)}{P_{uncoated}(\lambda)} \tag{6.5}$$
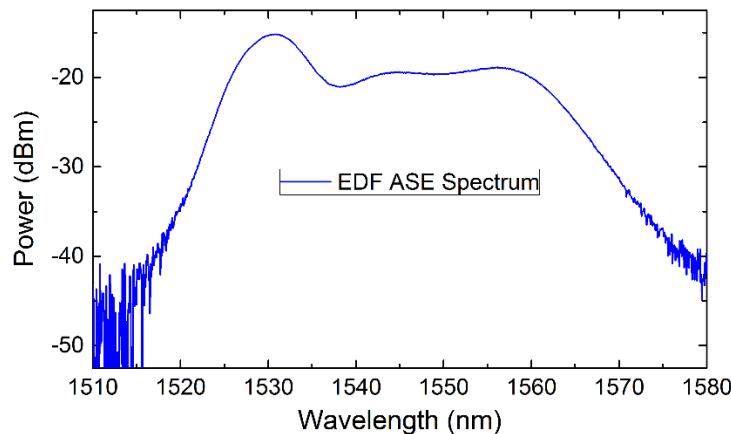
Figure A-9: Optical ASE spectrum of the unseeded Erbium doped fiber amplifier.

In Figure A-10 the spectral transmission for different coatings is shown. In this context every coating has a flat spectral transmission profile. The CNTs embedded within the P3HT solution have a transmission of about 66 %, which is relatively low compared to SESAM absorbers. However, fiber lases can cope with high intra-cavity losses due to the availability of high gain Erbium doped fibers. Solid State lasers on the other side are not functional with losses of more than some percent. Further the CNT absorbers were coated with a layer of Siloxane,

which shall prevent that the CNTs oxide with air during operation. Together with the Siloxane layer a transmission of just 26 % was determined.
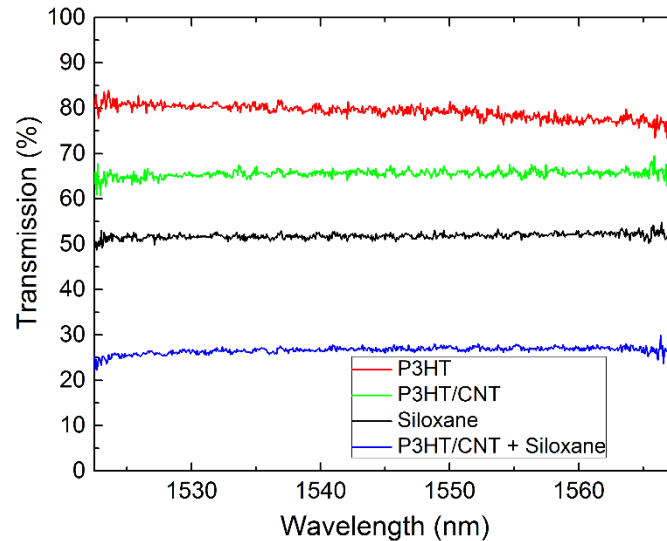
Figure A-10: Spectral transmission for different coatings of the FC/APC connector.

The same amplifier as above was seeded with pulses from a femtosecond oscillators to measure the CNT absorbers transmission as function of fluence. Hereby the seed pulse duration was temporally stretched (or chirped) from 0.4 ps to 1 ps in a 6 m long PM fiber before entering the anormal dispersive amplifier. The pulses were pre-chirped to avoid any pulse break up during or after amplification. Also here reference measurements were taken to consider the loss of the FC/APC connectors. The fluence is described in section 2.5 by equation (2.30)
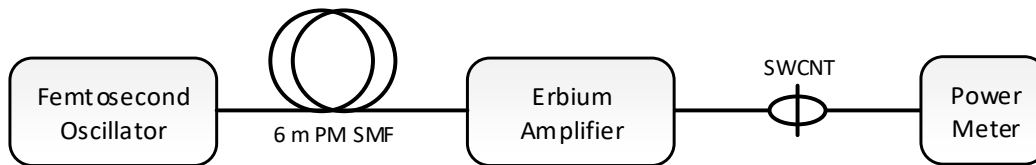
Figure A-11: Setup to estimate the carbon nanotube absorber's transmission as function of fluence.

The transmission as function of fluence for the CNT absorber without and with Siloxane coating is depicted in Figure A-12. The modulation depth is 10.6% and 8.9% for the uncoated and coated CNT absorber, respectively. This modulation depth is sufficient for stable mode-locked operation. It has to be notified that the difference in modulation depth between both absorbers most probably occurs due to reproducibility of the CNT absorber. The saturation fluence is with 16.5 μJ/cm^2 and 2.3 μJ/cm^2 quite low, which helps to start mode-locked operation without over-pumping the laser oscillator. A comparable SESAM absorber (Batop-

SAM-1550-10-2ps) has a saturation fluence of 70 µJ/m². The Siloxane coated absorber has a high non-saturable loss of 65.4%, which is 41.6% more compared to the uncoated CNT. Further the coated absorber starts to degenerate at a fluence of 160 µJ/cm² probably caused due to the higher absorption induced heat dissipation.
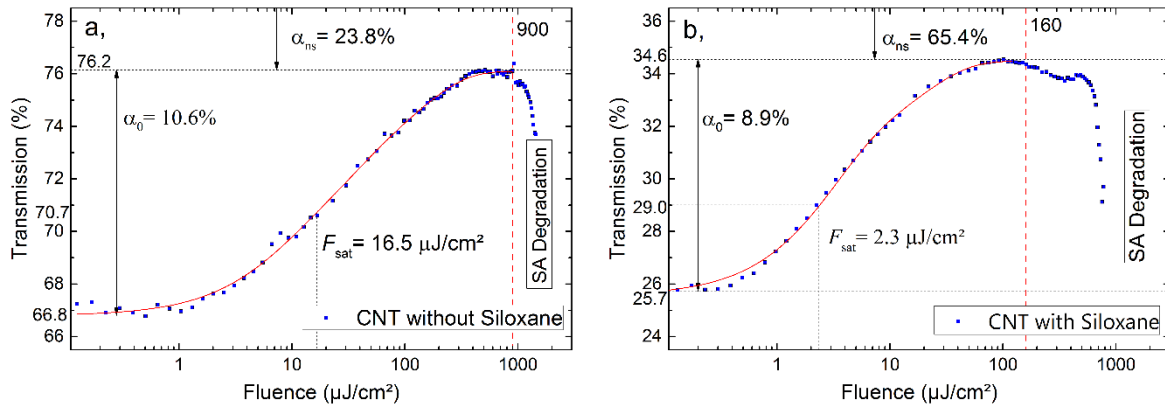
Figure A-12: Transmission as function of fluence for the (a,) uncoated and (b,) coated CNT absorber.

On the other side the uncoated absorber degenerates upon a fluence of about 900 µJ/cm². The low degradation fluence shows a major drawback of the siloxane coated absorber. However, the siloxane coating prevents the CNT layers from oxidation.

Some of the self-built CNT absorbers degenerated very quickly right away the laser was operated about more than 70% of the maximum pump power. On the one side the absorber has to withstand some hundreds of Watts peak power. Therefore an average intra-cavity power of 30 mW is often sufficient to initiate degradation of the absorber [84]. In this context the degeneration process is driven due to graphitization of the carbon nanotubes. Further it was assumed that the degeneration is supported by oxidation of the absorber.
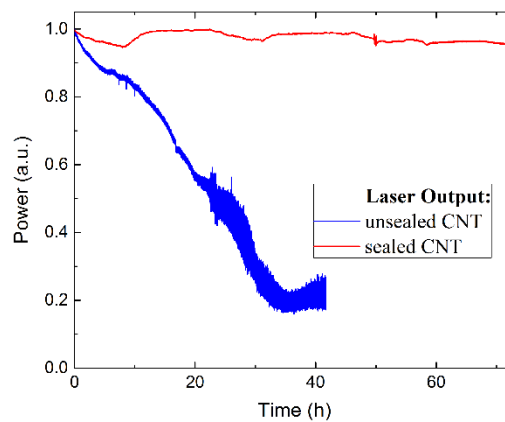
Figure A-13: Relative output power as a function of time of a femtosecond laser with a CNT absorber which is sealed with a layer of Siloxane and for a CNT absorber which is unsealed.

Figure A-13 illustrates the output power of a CNT femtosecond laser with a P3HT/CNT absorber and a CNT absorber coated with siloxane. The uncoated CNT absorber decreases in output power from the start, where the coated CNT absorber shows an almost constant output power during operation. This means that the risk for degeneration of a femtosecond laser with an uncoated P3HT/CNT absorber is very high. Out of this reason only Siloxane coated absorbers were employed in the laser cavity, despite having a tremendously higher loss.

In Figure A-14 the output spectrum and output power of the femtosecond laser with the coated CNT absorber was continuously measured for more than 20 days. Hereby the output spectrum was stable until day 18, where a cw peak occurred resulting into q-switching like disturbances of the laser output. In a previous characterization the cw occurred when the laser reached a bandwidth of 10.4 nm. Here, the cw peak occurs at a bandwidth of 9.7 nm probably resulting in a degeneration in the absorber's modulation depth.
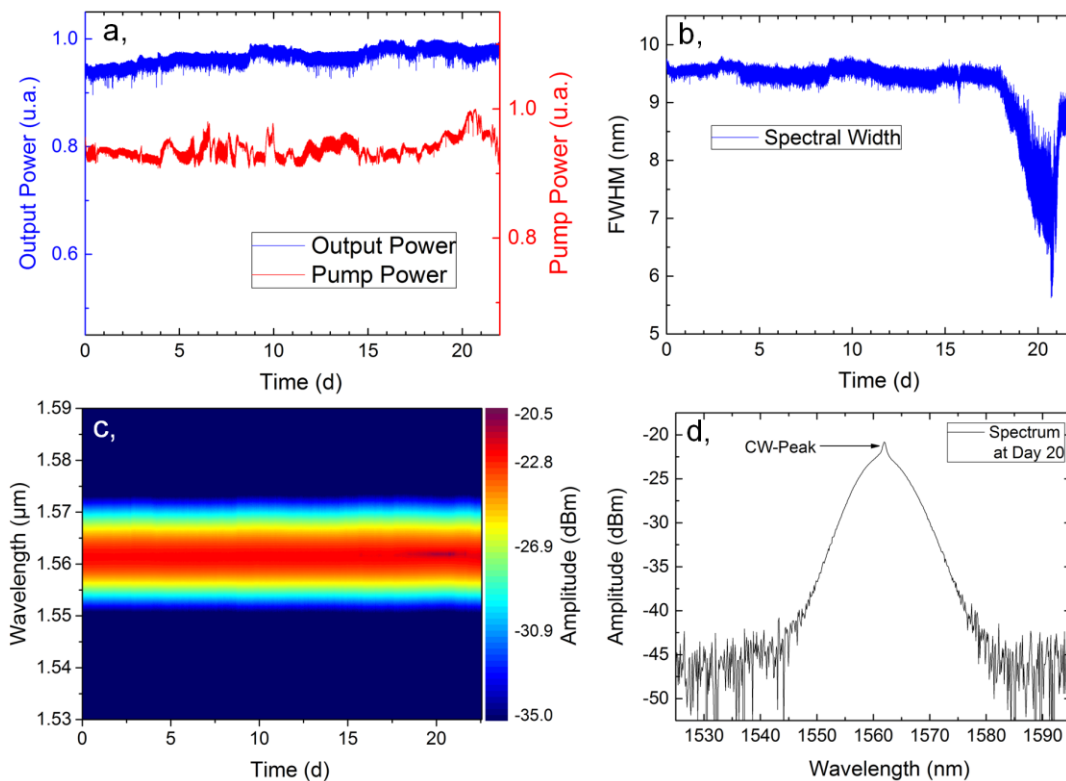
Figure A-14: Results of the second long-term test with (a) relative in-and output power, (b) spectral FWHM, (c) spectral evolution as function of time and (b) spectrum with cw-peak at day 20.

Nevertheless, the rate of degeneration could be slowed down by operating the laser at an bandwidth lower than 8 nm resulting into a lower intra-cavity power. In this context it has to be notified that the FSL2 oscillator is in laboratory use without degeneration since 1.5 years. However, no effort was made to stabilize f_{CEO} and f_{rep} of the femtosecond oscillator, since the degeneration mechanism of the absorbers needs to be studied further and so the manufacturing of the absorbers had to be optimized to guarantee a robust and long life time femtosecond laser operation. Therefore it made no sense to take the risk to use the self-build CNT laser as engine for the all-in-fiber frequency comb system.

The benefit on the other side was that cheap PM femtosecond oscillators for a price less than 500 € each (excluding pump diode and pump diode driver) could be manufactured serving for other laboratory experiments.

Abbreviations

AOM	Acoustic Optic Modulator
ASE	Amplified Spontaneous Emission
CCW	Counter clockwise
CW	Clockwise
cw	Continuous wave
CEO	Carrier Envelope Offset
CNT	Carbon Nanotubes
EDF	Erbium doped fiber
EOM	Electro optic modulator
ESA	Electrical Spectrum Analyzer
FRM	Fiber Resistive Modulator
FWHM	Full Width Half Maximum
GM	Graphene Modulator
HNF	Highly Nonlinear Fiber
IWDM	WDM with integrated isolator
LDD	Laser Diode Driver
NPE	nonlinear polarization evolution
O.C.	optical coupler
OAC	Optical Atomic Clock
OOM	Opto-Optical Modulator
OSA	Optical Spectrum Analyzer
PBS	Polarization Beam Splitter
PID	Propotional-Integrator-Derivator
PLL	Phase Locked Loop
PM	Polarization Maintaining
PMMA	Poly(methyl methacrylate)
PPKTP	Periodic Poled Kalium Tassium Phosphore
PPLN	Periodic Poled Lithium Niobate
PPM	Pump Power Modulation
RF	Radio Frequency
RIN	Relative Intensity Noise
SC	Supercontinuum
SESAM	Semiconductor Saturable Absorber Mirror
SHG	Second Harmonic Generation
TEC	Thermo Electric Cooler
tf	Tapered fiber
WDM	wavelength division multiplexing coupler

References

[1]   L. Sinclair, I. Coddington, W. Swann, G. Rieker, A. Hati, K. Iwakuni, and N. Newbury, "Operation of an optically coherent frequency comb outside the metrology lab", Opt. Express 22, 6996-7006 (2014).

[2]   Y. Feng, X. Xu, X. Hu, Y. Liu, Y. Wang, W. Zhang, Z. Yang, L. Duan, W. Zhao, and Z. Cheng, "Environmental-adaptability analysis of an all polarization-maintaining fiber-based optical frequency comb," Opt. Express 23, 17549–17559 (2015).

[3]   B. J. Bloom, T. L. Nicholson, J. R. Williams, S. L. Campbell, M. Bishof, X. Zhang, W. Zhang, S. L. Bromley, and J. Ye, "An Optical Lattice Clock with Accuracy and Stability at the 10^{-18} Level," Nature 506, 71–75 (2014).

[4]   J. Millo, M. Abgrall, M. Lours, E. M. L. English, H. Jiang, J. Guéna, A. Clairon, M. E. Tobar, S. Bize, Y. Le Coq, and G. Santarelli, "Ultralow noise microwave generation with fiber-based optical frequency comb and application to atomic fountain clock," Appl. Phys. Lett. 94, 141105 (2009).

[5]   B. Bernhardt, A. Ozawa, P. Jacquet, M. Jacquey, Y. Kobayashi, T. Udem, R. Holzwarth, G. Guelachvili, T. W. Hänsch, and N. Picqué, "Cavity-enhanced dual-comb spectroscopy," Nat. Photonics 4, 55–57 (2010).

[6]   J. Ye, "Absolute measurement of a long, arbitrary distance to less than an optical fringe," Opt. Lett. 29, 1153–1155 (2004).

[7]   F. R. Giorgetta, W. C. Swann, L. C. Sinclair, E. Baumann, I. Coddington and N. R. Newbury, "Optical two-way time and frequency transfer over free space," Nature Photonics volume 7, pages 434–438 (2013).

[8]   R. Holzwarth, Th. Udem, and T. W. Hänsch, J. C. Knight, W. J. Wadsworth, and P. St. J. Russell, "Optical Frequency Synthesizer for Precision Spectroscopy," Phys Rev Lett., 85(11):2264-7 (2000).

[9]   N. R. Newbury, "Searching for applications with a fine-tooth comb," Nature Photonics 5, 186–188 (2011).

[10]   Urs Hugentobler. "Optical clock technologies and their applications for globally optimized navigation," Technical report, Forschungseinrichtung Satellitengeodäsie, (2010).

[11]   Urs Hugentobler. "Optical clock technologies and their applications for globally optimized navigation – 2," Technical report, Forschungseinrichtung Satellitengeodäsie, (2013).

[12]   Advantage - Advanced Technologies for Navigation and Geodesy (23.11.2018), https://www.dlr.de/kn/en/desktopdefault.aspx/tabid-4305/6933_read-51540/admin-1/

[13]   R. Bondarescu, M. Bondarescu, G. Hetényi, L. Boschi, P. Jetzer and J. Balakrishna; "Geophysical applicability of atomic clocks: direct continental geoid mapping," Geophysical Journal International, Volume 191, Issue 1, Pages 78–82, (2016).

[14]   Tanja E Mehlstäubler, Gesine Grosche, Christian Lisdat, Piet O Schmidt and Heiner Denker, "Atomic clocks for geodesy," Reports on Progress in Physics, Volume 81, Number 6, (2018).

[15]   B. G. Levi, "GRACE Satellites Start to Map Earth's Gravity Field," Physics Today 56, 2, 18 (2003).

[16]   L. Buinhas, E. Ferrer-Gil and R. Forstner, "IRASSI: InfraRed astronomy satellite swarm interferometry — Mission concept and description," 2016 IEEE Aerospace Conference, Big Sky, MT, pp. 1-20, (2016).

[17]   Gerhard Ehret, Pierre Flamant, Axel Amediek, Philippe Ciais, Fabien Gibert, Andreas Fix, Christoph Kiemle, Mathieu Quatrevalet, Martin Wirth, "The French-German Climate Monitoring Initiative on Global Observations of Atmospheric Methane," ILRC 25 (25th International Laser Radar Conference), St. Petersburg, Russia, July 5-9, pp 1348-1351 (2016).

[18]   S. Kolkowitz, I. Pikovski, N. Langellier, M. D. Lukin, R. L. Walsworth, and J. Ye, "Gravitational wave detection with optical lattice atomic clocks," arXiv preprint arXiv:1606.01859 (2016).

[19]   S. M. Schweyer, B. Eder, P. Putzer, M. Mayerbacher, N. Lemke, K. U. Schreiber, U. Hugentobler, and R. Kienberger, "All-in-fiber SESAM based comb oscillator with an intra-cavity electro-optic modulator for coherent high bandwidth stabilization," Opt. Express 26, 23798-23807 (2018).

[20]   T. W. Hänsch, "Noble Lecture: Passion for precision," Rev. Mod. Phys. 78, 1297, (2006).

[21]   K. U. Schreiber and J.-P. R. Wells, "Invited Review Article: Large ring lasers for rotation sensing," Scientific Instruments, 84(4), 041101–041101–26, (2013).

[22]   U. Keller, F. W. Helbing and G. Steinmeyer, "Carrier-envelope control of femtosecond lasers with attosecond timing jitter," Postconference Digest Quantum Electronics and Laser Science, 2003. QELS., Baltimore, MD, USA , pp. 4 pp., (2003).

[23]   E. Benkler, H. R. Telle, A. Zach, and F. Tauser, "Circumvention of noise contributions in fiber laser based frequency combs," Opt. Express 13, 5662–5668 (2005).

[24]   N. R. Newbury and B. R. Washburn, "Theory of the frequency comb output from a femtosecond fiber laser," IEEE J. Quantum Electron. 41, 1388–1402 (2005).

[25]   H. R. Telle, G. Steinmeyer, A. E. Dunlop, J. Stenger, D. H. Sutter, and U. Keller, "Carrier-envelope offset phase control: A novel concept for absolute optical frequency measurement and ultrashort pulse generation," Appl. Phys. B, vol. 69, no. 4, pp. 327–332 (1999).

[26]   I. Hartl, M. E. Fermann, C. Langrock, M. M. Fejer, J. W. Nicholson and D. J. DiGiovanni, "Integrated fiber-frequency comb using a PPLN waveguide for spectral broadening and CEO phase detection," Conference on Lasers and Electro-Optics and Quantum Electronics and Laser Science Conference, Long Beach, CA, 2006, pp. 1-2, (2006).

[27]   Marcus Zimmermann, Christoph Gohle, Ronald Holzwarth, Thomas Udem, and Theodor W. Hänsch, "Optical clockwork with an offset-free difference-frequency comb: accuracy of sum- and difference-frequency generation," Opt. Lett. 29, 310-312 (2004).

[28]   P. Rochat, F. Droz, Q. Wang, S. Froidevaux, "Atomic Clocks and Timing Systems in Global Navigation Satellite Systems," the European navigation conference, (2012).

[29]   D. J. Jones, S. A. Diddams, J. K. Ranka, A. Stenz, R. S. Windeler, J. L. Hall, and S. T. Cundiff," Carrier-envelope phase control of femtosecond mode-locked lasers and direct optical frequency synthesis," Science 288, 635 (2000).

[30]   H. R. Telle, B. Lipphardt, and J. Stenger, "Kerr-lens, modelocked lasers as transfer oscillators for optical frequency measurements," Appl. Phys. B 74, 1–6 (2002).

[31]   L. E. Nelson, D. J. Jones, K. Tamura, H. A. Haus, and E. P. Ippen, "Ultrashort-pulse fiber ring lasers," Appl. Phys. B 65, 277–294 (1997).

[32]   B. R. Washburn, W. C. Swann, and N. R. Newbury, "Response dynamics of the frequency comb output from a femtosecond fiber laser," Opt. Express 13, 10622-10633 (2005).

[33]   Nathan R. Newbury and William C. Swann, "Low-noise fiber-laser frequency combs (Invited)," J. Opt. Soc. Am. B 24, 1756-1770 (2007).

[34]   R. Paschotta, A. Schlatter, S. C. Zeller, H. R. Telle, and U. Keller, "Optical phase noise and carrier-envelope offset noise of mode-locked lasers," Appl. Phys. B 82, 265–273 (2006).

[35]   J. J. McFerran, W. C. Swann, B. R. Washburn, and N. R. Newbury, "Elimination of pump-induced frequency jitter on fiber-laser frequency combs," Opt. Lett. 31, 1997–1999 (2006).

[36]   J. J. McFerran, W. C. Swann, B. R. Washburn, and N. R. Newbury, "Suppression of pump-induced frequency noise in fiber-laser frequency combs leading to sub-radian f_{ceo} phase excursion," Appl. Phys. B 86, 219–227 (2007).

[37]   R. Paschotta, "Noise of mode-locked lasers (Part II): timing jitter and other fluctuations," Appl. Phys. B 79, 163–173 (2004).

[38]   H. A. Haus and A. Mecozzi, "Noise of mode-locked lasers," IEEE J. Quantum Electron. 29, 983–996 (1993).

[39]   Holly Leopardi, Josue Davila-Rodriguez, Franklyn Quinlan, Judith Olson, Jeff A. Sherman, Scott A. Diddams, and Tara M. Fortier, "Single-branch Er:fiber frequency comb for precision optical metrology with 10^{-18} fractional instability," Optica 4, 879-885 (2017).

[40]   L.-S. Ma, P. Jungner, J. Ye, and J. L. Hall, "Delivering the same optical frequency at two places: accurate cancellation of phase noise introduced by an optical fiber or other time-varying path," Opt. Lett. 19, 1777-1779 (1994).

[41]   M. Giunta, W. Hänsel, M. Fischer, M. Lezius, and R. Holzwarth, "Multi-branch Ultra-Low Noise Er:fiber Frequency Comb Comparison," European Conference on Lasers and Electro-Optics and European Quantum Electronics Conference, (Optical Society of America), paper ED_2_3, (2017).

[42]   J. P. Gordon and H. A. Haus, "Random walk of coherently amplified solitons in optical fiber transmission", Opt. Lett. 11 (10), 665 (1986).

[43]   A. L. Schawlow and C. H. Townes, "Infrared and optical masers," Phys. Rev. 112 (6), 1940 (1958).

[44]   F. Riehle, "Frequency Standards: Basics and Applications," Wiley-VCH-Verlag, ISBN 3-527-40230-6, (2005).

[45]   Vig, John R.; Ferre-Pikal, Eva. S.; Camparo, J. C.; Cutler, L. S.; Maleki, L.; Riley, W. J.; Stein, S. R.; Thomas, C.; Walls, F. L.; White, J. D., IEEE Standard Definitions of Physical Quantities for Fundamental Frequency and Time Metrology---Random Instabilities," in IEEE Std Std 1139-2008 , vol., no., pp.c1-35, (2009).

[46]   W. J. Riley, "Handbook of Frequency Stability Analysis", Physics Laboratory (U.S.). Time and Frequency Division, U.S. Department of Commerce, NIST Special Publication 1065

[47]   S. T. Dawkins, J. J. McFerran and A. N. Luiten, "Considerations on the measurement of the stability of oscillators with frequency counters," in IEEE Transactions on Ultrasonics, Ferroelectrics, and Frequency Control, vol. 54, no. 5, pp. 918-925, (2007).

[48]   E. Rubiola, F. Vernotte and V. Giordano, "On the measurement of frequency and of its sample variance with high-resolution counters," Proceedings of the 2005 IEEE International Frequency Control Symposium and Exposition, Vancouver, BC, (2005).

[49]   E. Rubiola, M. Lenczner, P. Y. Bourgeois and F. Vernotte, "The Omega Counter, a Frequency Counter Based on the Linear Regression," in IEEE Transactions on Ultrasonics, Ferroelectrics, and Frequency Control, vol. 63, no. 7, pp. 961-969 (2016).

[50]   Gianni Di Domenico, Stéphane Schilt, and Pierre Thomann, "Simple approach to the relation between laser frequency noise and laser line shape," Appl. Opt. 49, 4801-4807 (2010).

[51]   P. Brochard, T. Südmeyer and S. Schilt, "Power Spectrum Computation for an Arbitrary Phase Noise Using Middleton's Convolution Series: Implementation Guideline and Experimental Illustration," in IEEE Transactions on Ultrasonics, Ferroelectrics, and Frequency Control, vol. 64, no. 11, pp. 1766-1775, Nov. (2017).

[52]   Stefan Mayerhofer, "Development and characterization of an Erbium femtosecond fibrelaser based on carbon nanotubes," University of Applied Sciences Munich, Master Thesis, (2016)

[53]   M. Hofer et al., "Characterization of ultrashort pulse formation in passively mode-locked fiber lasers", IEEE J. Quantum Electron. 28 (3), 720 (1992).

[54]   M. E. Fermann, "Passive mode locking by using nonlinear polarization evolution in a polarization-maintaining erbium-doped fiber", Opt. Lett. 18 (11), 894 (1993).

[55]   M. E. Fermann, F. Haberl, M. Hofer, and H. Hochreiter, "Nonlinear amplifying loop mirror," Opt. Lett. 15, 752-754 (1990).

[56]   A. J. DeMaria, D. A. Stetser, and H. Heynau, "Self mode-locking of lasers with saturable absorbers," Appl. Phys. Lett. 8, 174 (1966).

[57]   J. Lee, K. Lee, Y.-S. Jang, H. Jang, S. Han, S.-H. Lee, K.-I. Kang, C.-W. Lim, Y.-J. Kim and S.-W. Kim, "Testing of a femtosecond pulse laser in outer spacem", Sci. Rep. 4, 5134 (2014).

[58]   U. Keller et al., "Semiconductor saturable absorber mirrors (SESAMs) for femtosecond to nanosecond pulse generation in solid-state lasers," IEEE J. Sel. Top. Quantum Electron. 2, 435 (1996)

[59]   T. R. Ganka, "Optical Frequency Comb for Space Measurement, Stabilization and Characterization ," Master Thesis, University of Applied Sciences Munich, (2011).

[60]   J. M. Dudley, A. Peacock, G. Millot, "The cancellation of nonlinear and dispersive phase components on the fundamental optical fiber soliton: A pedagogical note. ," Optics Communications. 193. 253-259 (2001).

[61]   R. Paschotta, "Timing jitter and phase noise of mode-locked fiber lasers," Opt. Express **18**, 5041-5054 (2010).

[62]   S. Wang, S. Droste, L. Sinclair, I. Coddington, N. Newbury, T. Carruthers, and C. Menyuk, "Wake mode sidebands and instability in mode-locked lasers with slow saturable absorbers," Opt. Lett. 42, 2362-2365 (2017).

[63]   Lora Nugent-Glandorf, Todd A. Johnson, Yohei Kobayashi, and Scott A. Diddams, "Impact of dispersion on amplitude and frequency noise in a Yb-fiber laser comb," Opt. Lett. 36, 1578-1580 (2011)

[64]   R. Paschotta, "Noise of mode-locked lasers (Part I): numerical model," Appl. Phys. B 79, 153–162 (2004).

[65]   K. Tamura et al., "77-fs pulse generation from a stretched-pulse mode-locked all-fiber ring laser", Opt. Lett. 18 (13), 1080 (1993).

[66]   Batop Optoelectronics. Data Sheet SAM-1550-41-1.5ps-x, 1550 nm, (2016)

[67]   J. Sotor, G. Sobon, J. Jagiello, L. Lipinska, and K. Abramski,"Repetition frequency scaling of an all-polarization maintaining erbium-doped mode-locked fiber laser based on carbon nanotubes saturable absorber" Journal of Applied Physics, 117(13):133103, (2015).

[68]   https://www.fiberdesk.com/, (23.10.2018).

[69]   P. V. Mamyshev and S. V. Chernikov, "Ultrashort-pulse propagation in optical fibers," Opt. Lett. 15, 1076-1078 (1990).

[70]   C. R. Giles and E. Desurvire, "Modeling erbium-doped fiber amplifiers," in *Journal of Lightwave Technology*, vol. 9, no. 2, pp. 271-283 (1991).

[71]   P. Peterka, J. Kanka, P. Honzatko, D. Kacik, "Measurement of chromatic dispersion of microstructure optical fibers using interferometric method,". Optica Applicata. 38. (2008).

[72]   D. Brida, G. Krauss, A. Sell und A. Leitenstorfer, "Ultrabroadband Er:fiber lasers," Laser & Photonics Reviews 8, 409-428 (2014).

[73]   G. P. Agrawal, "Nonlinear Fiber Optics," Optics and Photonics, Third Edition, Academic Press, ISBN: 9780120451432, (2001).

[74]   R. H. Stolen and C. Lin, "Self-phase-modulation in silica optical fibers," Phys. Rev. A 17 (4), 1448 (1978).

[75]   R. H. Stolen, J. P. Gordon, W. J. Tomlinson, and H. A. Haus,"Raman response function of silica-core fibers," J. Opt. Soc. Am. B 6, 1159-1166 (1989).

[76]   R. H. Stolen, "Phase-matched-stimulated four-photon mixing in silica-fiber waveguides," IEEE J. Quantum Electron. 11 (3), 100 (1975).

[77]   D. Anderson et al., "Wave-breaking-free pulses in nonlinear-optical fibers," J. Opt. Soc. Am. B 10 (7), 1185 (1993).

[78]   V. I. Kruglov, A. C. Peacock, J. D. Harvey, and J. M. Dudley, "Self-similar propagation of parabolic pulses in normal-dispersion fiber amplifiers," J. Opt. Soc. Am. B **19**, 461-469 (2002).

[79]   K. Tamura and M. Nakazawa, "Pulse compression by nonlinear pulse evolution with reduced optical wave breaking in erbium-doped fiber amplifiers," Opt. Lett. 21 (1), 68 (1996).

[80]   Chur Kim, Kwangyun Jung, Khanh Kieu, and Jungwon Kim, "Low timing jitter and intensity noise from a soliton Er-fiber laser mode-locked by a fiber taper carbon nanotube saturable absorber," Opt. Express 20, 29524-29530 (2012).

[81]   Sebastian Wick, "Characterisation and Modelling of an in-fibre Ultra-Short Pulse Amplifier for a Frequency Comb Device," Master Thesis, University of Applied Sciences, (2015).

[82]   G. Boyd and D. Kleinman, "Parametric interaction of focused Gaussian light beams," in *IEEE Journal of Quantum Electronics*, vol. 4, no. 5, pp. 353-353 (1968).

[83]   Curtis R. Menyuk, Jared K. Wahlstrand, John Willits, Ryan P. Smith, Thomas R. Schibli, and Steven T. Cundiff, "Pulse dynamics in mode-locked lasers: relaxation oscillations and frequency pulling," Opt. Express 15, 6677-6689 (2007).

[84]   Sung Yoon Ryu, Kyung-Soo Kim, Jungwon Kim, and Soohyun Kim, "Degradation of optical properties of a film-type single-wall carbon nanotubes saturable absorber (SWNT-SA) with an Er-doped all-fiber laser," Opt. Express 20, 12966-12974 (2012).

[85]   T. Lamour et. al., "High-Bandwidth Intensity and Phase Noise Stabilization of an Yb:fiber Femtosecond Frequency Comb," European Frequency and Time Conference, (2014).

[86]   C.-C. Lee, J. M. Miller, and T. R. Schibli, "Doping-induced changes in

the saturable absorption of monolayer graphene," Appl. Phys. B 108(1), 129–135 (2012).

[87]   Esther Baumann, Fabrizio R. Giorgetta, Jeffrey W. Nicholson, William C. Swann, Ian Coddington, and Nathan R. Newbury, "High-performance, vibration-immune, fiber-laser frequency comb," Opt. Lett. 34, 638-640 (2009).

[88]   W. Hänsel, M. Giunta, M. Lezius, M. Fischer, and R. Holzwarth, "Electro-optic modulator for rapid control of the carrier-envelope offset frequency," in *Conference on Lasers and Electro-Optics*, OSA Technical Digest, paper SF1C.5. (2017).

[89]   Kana Iwakuni, Hajime Inaba, Yoshiaki Nakajima, Takumi Kobayashi, Kazumoto Hosaka, Atsushi Onae, and Feng-Lei Hong, "Narrow linewidth comb realized with a mode-locked fiber laser using an intra-cavity waveguide electro-optic modulator for high-speed control," Opt. Express 20, 13769-13776 (2012).

[90]   K. Gürel, S. Hakobyan, V. J. Wittwer, S. Schilt and T. Südmeyer, "Frequency Comb Stabilization of Ultrafast Lasers by Opto-Optical Modulation of Semiconductors," in IEEE Journal of Selected Topics in Quantum Electronics, vol. 24, no. 5, pp. 1-9 (2018).

[91]   P. Manurkar, E. Perez, D. D. Hickstein, D. R. Carlson, J. Chiles, E. Baumann, S. A. Diddams, N. R. Newbury, K. Srinivasan, S. B. Papp, and I. Coddington, "Operating an optical frequency comb using a 5-W handheld USB charger," in Conference on Lasers and Electro-Optics, OSA Technical Digest, paper SM4L.1. (2018).

[92]   Tsung-Han Wu, K. Kieu, N. Peyghambarian, and R. J. Jones, "Low noise erbium fiber fs frequency comb based on a tapered-fiber carbon nanotube design," Opt. Express **19**, 5313-5318 (2011).

[93]   H. Hu, R. Ricken, and W. Sohler, "Low-loss ridge waveguides on lithium niobate fabricated by local diusion doping with titanium," Appl. Phys. B, (2010).

[94]   K. W. Holman, R. J. Jones, A. Marian, S. T. Cundiff and Jun Ye, "Detailed studies and control of intensity-related dynamics of femtosecond frequency combs from mode-locked Ti:sapphire lasers," in IEEE Journal of Selected Topics in Quantum Electronics, vol. 9, no. 4, pp. 1018-1024 (2003).

[95]   C. Benko, A. Ruehl, M. Martin, K. Eikema, M. Fermann, I. Hartl, and J. Ye, "Full phase stabilization of a Yb:fiber femtosecond frequency comb via high-bandwidth transducers," Opt. Lett. 37, 2196-2198 (2012).

[96]   S. Schweyer, R. Kienberger, B. Eder, P. Putzer, A. Kölnberger and N. Lemke, "Characterization of a SESAM mode-locked erbium fiber laser frequency comb with an integrated electro-optic modulator," European Frequency and Time Forum (EFTF), Neuchatel, (2014).

[97]   Martin Hoffmann, Stéphane Schilt, and Thomas Südmeyer, "CEO stabilization of a femtosecond laser using a SESAM as fast opto-optical modulator," Opt. Express 21, 30054-30064 (2013).

[98]   Q. Bao, H. Zhang, Y. Wang, Zhenhua Ni, Yongli Yan, Ze Xiang Shen, Kian Ping Loh, Ding Yuan Tang,"Atomic-Layer Graphene as a Saturable Absorber for Ultrafast Pulsed Lasers," Adv. Funct. Mater. 19, 3077–3083 (2009).

[99]   N. Kuse, C.-C. Lee, J. Jiang, C. Mohr, T. R. Schibli, and M.E. Fermann, "Ultra-low noise all polarization-maintaining Er fiber-based optical frequency combs facilitated with a graphene modulator," Opt. Express 23, 24342-24350 (2015).

[100] N. Kuse, J. Jiang, C.-C. Lee, T. R. Schibli, and M.E. Fermann, "All polarization-maintaining Er fiber-based optical frequency combs with nonlinear amplifying loop mirror," Opt. Express 24, 3095-3102 (2016).

[101] L. C. Sinclair, J.-D. Deschênes, L. Sonderhouse, W. C. Swann, I. H. Khader, E. Baumann, N. R. Newbury, and I. Coddington, "A compact optically coherent fiber frequency comb," Review of Scientific Instruments 86, 081301 (2015).

[102] J. Kim, J. Chen, Z. Zhang, F. N. C. Wong, F. X. Kärtner, F. Loehl, and H. Schlarb, "Long-term femtosecond timing link stabilization using a single-crystal balanced cross correlator," Opt. Lett. 32, 1044-1046 (2007).

[103] S. Schweyer, P. Putzer, B. Eder, A. Kölnberger, M. Breuer, N. Lemke, A. Sell, A. Zach, R. Kienberger and U. Schreiber, "Stabilization of a SESAM Mode-Locked Erbium Laser Frequency Comb with an Integrated Electro-Optic Modulator to an Optical Reference," European Frequency and Time Forum (EFTF), York, (2016).

[104] F. Loehl, H.Schlarb, J. Müller, J.-W. Kim, J. Chen, F. Wong and F. X. Kaertner et al., "Sub-10 femtosecond stabilization of a fiber-link using a balanced optical cross-correlator," 2007 IEEE Particle Accelerator Conference (PAC), Albuquerque, NM, pp. 3804-3806 (2007).

[105] N. Kuse, C.-C. Lee, J. Jiang, C. Mohr, T. R. Schibli, and M. E. Fermann, "Ultra-low noise all polarization-maintaining Er fiber-based optical frequency combs facilitated with a graphene modulator," Opt. Express 23(19), 24342–24350 (2015).

[106] K. U. Schreiber, A. Gebauer, and J.-P. R. Wells, "Closed-loop locking of an optical frequency comb to a large ring laser," Opt. Lett. 38, 3574-3577 (2013)

[107] http://www.fs.wettzell.de/LKREISEL/G/LaserGyros.html, (02.11.2018)

[108] S. Grop, P.-Y. Bourgeois, N. Bazin, Y. Kersalé, E. Rubiola, C. Langham, M. Oxborrow, D. Clapton, S. Walker, J. D.Vicente, and V. Giordano, "A crycooled 10 GHz oscillator with 10^{-15} frequency stability," Rev. of Sci. Instrum.81, 025102 (2010).

[109] http://sci.esa.int/sci-ft/50124-technology-readiness-level/, (02.11.2018)

[110] T. Lévèque, L. Antoni-Micollier, B. Faure and J. Berthon, "A laser setup for rubidium cooling dedicated to space applications," Applied Physics B. 116. 997-1004. 10.1007/s00340-014-5788-z, (2014).

[111] P. Manurkar, E. F. Perez, D. D. Hickstein, D. R. Carlson, J. Chiles, D. A. Westly, E. Baumann, S. A. Diddams, N. R. Newbury, K. Srinivasan, S. B. Papp and I. Coddington," A fully self-referenced frequency comb consuming 5 Watts of electrical power," arXiv:1802.04119 (2018).

[112] L. V. Radushkevich and B. Lukyanovich," Structure of the carbon formed by thermal decomposition of carbon monoxide in an iron contact," Journal of Physical Chemistry, 26(1):88–95 (1952).

[113] S. Iijima et al. "Helical microtubules of graphitic carbon," nature, 354(6348):56–58 (1991).

[114]   K. S. Novoselov, A. K. Geim, S. V. Morozov, D. Jiang, Y. Zhang, S. V. Dubonos,I. V. Grigorieva and A. A. Firsov, "Electric Field Effect in Atomically Thin Carbon Films," Science. Band306, Nr.5696, S.666–669 (2004).

[115]   S. Y. Set et al., "Mode-locked fiber lasers based on a saturable absorber incorporating carbon nanotubes," OFC 2003 Optical Fiber Communications Conference, pp. PD44-P1-3 vol.3. (2003).

[116]   H. B. Qin, G. Wang, H. B. Zhang, J. Liu and Z. Zhuo, "A passively mode-locked Nd:YVO 4 Laser with a carbon nanotube saturable absorber," Laser Physics. 22. 10.1134/S1054660X12040160, (2012).

[117]   A. Kis and A. Zettl, "Nanomechanics of carbon nanotubes,". Philosophical Transactions of the Royal Society of London A: Mathematical, Physical and Engineering Sciences, 366(1870):1591–1611 (2008).

[118]   A. Jorio, M. Pimenta, A. Souza Filho, R. Saito, G. Dresselhaus, and M. Dresselhaus, "Characterizing carbon nanotube samples with resonance Raman scattering", New Journal of Physics, 5(1):139, (2003).

[119]   Yim, J. H., Cho, W. B., Lee, S., Ahn, Y. H., Kim, K., Lim, H., F. Rotermund, "Fabrication and characterization of ultrafast carbon nanotube saturable absorbers for solid-state laser mode locking near 1μm," Applied Physics Letters, 93(16), 161106. doi:10.1063/1.2999593 (2008).

[120]   M. J. Bronikowski, P. A. Willis, D. T. Colbert, K. Smith, and R. E. Smalley, "Gas-phase production of carbon single-walled nanotubes from carbon monoxide via the HiPco process: A parametric study," Journal of Vacuum Science & Technology A", 19(4):1800–1805 (2001).

[121]   S. Kelly, "Characteristic sideband instability of periodically amplified average soliton," Electronics Letters, 28(8):806–807 (1992).